NATIONAL TECHNICAL UNIVERSITY OF ATHENS

DIPLOMA THESIS

PARAMETRIC EXCITATION AND ANTI-RESONANCE IN ROTATING SYSTEMS WITH GAS BEARINGS

Author:

Emmanuel D. Dimou

Supervisor:

Asst. Prof. Athanasios Chasalevris

A thesis submitted in fulfillment of the requirements

, for the degree of Diploma in Mechanical Engineering

Athens, July 2022

ABSTRACT

The linear and the non – linear dynamics of a parametrically excited turbo-pump rotor are investigated in this thesis. Realistic models of rotors, linear and non – linear bearings under the effect of vertical periodic loads are implemented to compose a set of differential equations for autonomous and non – autonomous cases. The solution branches of the dynamic system are evaluated by the pseudo arc – length continuation method and the respective limit cycles are evaluated by orthogonal collocation method, programmed by the author. The former are investigated in their stability properties and their quality of motion for the respective key design parameters of the whole rotor – bearing system. The main conclusion of this thesis is that parametric antiresonance (considered as the stabilization of unstable trivial solutions under the principles of parametric excitation at certain parameter regions) is feasible in rotor – gas foil bearing systems. Around a fundamental excitation frequency which can be approximately calculated by a closed form expression the stability margins of the (perfectly balanced) system are enhanced and the extent of the corresponding limit cycles is decreased. It is strongly believed that parametric excitation could have similar beneficial effects on unbalanced systems too.

ACKNOWLEDGEMENTS

This thesis is a result of 12 months of work in the Rotordynamics Group at the N.T.U.A. school of mechanical engineering. During this time I was supported and influenced by several people to whom I would like to express my sincere thanks. In addition I would like to honestly apologize to those I may have disappointed. This thesis is wholeheartedly dedicated to them.

This work would not be possible, without the consistent guidance, patience and persistence of my supervisor Asst. Prof. Athanasios Chasalevris. His knowledge on the physical principles under which a dynamic system operates and experience on the mechanical design are invaluable. Due to our common vision, I am getting used to both the difficulties and the beauty of the Rotordynamics research field. I am grateful to him.

Additionally, I would like to extend my gratitude to the fellow students who also worked on their theses in the Rotordynamics group. Their ideas of high quality regarding technical issues were really helpful.

I am also grateful to all the people I had more personal relationships with. Their continuous support and the experiences we shared helped me maintain spiritual balance during an otherwise pandemic – stricken and work – intensive period.

Last but certainly not least, I would like to try to put into words my love for my mother and sister. They fulfilled my desires before I even express them, they served my every – day necessities unselfishly. Their unwavering support during my studies and beyond is of much more than a master thesis dedication.

Emmanuel D. Dimou

Athens, July 2022

CONTENTS

LIST OF FIGURES

LIST OF TABLES

NOMENCLATURE

HELLENIC LETTERS

A_e	Cross – section area of e-th FBE
A_i	I-th const. term deriving from the discr. RE (zero order)
a	Coeff. for the Rayleigh damping
a_i	I-th const. term for the construction of FBE stiffness matrix
B_i	I-th const. term deriving from the discr. RE (first order)
β	Coefficient for the Rayleigh damping
γ	Dimensionless whirl frequency, $\gamma = \frac{\nu}{\Omega}$
δ	Amplitude ratio of the PE stiffness and bearing coefficients
E_e	Young's modulus of e-th FBE
ε	Eccentricity ratio
ζ	Dimensionless axial coordinate of a FBE
η	Loss factor
θ	Circumferential bearing coordinate
θ_0	Altitude angle
I_e	2nd moment of cross – section's area of e-th FBE
I_r	2nd moment of cross – section's area of the deformable ring
κ_i	Const. depending on the geom. and phys. properties of the ring
Λ	Bearing number according to the nonlinear model, $\Lambda = \frac{p_0 {c_r}^2}{6\mu R^2}$
Λ'	Bearing number according to the linear model, $\Lambda' = \frac{6\mu R^2 \Omega}{p_0 {c_r}^2}$
λ	Eigenvalue, according to the LHA
μ	Viscosity
μ_d	Diametrical mass moment of inertia per unit length
μ_e	Mass per unit length of e-th FBE
μ_p	Polar mass moment of inertia per unit length
N_m	Number of master nodes of the reduced rotor model
N_r	Number of nodes of the full rotor model
$N_{\bar{x}}$	Number of intervals in the circumferential bearing's direction
$N_{\bar{z}}$	Number of intervals in the axial bearing's direction
ν	Whirl frequency
ν_r	Poison's ratio of the deformable ring
ξ_0	Initial state vector belonging to a curve of periodic solutions
ρ	Density of the gas
ρ_e	Density of the e-th finite beam element
T_e	Kinetic energy of the e-th FBE
τ	Dimensionless time
$\mathbf{\Phi}$	Left eigenvector, according to the LHA
$\boldsymbol{\varphi}_e$	Lateral bending slope in both planes of the e-th FBE
χ	Angle of foil's fixation point
$\mathbf{\Psi}$	Right eigenvector, according to the LHA
$\boldsymbol{\psi}_e$	Elastic line in both planes of the e-th FBE
Ω, $\bar{\Omega}$	Rotating speed, $\bar{\Omega} = \frac{\Omega}{\Lambda}$
Ω_{2D}	2D-Domain on which RE is solved
Ω_{ex}	Excitation frequency

LATIN LETTERS

A, A'	Matrices of the customary state space form
a_f	Struct. compl. (of the BF) per area
B, B'	Matrices of the customary state space form
$\mathbf{C}$	Damping matrix of the full rotor model
$\mathbf{C}_e$	Damping matrix of the e-th FBM
$\mathbf{C}_r$	Damping matrix of the reduced rotor model
C_i	I-th const. term from the discr. RE (first order)
c_f	Struct. damp. coeff. (of the BF) per area,
c_i	I-th const. term for the constr. of FBM matrices
c_r	Radial clearance
dh	Horizontal displacement of the deformable ring
dv	Vertical displacement of the deformable ring
e	Const. term for the constr. of FBM matrices
$e_{\max}$	Max eccentricity ratio
e_u	Const. term regarding unbal. force's magnitude
F	Vertical periodic load applied to the PEGFB
$\mathbf{F}^B, \mathbf{F}^G, \mathbf{F}^U$	Bear., Gas and Unbal. nodal forces of full rotor model
$\mathbf{F}_e$	External nodal forces applied to the e-th FBM
$\mathbf{F}_m$	External nodal forces of reduced rotor model
$\mathbf{F}_m^B, \mathbf{F}_m^G, \mathbf{F}_m^U$	Bear., Gas and Unbal. forces of reduced rotor model
G_e	Shear modulus of the e-th FBM
g_i	I-th const. term for the constr. of the gyroscopic FBM
$\mathbf{G}$	Gyroscopic matrix of the full rotor model
$\mathbf{G}_e$	Gyroscopic matrix of the e-th FBM
$\mathbf{G}_r$	Gyroscopic matrices of the reduced rotor model
H_i	I-th Hermitian polynomial
H_i'	I-th derive. of the Her. pol. with resp. to the ax. coord.
$h, \bar{h}$	Gas film thickness $\bar{h} = \frac{h}{c_r}$
$h_0, \bar{h}_0$	Gas film thickness at journal's equilibrium position
$\bar{h}_{\bar{x}}, \bar{h}_{\bar{y}}, \bar{h}_{\dot{\bar{x}}}, \bar{h}_{\dot{\bar{y}}}$	Disturbances of the Gas film thickness
i_a	Const. term regard. the BF used in RERM
K_{ij}	Linearized stiffness coefficients
$k_f, \bar{k}_f$	Strut. stiffness coeff. (of the BF) per area
$\mathbf{K}$	Stiffness matrix of the full rotor model
$\mathbf{K}^G$	Cond. stiffness matrix of the full rotor model for SA
$\mathbf{K}_e$	Stiffness matrix of the e-th FBM
$\mathbf{K}_{ab}$	Stiff. sub-matrices regard. the master and slave nodes
$\mathbf{K}_r$	Stiffness matrices of the reduced rotor model
L_b	Bearing's length
l_e	Length of the e-th FBM
m_a	Const. term regard. the BF used in RERM
O_b	Geometrical bearing's centre
O_j	Geometrical journal's centre
$p, \bar{p}$	Pressure distribution $\bar{p} = \frac{p}{p_a}$
p_a	Ambient pressure
$\tilde{p}_a, \hat{p}_a$	Functions regard. pressure distribution used in RERM
$p_m, \bar{p}_m$	Mean pressure over bearing's half length
$p_0, \bar{p}_0$	Press. distribution at the journal's equilibrium position
$\bar{p}_{\bar{x}}, \bar{p}_{\bar{y}}, \bar{p}_{\dot{\bar{x}}}, \bar{p}_{\dot{\bar{y}}}$	Disturbances of the pressure distribution
$q, \bar{q}$	Foil deformation $\bar{q} = \frac{q}{c_r}$
$q_0, \bar{q}_0$	Foil deformation at journal's equilibrium position
$\bar{q}_{\bar{x}}, \bar{q}_{\bar{y}}, \bar{q}_{\dot{\bar{x}}}, \bar{q}_{\dot{\bar{y}}}$	Disturbances of the foil deformation
$q_r, \bar{q}_r$	Outer ring's deform. under the effect of the per. load
R	Bearing's radius
$R_{i_{m,e}}$	Inner mass radius of the e-th FBM
R_{i_r}	Inner radius of the outer deformable ring
$R_{i_{s,e}}$	Inner stiffness radius of the e-th FBM
R_j	Journal's radius
$R_{o_{m,e}}$	Outer mass radius of the e-th FBM
R_{o_r}	Outer radius of the outer deformable ring
$R_{o_{s,e}}$	Outer stiffness radius of the e-th FBM
r_a	Resid. Deriv. by the approx. of the pressure distr.
s_f	Shear factor for all FBMs
s_i	I-th constant term calculated via Simpson's rule
T	Period of the periodic solution
t	Time
U_e	Potential energy of the e-th FBM
v	Stability factor

W_{st}	Static load of each gas foil bearing	$\mathbf{x}_r$	Displ. and angular slopes of the full rotor model
w_a	Const. term regard. the BF used in RERM	$\mathbf{x}_{r_0}$	IC for displ. and angular slopes of the full rotor model
$\overline{X}$	Journal's vertical displacement, linear model $\overline{X} = \frac{X}{c_r}$	$\mathbf{x}_{s_r}$	State vector of the whole nonlinear system
$\mathbf{X}_{m_r}$	State vector of the reduced rotor model	$\mathbf{x}_{s_{r,0}}$	IC for the state vector of the whole nonlinear system
$\mathbf{X}_{m_{r,0}}$	IC of the state vect. of the reduced rotor model	$\overline{Y}$	Journal's horizontal displ., linear model $\overline{Y} = \frac{Y}{c_r}$
$x, \overline{x}$	Circumferential bearing coordinate $\overline{x} = \frac{x}{c_r}$	y_b	Bearing's centre vertical position
x_b	Bearing's centre horizontal position	y_j	Journal's vertical displacement, nonlinear model
x_j	Journal's horizontal displacement nonlinear model	$\mathbf{Y}_{m_r}$	State vector of the PE linearized system
x_e	Horizontal coordinate of the e-th FBM	$\mathbf{Y}_{m_{r,0}}$	IC for the state vector of the PE linearized system
$\mathbf{x}_{m_r}, \overline{\mathbf{x}}_{m_r}$	Dis. and slopes of the reduced rotor model $\overline{\mathbf{x}}_{m_r} = \frac{\mathbf{x}_{m_r}}{c_r}$	$z, \overline{z}$	Axial bearing coordinate $\overline{z} = \frac{z}{L_b}$
$\mathbf{x}_{m_{r,0}}, \overline{\mathbf{x}}_{m_{r,0}}$	IC for displ. and slopes of the reduced rotor model	z_e	Axial coordinate of the e-th FBM

1. INTRODUCTION

1.1 Gas foil bearings and parametric excitation

Gas foil bearings (GFBs) as modern oil-free technology have a vital role in high-speed rotating machinery[1]. Under normal working conditions, when a thin hydrodynamic gas film is developed, such bearings are proved to be beneficial for the operation of the whole foil bearing – rotor system. More specifically, GFBs are self-acting and therefore do not require any external pressurization. Furthermore, given the fact of solid lubrication, due to the absence of solid to solid contact between the rotor's journal and the foil's inner surface (top foil) low wear and power loss can be achieved[2]. This absence of solid to solid contact also contributes to remarkable reliability. The mean time between failures for aircraft turbo compressors has been dramatically enhanced during the last decades and today reaches 60000 h[3] [4]. Last but not least, if the bearing's surface is compliant, not rigid, rotors are capable to work under higher loads and at higher rotating speeds stably[5]. The motivation of the present work lies exactly on this special characteristic.

Numerous variations of GFBs are gaining more and more interest in the industry world widely, but the structure and the physical principles under which they operate are pretty much the same. Foil air bearings are similar to conventional, oil-lubricated bearings in size and shape (volume limitations are not arising) but use air as working fluid whose compressibility can't be neglected[6]. In contradiction, the time varying density of the fluid affects the development of hydrodynamic film and therefore the foil's deformations and the trajectory of the rotor's journal. In addition, the assumption of compressible flow has a significant role in the implementation of parametric excitation. The most commonly used compliant inner surface (top foil), is supported by a spring pack or a bump foil layer and this is the key characteristic of the whole bearing-rotor system. The aforementioned compliance allows on the one hand the bearing to accommodate shaft misalignment and thermal distortion and on the other hand the designer to enhance load capacity and stability[7]. The dumping characteristics depend on the GFB's design. For example, in multiple overleaf and tape GFBs the dry friction at the contact lines is quite significant[8]. In bump GFBs bump-strip layers under the top foil construct a complex foundation with nonlinear elastic properties and at the same time interesting dumping characteristics. Of course dry friction effects between the bumps and the top foil continue arising[9] [10].*Figure 1.1.1* schematically shows some GFB

---

[1] ***T.Leister, C.Baum, W.Seemann.*** *On the Importance of Frictional Energy Dissipation in the Prevention of Undesirable Self-Excited Vibrations in Gas Foil Bearing Rotor Systems. TECHNISCHE MECHANIK. 2017.*

[2] ***H. Heshmat, J. A. Walowit, O. Pinkus.*** *Analysis of gas-lubricated foil journal bearings. Journal of Lubrication Technology. 1983.*

[3] ***S. A. Howard, R. J. Bruckner, C. DellaCorte, K. C. Radil.*** *Gas foil bearing technology advancements for closed Brayton cycle turbines. United States of America : National Aeronautics and Space Administration, 2007.*

[4] ***Howard, S. A.*** *Rotordynamics and design methods of an oil-free turbocharger. United States of America : National Aeronautics and Space Administration, 1999.*

[5] ***S. A. Howard, R. J. Bruckner, K. C. Radil.*** *Advancements toward oil-free rotorcraft propulsion. United States of America : National Aeronautics and Space Administration, 2010.*

[6] ***C. DellaCorte, A. Zaldana, K. C. Radil.*** *A Systems Approach to the Solid Lubrication of Foil Air Bearings for Oil-Free Turbomachinery. STLE/ASME . Joint International Tribology Conference, 2004.*

[7] ***Gross, W. A.*** *Gas Film Lubrication. s.l. : John Wiley and Sons, Inc, 1962.*

[8] ***C. A. Heshmat, H. Heshmat.*** *An Analysis of Gas Lubricated Multileaf Foil Journal Bearings with Backing Springs. J. Tribol. 1995, 117. pp. 437-443.*

[9] ***M. J. Baum, F. K. Choy, M. Dzodzo, J. Hsu.*** *Two-Dimensional Dynamic Simulation of a Continuous Foil Bearing. Tribology International. 1996, pp. 61-68.*

[10] ***H. Heshmat, W. Sharpino, S. Gray.*** *Development of Foil Journal Bearings for High Load Capacity and High Speed Whirl Stability. J. Lubr. Technol. 1982, pp. 149-156.*

designs. The solid lubrication is of a great importance too, especially when low rotating speeds are encountered (run-up, run-down) and the hydrodynamic gas film has not been developed. A common strategy which provides it is the application of a thin polymer film or coating whose mass properties are negligible[11].

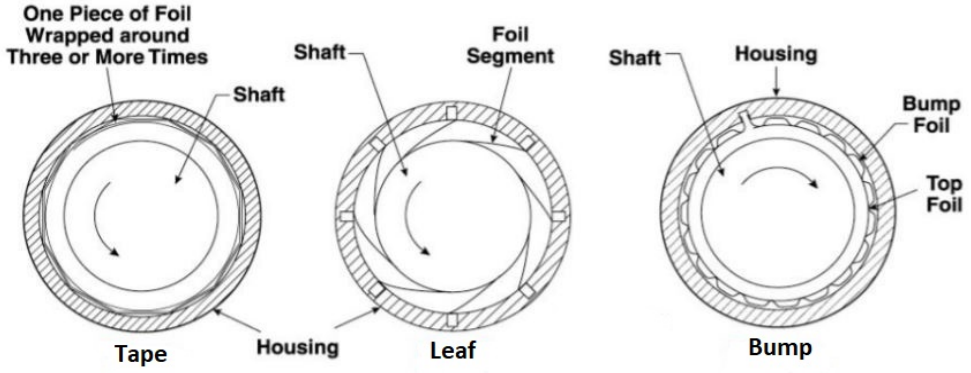

Figure 1.1.1 *Schematic example of typical Generation I foil bearings with axially and circumferentially uniform support elements*

In general, the plethora of gas foil bearing designs can be categorized in three different Generations presented in *Figure 1.1.2* , *Figure 1.1.3*. First Generation bearings normally replace rigid gas bearings of the same size in air cycle machines, since they share common load capacities. Second Generation bearings exhibit a more complex elastic foundation as its stiffness properties are capable to be tailored in one direction. For example, if the designer's main goal is to adopt in shaft's misalignment or to avoid leakage of hydrodynamic fluid, then stiffness properties are tailored in the axial direction. This type of bearings has significantly higher load capacities and this is why they are preferred in turbo-compressors and micro-turbines. Finally, third Generation bearings carry the most complex elastic foundations with properties able to be tailored in both axial and radial direction. The designer can adopt to load capacities three or four times greater than the load capacity of Generation one bearings and optimize the bearing stiffness for varying loads. The superiority of this type is profound but still the stability of the whole bearing-rotor system in really high rotating speeds is not ensured[12]. In this Master Thesis, the potential to enhance the stability margins under the principles of the parametric excitation is investigated.

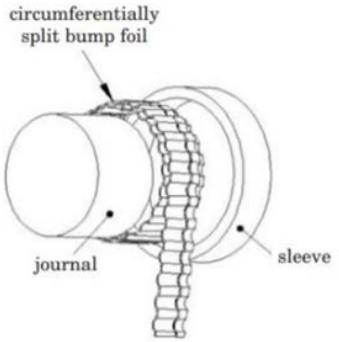

Figure 1.1.2 *Generation II foil air bearings*

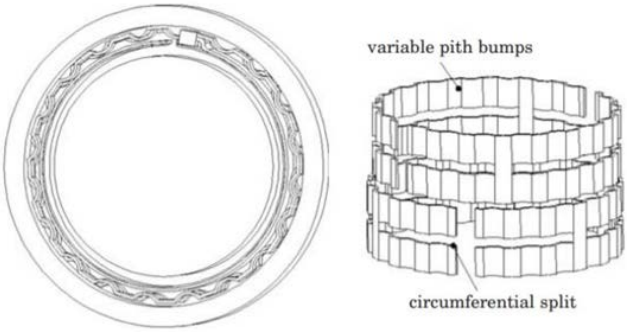

Figure 1.1.3 *Generation III foil air bearings*

[11] ***C. DellaCorte, J. C. Wood.*** *High Temperature Solid Lubricant Materials for Heavy Duty and Advanced Heat Engines. NASA TM-106570. 1994.*

[12] ***C. DellaCorte, K. C. Radil, R. J. Bruckner, S. A. Howard.*** *Design, Fabrication and Performance of Open Source Generation I and II Compliant Hydrodynamic Gas Foil Bearings. NASA TM-214691. 2007.*

Parametrically excited systems have been studied extensively in mathematics and engineering applications[13][14][15]. Maybe the most reputable examples of parametrically excited systems are the simple pendulum with a periodically moving support and the simple beam with pulsating axial load. Mathieu equations can easily describe the linearized equations of motion of both aforementioned systems and the trivial solution of these equations can easily be destabilized by parametric excitation. Unstable parameter regions caused by parametric excitation are called parametric resonances.

In systems with two or more degrees of freedom a well-chosen parametric excitation can have stabilizing effects too, first discovered and described by Tondl[16] [17]. These effects can be simplistically interpreted as couplings of certain modal degrees of freedom which allow a better usage of the existing system dumping. Thus, parametric excitation does not enhance the dumping properties of a system, it just highlights them. If the trivial solutions of an unstable, system can be stabilized in certain parameter regions by introducing parametric excitation then these regions are called parametric anti-resonances. For applications which can't operate unstably in high rotating speeds, parametric anti – resonances are significant engineering benefits.

1.2 Models of gas foil bearings and parametric excitation implementation

An important amount of research has been conducted on the bump type foil bearing dynamics. First, H. Heshmat[2] proposed the so called simple elastic foundation model for foil journal bearings and compliant thrust bearings whose simplicity made it widely accepted even if the prediction of the equivalent stiffness is not sufficient. More specifically, Heshmat substituted the bump-strip layers with separated linear springs. Thus, the structural stiffness was assumed linear, equally distributed and independent of the carrying loads. The static Reynolds equation (zero order) was coupled with the linear structural equations in order to obtain the pressure distribution. Low stiffness predictions were expected since the interactions between the bumps where neglected and the zero order Reynolds equation provides information of poor accuracy about the pressure distribution. Later, Peng and Carpino[18] [19] presented a novel method to predict the linear dynamic stiffness and damping coefficients of bump foil bearings. Even if their structural model consisted only of an elastic foundation, the structural equations of motion can easily be modified in order to incorporate structural damping too. They used perfect gas whose behavior can be described by the Reynolds equation and they coupled structural and fluid equations. A perturbation method was applied to both zero and first order Reynolds equations and a finite difference (FD) formulation was developed to solve for the four stiffness and the four damping coefficients. Last but not least,

---

[13] ***Bolotin, V.*** *The Dynamic Stability of Elastic Systems. Holden-Day. 1964.*

[14] ***A. P. Seyramian, A. A. Mailybaev.*** *Multiparameter Stability Theory with Mechanical Applications. World Scientific Pub. Co. 13, 2003.*

[15] ***Schmidt, G.*** *Parametererregte Schwingungen (In German, Translated Title 'Parametrically Excited Oscillations'). Deutcher Verlag der Wissenschaften. 1975.*

[16] ***Tondl, A.*** *On the interaction between self excited and parametric vibrations. Monographs and Memoranda, National Research Institute for Machine Design. 25, 1978.*

[17] ***Tondl, A.*** To the problem of quenching self-excited vibrations. ACTA Technology. 1998, pp. 109-116.

[18] ***J. P. Peng, M. Carpino.*** *Calculation of stiffness and damping coefficients for elastically supported gas foil bearings. Journal of Tribology. 115, pp. 20-27.*

[19] ***J. P. Peng, M. Carpino.*** *Finite element approach to the prediction of foil bearing rotor dynamic coefficients. Journal of Tribology. 119, pp. 85-90.*

L. San Andres and Kim[20] [21] [22] developed a numerical model in which 1D and 2D finite element (FE) approaches were introduced in order to calculate the top foil deflection. They managed to obtain frequency dependent linear dynamic coefficients for heavily loaded foil bearings and therefore a linear response of a rotor supported by them. Moreover, they compared the results with the non-linear response of the same rotor and the non-linear nature of stiffness characteristics were modeled using experimental data. They concluded in that the linear force coefficients are not reliable to represent the dynamic behavior of a rotor supported by GFBs.

In general, when simulating the rotor's behavior in gas foil bearings different approaches are conceivable. The common approach of deriving the linearized stiffness and damping coefficients, around a static equilibrium position of the journal is proved to be quite inaccurate. In other words, if the equilibrium position is stable, the method might be sufficient, but if the equilibrium position is unstable some non-linear effects like sub-synchronous vibrations might not be predicted by the linear approach. Another possible approach, mainly implemented on oil-lubricated bearings, is look-up tables. The main idea is, predicting the bearing force in advance for various journal states without coupling to the rotor model, save it to a look-up table and finally run the rotor simulation linked to that table. Since the fluid equation does not include the time dependent part, this approach might be practical, but in GFBs, at least the pressure distribution is function of time. Therefore, at least one extra dimension of the data field is required making the approach rather impractical. So, when fluid-structure models of bearings are coupled to dynamic rotor models the time integration of both models has to be synchronized. C. Baum, H. Hetzler, S. Schroders, T. Leister and W. Seemann[23] suggested a model order reduction for the fluid equations in order to obtain an overall bearing model suitable for fully coupled non-linear rotor-dynamic investigations.

Obviously, the computational efficiency of an approach which combines a fully coupled non-linear rotor-bearing model with a well-chosen parametric excitation implementation is of great importance. As far as the author knows, one of the first attempts to implement parametric excitation has been done by F. Dohnal, H. Ecker, and H. Springer[24]. A uniform cantilever beam under the effect of a periodic axial load was investigated. The beam structure was discretized by a finite element approach, so the linearized equations of motion which described the one planar bending vibrations of the beam led to a system with periodic stiffness matrices. Numerical methods based on Floquet's theorem and other analytical methods proved that given the fact that a certain level of the forcing amplitude is exceeded the damping properties of the beam are high lightened. In other words, parametric excitation mainly resulted in suppressed vibrations. T. Breunung, F. Dohnal, B. Pfau [25] investigated two quite realistic rotor systems from the literature in order to prove that an initially unstable equilibrium position can be stabilized by introducing a parametric excitation. The first was a

[20] ***L. San Andres, T. H. Kim.*** *Improvements to the analysis of gas foil bearings: Integration of top foil 1D and 2D structural models. ASME turbo expo 2007, Power for land, sea and air pp.779-789.*

[21] ***T. H. Kim, L. San Andres.*** *Heavily loaded gas foil bearings: a model anchored to test data. Journal Engineering for Gas Turbines and Power 012504-012508. 130, 2007.*

[22] ***T. H. Kim, L. San Andres.*** *Forced non-linear response of gas foil bearing supported rotors. Tribology International. 41, pp. 704-715.*

[23] ***C. Baum, H. Hetzler, S. Schroders, T. Leister, W. Seemann.*** *A Computationally Efficient Nonlinear Foil Air Bearing Model for Fully Coupled Transient Rotor Dynamic Investigations. Tribology International. 2020.*

[24] ***F. Dohnal, H. Ecker, H. Springer.*** *Enhanced damping of a cantilever beam by axial parametric excitation. Archive of Applied Mathematics. December 2008.*

[25] ***T. Breunung, F. Dohnal, B. Pfau.*** *An approach to account for interfering parametric resonances and anti-resonances applied to examples from rotor dynamics. Springer Nature B.V. 2019.*

self-excited rotor system proposed by Tondl and Ecker[26], which consisted of two bearing housings with known masses and one rigid rotor. Each one of the three masses had two translational degrees of freedom and the rotor mass had two extra rotational degrees of freedom. Bearing forces were modeled phenomenologically and the parametric excitation was introduced by the time variant stiffness of the bearing support. The second was a Jeffcott rotor consisted of a flexible shaft, a centered disc, and two journal masses at both ends of the shaft. The bearing forces were calculated by numerical integration of the Reynolds equation of the incompressible flow and the parametric excitation was introduced by a harmonic adjustment of the upper segment of the lemon bore bearing. F. Dohnal, A. Chasalevris[27] proposed an even more realistic concept of adjustable fluid film journal bearings. The main goal was the enhancement of the stability margins of a turbine rotor discretized by a finite element (FE) method. The parametric excitation was introduced by a predefined sinusoidal displacement (of certain amplitude and frequency) of the movable pads of two and three lobe bearings.

In this Master Thesis, a rather simplistic model for bump foils properties of linearized stiffness and damping coefficients is utilized and the interesting parameters are introduced as foil compliance and foil loss factor. Due to its complex geometry, the slender rotor is discretized with continuous beam elements, each element having two nodes and eight total degrees of freedom. The rotor's behavior in gas foil bearings is approached by deriving the linearized stiffness and damping coefficients of the bearings (linear approach) and by following the model order reduction for the fluid equations (nonlinear approach) [23]. The linear approach is inspired by the idea of Peng and Carpino[18, 19]. A modified method for obtaining the equilibrium position of the journal is presented, according to which, the zero order Reynolds equation and the corresponding time invariant structural equation are coupled to two extra equations relative to the static bearing forces. The parametric excitation is implemented by a predefined displacement (of heavily investigated amplitude and frequency) of the initially circular ring. The aforementioned configuration of the rotor-bearing model is depicted in *Figure 1.2.1*.

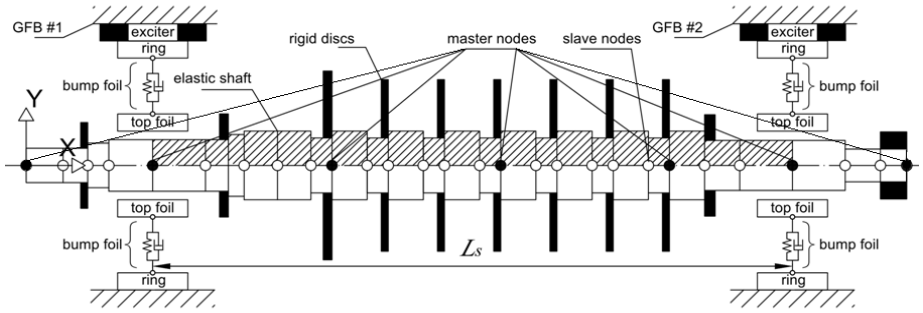

Figure 1.2.1 *The configuration of the G.F.B.s (linear approach) - Rotor system*

1.3 Methods of limit cycle calculation and continuation

As clearly mentioned before, the non-linear phenomena in high speed rotor systems are strong and can't be neglected. Thus, numerical integration of the equations of motion is most commonly implied, even if it imposes several limitations. At first, particularly for large order systems numerical integration is of large computational cost which makes the system's design

[26] ***H. Ecker, A. Tondl.*** *Stabilization of a rigid rotor by a time-varying stiffness of the bearing mounts. Vibration of Rotating Machinery. 2004.*
[27] ***F. Dohnal, A. Chasalevris.*** *Improving stability and operation of turbine rotors using adjustable journal bearings. Tribology International. 2016.*

rather impractical. Furthermore, numerical integration is unable to compute unstable steady state solutions (unstable limit cycles) and difficultly computes the corresponding stable steady state solutions (attracting limit cycles). Since the current work primarily aims to investigate the threshold speed of instability of large order rotating systems under the principles of parametric excitation, another more effective and computationally efficient method for calculating limit cycles should be utilized.

Maybe the most popular method for the calculation of periodic solutions of non-linear systems with multiple degrees of freedom (MDoF) is the collocation method[28]. N. J. Mallon in that report showed that a good approximation of the solutions of ordinary differential equations (ODEs) can be discretized properly and satisfy the set of ODEs at certain preselected points, the collocation points. They also showed that the computation of periodic solutions could be defined as a two point boundary value problem (BVP) with an extra unknown parameter, the period. A quasi-linearization technique was utilized to transform the non-linear BVP in a sequence of linear BVPs. Finally, in order to eliminate the unknowns of the linear problem he proposed a parameter condensation technique which incorporates a quadrature scheme. The main drawback of the method is the 'necessity' of analytically computed Jacobian matrices.

Nevertheless, it is far from enough just to compute a periodic solution. The main goal is to find solution branches as one or more design or operating parameters change (as bifurcation parameters) and therefore numerical continuation tools are of great importance[29] [30] [31] [32]. The numerical continuation method in one of its most popular version (pseudo arc-length continuation) has the primary advance to study MDoF systems[33]. Among the various contributions, in[34] [35] [36] simplified models of high speed rotors on floating ring bearings were studied while in[37] [38] [39] [40] the bifurcation sets of Jeffcott rotor models mounted on oil film bearings were investigated. More recently, pseudo arc length continuation method was implemented on simple rotor models on adjustable bearings[41] or on gas foil bearings.

---

[28] ***Mallon, N. J.*** *Collocation: A method for computing periodic solutions of ordinary differential equations. Eindhoven : s.n., 2002.*

[29] ***K. Georg, E. L. Allgower.*** *Introduction to Numerical Continuation Methods. Society for Industrial and Applied Mathematics. 2003.*

[30] ***H. Meijer, F. Dercole, B. Olderman.*** *Numerical bifurcation analysis. Encyclopedia of Complexity and Systems Science. 2003, pp. 6329-6352.*

[31] ***Kuznetsov, Y. A.*** *Elements of applied bifurcation theory. New York : Applied Mathematical Sciences, Springer, 1998. 2.*

[32] ***A. H. Nayfeh, B. Balachandran.*** *Applied Nonlinear Dynamics. s.l. : Wiley Series in nonlinear science, J.Wiley & Sons, 1995. 1.*

[33] ***Doedel, E. J.*** *Lecture Notes on Numerical Analysis of Nonlinear Equations. Montreal, Canada : Department of Computer Science.*

[34] ***Boyaci, A.*** *Analytical bifurcation Analysis of a rotor supported by floating bearings. Nonlinear Dunamics. 57, 497-507.*

[35] ***A. Boyaci, D. Lu, B. Schweizer.*** *Stability and bifurcation phenomena of Laval/Jeffcott rotors in semi-floating ring bearings. Nonlinear Dynamics. 2015, pp. 1535-1561.*

[36] ***Breemen, F. C. Van.*** *Stability analysis of a laval rotor on hydrodynamic bearings by numerical continuation: Investigating the influence of rotor flexibility, rotor damping and external rotor oil pressure on the rotordynamic behavior. M.Sc Thesis, Delft University of Technology. 2016.*

[37] ***Rubel, J.*** *Vibrations in nonlinear rotordynamics, Ph.D. Thesis. Heidelberg : Ruprecht-Karls-Universitat, 2009.*

[38] ***A. Amanou, M. Couchane.*** *Bifurcation of limit cycles in fluid film bearings. International Journal of Non-Linear Mechanics. 2011, pp. 1258-1264.*

[39] ***R. Sghir, M. Couchane.*** *Prediction of the nonlinear hysterisis loop for fluid-film bearings by numerical continuation. Proc. IMechE Part C: Mechanical Engineering Science . 2015, pp. 651-662.*

[40] ***R. Sghir, M. Couchane.*** *Non-linear stability analysis of a flexible rotor-bearing system by numerical continuation. Journal of Vibration and Control. 2016, pp. 3079-3089.*

[41] ***Becker, K.*** *Dynamisches Verhalten hydrodynamisch gelagerter Rotoren unter berucksichtigung veranderlicher Lagergeometrien, Ph.D Thesis. Karlsruhe : Karlsruhe Institute of Technology, 2019.*

2. MODELING AND FORMULATION OF THE ROTOR DYNAMIC SYSTEM

In this chapter, the methods used to formulate the rotor model are presented. The main objective of this chapter is to give the reader a brief overview of the linear and non-linear approach to the elastoaerodynamic lubrication problem, the parametric excitation implementation, the finite element method and the element order reduction method for modeling rotors. Where deemed necessary, references to the existing literature and appendices are incorporated.

2.1 Elastoaerodynamic lubrication problem, non-linear approach

Figure 2.1.1 shows the simplistic configuration of a bump type GFB mainly utilized in current work. Journals' and bearings' rotational axes are considered parallel and their geometrical centers are denoted by $O_j\left(x_j, y_j\right)$ and $O_b\left(x_b, y_b\right)$ respectively. Coordinate θ is measured from the horizontal positive semi-axis of the bearing and therefore the circumferential spatial coordinate is denoted by $x = R\cdot\theta$ and the axial spatial coordinate is denoted by z. The pressure distribution $p = p\left(x, z, t\right)$ is a function of time since the flow in the gap between the journal and the top foil is considered compressible and the analysis being held is transient. In addition, due to the very small film height in the radial direction compared to the circumferential and axial dimensions of the film, a dependency of the pressure on a height coordinate is typically not taken into account. The top foil deformation $q = q\left(\theta, t\right)$ is not a function of the axial spatial coordinate since the coupling of the structural and the fluid equation considers a mean gas pressure among the aforementioned coordinate. The last deformation is considered positive when it is developed towards the outer side of the bearing. In this project, the foil's starting and ending angle is denoted by χ, thus by definition $q\left(\theta = \chi, t\right) = 0$.

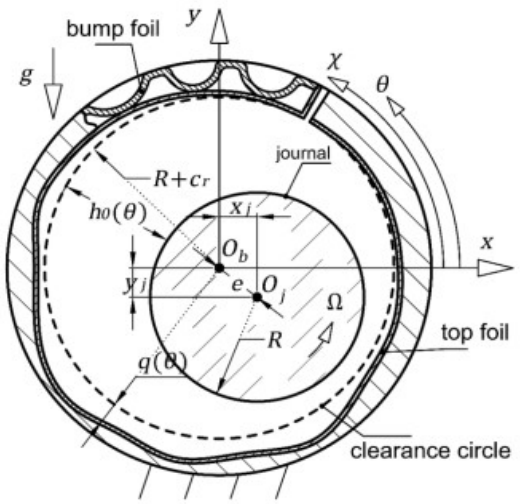

Figure 2.1.1 *Representation of a G.F.B. cross section, key geometry and operating parameters*

Eventually, since the maximum eccentricity is typically small compared to geometrical parameters of the bearing ($e_{\max} \ll R, R_j$) the film thickness can be written as:

$$h = h\left(\theta, t\right) = c_r - x_j\cos\theta - y_j\sin\theta + q \tag{2.1.1}$$

The necessary assumptions of the lubrication problem are quite common: Isothermal gas film described by ideal gas law ($\frac{p}{\rho} = ct$), laminar, continuum flow under no-slip boundary conditions, negligible fluid inertia, entrance/exit effects and curvature ($R \simeq R + c_r$). Under these assumptions, the Navier-Stokes equations and the continuity equation can be simplified to the Reynolds equation for compressible fluids and unsteady motions of the journal:

$$\frac{\partial}{\partial x}\left(\frac{ph^3}{\mu}\frac{\partial p}{\partial x}\right)+\frac{\partial}{\partial z}\left(\frac{ph^3}{\mu}\frac{\partial p}{\partial z}\right)-6\Omega R\frac{\partial}{\partial x}(ph)-12\frac{\partial}{\partial t}(ph)=0 \qquad (2.1.2)$$

on the domain $\Omega_{2D}=\left\{(x,z)\,|\,\chi R \le x \le \chi R + 2\pi R, 0 \le z \le \frac{L_b}{2}\right\}$, whereas the viscosity μ is considered to be constant in space as well as in time. The boundary conditions for the pressure distribution are:

$$p\left(x, z=\frac{L_b}{2}, t\right)=p_0,\ \frac{\partial p(x, z=0, t)}{\partial z}=0 \qquad (2.1.3)$$

$$p(x=\chi R, z, t)=p_0,\ \ p(x=\chi R+2\pi R, z, t)=p_0 \qquad (2.1.4)$$

, and are accompanied by the corresponding initial condition:

$$p(x, z, t=0)=p_0 \qquad (2.1.5)$$

It is quite common in G.F.B.s for sub-ambient pressures to arise. These sub-ambient pressures can cause the top foil to separate from the bump into positions where the pressure on both sides of the pads is equalized. Heshmat et al[42], introduced a set of boundary conditions meaning that sub-ambient pressures are discarded when integrating pressure in order to obtain the bearing forces. This assumption, in terms of numerical calculations can be simply expressed as follows: In case fluid pressure p is lower than the ambient pressure p_0, then the former should be considered equal to p_0 and the foil's deformation at these areas should be considered zero. The last two boundary conditions recognize that the flow is continuous in the circumferential direction and gas does not enter or leave the lubricant film, even if sub-ambient pressures are occurred. Finally, the reduced domain Ω_{2D} and the first boundary condition is due to the assumption of the symmetry of the problem.

The simplified model for the bump structure is depicted in *Figure 2.1.2*. Since a thin and extendable material is used for the foil's surface, the membrane and bending effects are negligible compared with the elastic foundation effects. Therefore, the structure consists of linear, massless elements with one finite dimension in the radial direction and no coupling of the elements in the circumferential direction. These elements are of stiffness k_f and damping c_f and mount the corresponding top foil stripes of area $\Delta x \cdot L_b$. For computational reasons, it should be noted that the top foil is not covering a full cylinder. Instead, a single gap can be found at $x = \chi R$ where foil is clamped to the bearing housing. These top foil stripes are assumed to remain parallel to the bearing surface during their motion, so no axial coordinate is required for their description.

[42] ***H. Heshmat, J. A. Walowit, O. Pinkus.*** *Analysis of gas-lubricated foil journal bearings. Journal of Lubrication Technology. 1983.*

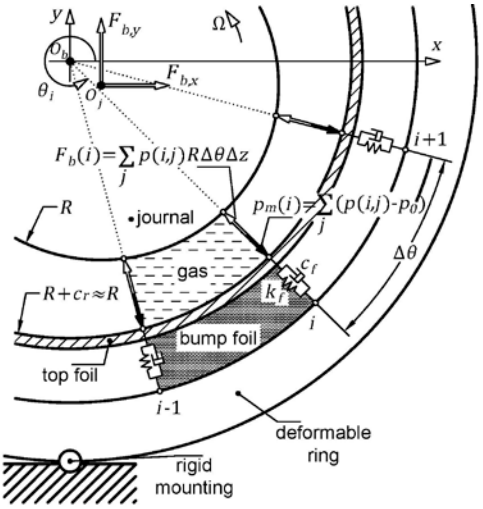

Figure 2.1.2 *Model of gas pressures and forces acting on the rotating journal and the compliant foil structure*

The proposed relationship between the applied pressure and the deflection of each top foil stripe is given by:

$$p_m = c_f \dot{q} + k_f q \tag{2.1.6}$$

Whereas:

$$p_m(\theta,t) = p_m = \frac{2}{L_b}\int_0^{L_b/2}(p - p_0)\,dz \tag{2.1.7}$$

The necessary initial condition for the foil deflection is:

$$q(\theta, t=0) = q_0 \tag{2.1.8}$$

It is of great importance to note that in terms of (2.1.8) if sub-ambient pressure is occurred then this pressure is discarded, as explained in the previous paragraph. Additionally, the multiplication is due to the assumption of the symmetry of the pressure distribution in the axial direction.

In general, solving the dimensional form of the problem is computationally inefficient. Obviously, the pressure distribution and the top foil deflection will be both parts of the state vector of the non-linear equations of motion. As clearly stated in 1.3, there is a necessity of analytically computed Jacobian matrix, but if numerically computed Jacobian matrix is provided, then it should be very accurate. It is beyond any doubt, that carrying dimensional pressures and foil deformations in the same state vector makes this computation quite difficult. Thus, the non-dimensional form of the problem is preferred. The following transformations (of the independent and dependent variables respectively) take place in order to define the dimensionless form:

$$\overline{x} = \frac{x}{R}, \overline{z} = \frac{z}{L_b}, \tau = \frac{p_0 {c_r}^2}{6\mu R^2}t = \Lambda t \tag{2.1.9}$$

$$\overline{p} = \frac{p}{p_0}, \overline{\Omega} = \frac{\Omega}{\Lambda}, \overline{h} = \frac{h}{c_r}, \overline{q} = \frac{q}{c_r}, \overline{x}_j = \frac{x_j}{c_r}, \overline{y}_j = \frac{y_j}{c_r} \tag{2.1.10}$$

Substituting (2.1.9) and (2.1.10) in (2.1.1) - (2.1.8) results in the non-dimensional Reynolds equation:

$$\frac{\partial}{\partial \bar{x}}\left(\bar{p}\bar{h}^3\frac{\partial \bar{p}}{\partial \bar{x}}\right)+\frac{R}{L_b}\frac{\partial}{\partial \bar{z}}\left(\bar{p}\bar{h}^3\frac{\partial \bar{p}}{\partial \bar{z}}\right)-\bar{\Omega}\frac{\partial}{\partial \bar{x}}\left(\bar{p}\bar{h}\right)-2\frac{\partial}{\partial \tau}\left(\bar{p}\bar{h}\right)=0 \quad (2.1.11)$$

on the domain $\Omega_{2D'}=\left\{(\bar{x},\bar{z})\,|\,\chi\le\bar{x}\le\chi+2\pi,0\le\bar{z}\le\frac{1}{2}\right\}$

, and the non-dimensional structural equations:

$$\bar{p}_m=\bar{c}_f\dot{\bar{q}}+\bar{k}_f\bar{q} \quad (2.1.12)$$

, whereas:

$$\bar{p}_m=2\int_0^{1/2}\left(\bar{p}-1\right)d\bar{z} \quad (2.1.13)$$

, while the non-dimensional film thickness is defined by:

$$\bar{h}=1-\bar{x}_j\cos\theta-\bar{y}_j\sin\theta+\bar{q} \quad (2.1.14)$$

Boundary and initial conditions in non-dimensional form can be expressed as:

$$\bar{p}\left(\bar{x},\bar{z}=\frac{1}{2},\tau\right)=1,\ \frac{\partial\bar{p}\left(\bar{x},\bar{z}=0,\tau\right)}{\partial\bar{z}}=0 \quad (2.1.15)$$

$$\bar{p}\left(\bar{x}=\chi,\bar{z},\tau\right)=1,\ \bar{p}\left(\bar{x}=\chi+2\pi,\bar{z},\tau\right)=1 \quad (2.1.16)$$

$$\bar{p}\left(\bar{x},\bar{z},\tau=0\right)=1,\ \bar{q}\left(\bar{x},\bar{z},\tau=0\right)=\bar{q}_{0,} \quad (2.1.17)$$

In order to couple the fluid-structural model of the G.F.B. to the rotor model, the bearing forces are essential. Once the fluid pressure is evaluated, the non-dimensional bearing forces can be expressed as:

$$\bar{F}_{b_x}=-2\int_{\chi}^{\chi+2\pi}\int_0^{1/2}\left(\bar{p}-1\right)\cos\bar{x}d\bar{x}d\bar{z} \quad (2.1.18)$$

$$\bar{F}_{b_Y}=-2\int_{\chi}^{\chi+2\pi}\int_0^{1/2}\left(\bar{p}-1\right)\sin\bar{x}d\bar{x}d\bar{z} \quad (2.1.19)$$

Analytical solutions of (2.1.11) can't be found, so a Finite Difference Method (F.D.M.) is applied in order to evaluate an approximation of the pressure distribution. According to this method, second order derivatives with respect to the dimensionless spatial coordinates are approximated by central differences:

$$\frac{\partial^2\bar{p}}{\partial\bar{x}^2}\approx\frac{\bar{p}_{i+1,j}-2\bar{p}_{i,j}+\bar{p}_{i-1,j}}{\Delta\bar{x}^2},\frac{\partial^2\bar{p}}{\partial\bar{z}^2}\approx\frac{\bar{p}_{i,j+1}-2\bar{p}_{i,j}+\bar{p}_{i,j-1}}{\Delta\bar{z}^2} \quad (2.1.20)$$

, and first order derivatives with respect to the same spatial derivatives are approximated by backward differences:

$$\frac{\partial\bar{p}}{\partial\bar{x}}\approx\frac{\bar{p}_{i,j}-\bar{p}_{i-1,j}}{\Delta\bar{x}},\frac{\partial\bar{p}}{\partial\bar{z}}\approx\frac{\bar{p}_{i,j}-\bar{p}_{i,j-1}}{\Delta\bar{z}} \quad (2.1.21)$$

In general, F.D.M. includes truncation error. Thus, approximating first order derivatives by backward differences might be less accurate than approximating them by central differences. Our decision though, enhances numerical stability of the method. Given the fact that the G.F.B.s will be parametrically excited, our primal goal is to ensure the stability of the numerical method, even if accuracy might be sacrificed. The domain $\Omega_{2D'}$ is divided into a

grid of $i=1,...,N_{\bar{x}}+1,\ j=1,...,N_{\bar{z}}+1$ mesh points $\bar{p}_{i,j}$. By applying the discretization formulas (2.1.20) and (2.1.21) the Partial Differential Equation (P.D.E.) (2.1.11) is converted into $(N_{\bar{x}}+1)\cdot(N_{\bar{z}}+1)$ coupled first order O.D.E.s with respect to τ. This set of equations can be solved explicitly for time derivatives $\dot{\bar{p}}_{i,j}$. Additionally, after solving (2.1.12) for the time derivatives of the top foil deflection $\dot{\bar{q}}_i$ and introducing a state space vector:

$$\begin{aligned}&\bar{\mathbf{x}}_s=\left[\,\bar{p}_{1,1},...,\bar{p}_{N\bar{x}-1,N\bar{z}-1},\bar{q}_1,...,\bar{q}_{Nx+1},\bar{\mathbf{x}}_{m,r}\,\right]^T\\&,\bar{\mathbf{x}}_s\in\mathbb{R}^{(N\bar{x}-1)\cdot(N\bar{z}-1)+(N\bar{x}+Nm+1)}\end{aligned}\tag{2.1.22}$$

, whereas $\bar{\mathbf{x}}_{m,r}\in\mathbb{R}^{Nm}$ is the dimensionless state vector of the reduced discretized rotor model, which includes journal's displacements $\bar{x}_j,\bar{y}_j$ the discretized overall bearing rotor model can be written as non-linear system of first order O.D.E.s:

$$\begin{aligned}&\dot{\bar{\mathbf{x}}}_s=f\left(\bar{x}_s\right),\mathbf{f}:\mathbb{R}^{(N\bar{x}-1)*(N\bar{z}-1)+(N\bar{x}+Nm+1)}\rightarrow\mathbb{R}^{(N\bar{x}-1)*(N\bar{z}-1)+(N\bar{x}+Nm+1)}\\&,\bar{\mathbf{x}}_s(\bar{x},\bar{z},t=0)=\bar{\mathbf{x}}_{s,0}\end{aligned}\tag{2.1.23}$$

Solving the aforementioned non-linear system might be very expensive in terms of computational costs. This motivates the usage of a model order reduction method. In this Master Thesis, the Galerkin's method, firstly proposed by C. Baum et al[43] is used. This method can be categorized within the theory of weighted residuals and assumes that the pressure distribution can be approximated by the product:

$$\bar{p}\left(\bar{x},\bar{z},\tau\right)\approx\bar{p}_a\left(\bar{x},\bar{z},\tau\right)+1=\hat{p}_a\left(\bar{x},\tau\right)\cdot\tilde{p}_a\left(\bar{z}\right)+1\tag{2.1.24}$$

A non-linear differential operator is introduced:

$$D\{\bar{p}\}=\frac{\partial}{\partial\bar{x}}\left(\bar{p}\bar{h}^3\frac{\partial\bar{p}}{\partial\bar{x}}\right)+\frac{R}{L_b}\frac{\partial}{\partial\bar{z}}\left(\bar{p}\bar{h}^3\frac{\partial\bar{p}}{\partial\bar{z}}\right)-\bar{\Omega}\frac{\partial}{\partial\bar{x}}\left(\bar{p}\bar{h}\right)-2\frac{\partial}{\partial\tau}\left(\bar{p}\bar{h}\right)\tag{2.1.25}$$

, so potentially the Reynolds equation (2.1.11) leads to:

$$D\{\bar{p}\}=0,D\{\bar{p}_a\}=r_a\tag{2.1.26}$$

Since $\tilde{p}_a\left(\bar{z}\right)$ is treated as a base function and the Galerkin's method is implied, the so-called error orthogonality equation is introduced too:

$$\int_0^{1/2}\tilde{p}_a\cdot r_a\cdot d\bar{z}=\int_0^{1/2}\tilde{p}_a\cdot D\{\bar{p}_a\}\cdot d\bar{z}=0\tag{2.1.27}$$

Evaluating (2.1.27) will eliminate the dependency of non-dimensional axial direction. Hence, the domain $\Omega_{2D'}$ reduces to $\Omega_{2D'_r}=\{\bar{x}\mid\chi\le\bar{x}\le\chi+2\pi\}$ and the state vector $\bar{x}_s$ reduces to:

[43] ***C. Baum, H. Hetzler, S. Schroders, T. Leister, W. Seemann.*** *A Computationally Efficient Nonlinear Foil Air Bearing Model for Fully Coupled Transient Rotor Dynamic Investigations. Tribology International. 2020.*

$$\begin{aligned}&\overline{\mathbf{x}}_{s_r} = \left[\, \overline{p}_1, \ldots, \overline{p}_{N\overline{x}-1}, \overline{q}_1, \ldots, \overline{q}_{Nx+1}, \overline{\mathbf{x}}_{m,r} \,\right]^T \\ &, \overline{\mathbf{x}}_{s_r} \in \mathbb{R}^{2\cdot N\overline{x}+Nm}\end{aligned} \tag{2.1.28}$$

Accordingly, the non-linear system of first order O.D.E.s (2.1.23) is reduced as well to:

$$\begin{aligned}&\dot{\overline{\mathbf{x}}}_{s_r} = f\left(\overline{x}_{s_r}\right), \mathbf{f} : \mathbb{R}^{2\cdot N\overline{x}+Nm} \rightarrow \mathbb{R}^{2\cdot N\overline{x}+Nm} \\ &, \overline{\mathbf{x}}_{s_r}(\overline{x}, \overline{z}, t=0) = \overline{\mathbf{x}}_{s_r,0}\end{aligned} \tag{2.1.29}$$

However, as far as the base function $\tilde{p}_a\left(\overline{z}\right)$ is not determined, the reduction method can't be finalized. C. Baum et al[44] had been motivated by the short bearing theory for journal bearings in order to choose the proper base function. In the current work, the same generalized shape function has been introduced.

$$\begin{aligned}&\tilde{p}_a\left(\overline{z}\right) = \left(1-w_a\right)\cdot\left(1-2\overline{z}^{2i_a}\right) + w_a\cdot\left(1-2\overline{z}^{2i_a+2}\right) \\ &i_a = floor\left(m_a\right), w_a = m_a - i_a \\ &m_a \geq 1, m_a \in \mathbb{R}\end{aligned} \tag{2.1.30}$$

It is more than obvious that an optimal parameter m_a should be identified. This can be achieved by introducing an error function which includes the difference between the pressure field of the full domain model and the pressure field of the reduced one. The optimal parameter minimizes the aforementioned error function. But it is proven that m_a presents significant discrepancies depending on the journal states, the rotating speed and the foil properties. Thus the introduction of the error function is rather inefficient, especially if the reduction method is integrated in a limit cycle continuation method. In this Master Thesis a fixed value for the parameter m_a is chosen.

[44] ***C. Baum, H. Hetzler, S. Schroders, T. Leister, W. Seemann.*** *A Computationally Efficient Nonlinear Foil Air Bearing Model for Fully Coupled Transient Rotor Dynamic Investigations. Tribology International. 2020.*

2.2 Elastoaerodynamic lubrication problem, linear approach

The main purpose of the linear approach is to evaluate the stiffness and damping coefficients of a bump type G.F.B utilizing a perturbation method. *Figure 2.2.1* depicts the new coordinate system and the sign convention of the journal's forces. The assumptions about the lubrication problem are the same as mentioned in 2.1 but the variables (dependent and independent) in the governing equations are normalized slightly differently.

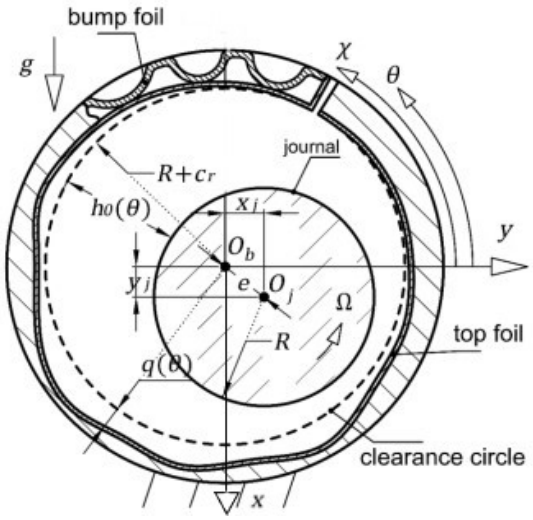

Figure 2.2.1 *The coordinate system and the sign convention according to the linear approach*

More specifically:

$$\overline{z} = \frac{z}{L_b}, \tau = \nu t \tag{2.2.1}$$

$$\overline{p} = \frac{p}{p_0}, \overline{h} = \frac{h}{c_r}, \overline{q} = \frac{q}{c_r} \tag{2.2.2}$$

It can easily be observed that the dimensionless time variable depends on the whirl frequency ν , the rate at which the journal will orbit about the equilibrium position in the perturbation analysis. For simplification purposes, synchronous whirling is assumed thus whirl frequency is by definition equal to the rotating speed of the journal. In addition, the symmetry of the lubrication problem is not taken into account. In terms of the structural model proposed in 2.1only one assumption is differentiated. The top foil stripes are not assumed to remain parallel to the bearing surface during their motion. Therefore the axial coordinate is essential for their description. Under these principles, the non-dimensional Reynolds equation is rewritten:

$$-\frac{\partial}{\partial\theta}\left(\overline{p}\overline{h}^3\frac{\partial\overline{p}}{\partial\theta}\right)-\frac{R}{L_b}\frac{\partial}{\partial\overline{z}}\left(\overline{p}\overline{h}^3\frac{\partial\overline{p}}{\partial\overline{z}}\right)+\Lambda'\frac{\partial}{\partial\theta}\left(\overline{p}\overline{h}\right)+2\Lambda'\gamma\frac{\partial}{\partial\tau}\left(\overline{p}\overline{h}\right)=0 \tag{2.2.3},$$

whereas:

$$\Lambda' = \frac{6\mu R^2\Omega}{p_0 c_r^{\,2}}, \gamma = \frac{\nu}{\Omega} \tag{2.2.4}$$

,on the domain $\Omega_{2D"}=\left\{(\theta,\bar{z})\,|\,\chi\le\vartheta\le\chi+2\pi,-\frac{1}{2}\le\bar{z}\le\frac{1}{2}\right\}$ and with the respective boundary conditions:

$$\bar{p}\left(\theta,\bar{z}=\frac{1}{2},\tau\right)=1,\bar{p}\left(\theta,\bar{z}=-\frac{1}{2},\tau\right)=1 \tag{2.2.5}$$

$$\bar{p}\left(\theta=\chi,\bar{z},\tau\right)=1,\bar{p}\left(\theta=\chi+2\pi,\bar{z},\tau\right)=1 \tag{2.2.6}$$

Similarly, the non-dimensional structural equation is rewritten:

$$\bar{p}=\bar{k}_f\bar{q}+\bar{c}_f{}'\gamma\frac{d\bar{q}}{d\tau} \tag{2.2.7}$$

, whereas:

$$\bar{k}_f=\frac{k_f c_r}{p_0},\bar{c}_f{}'=\Omega\frac{c_f c_r}{p_0} \tag{2.2.8}$$

It is of great importance to note that initial conditions are not necessary to be given, since a perturbation method will be implied. In addition, the boundary condition for the foil deformation which is introduced in [45] is neglected due to our desire to compare the linear approach to the non-linear one.

The modified perturbation method can now be explained. Suppose that the perturbed motion of the journal about an equilibrium position (subscript '0' indicates a quantity in this equilibrium position) is a circular orbit, the normalized perturbations (small displacements and small velocities among the axes illustrated in Figure 2.2.1) are given by:

$$\begin{aligned}\Delta\bar{X}(\tau)&=\frac{\Delta X(\tau)}{c_r}=\left|\Delta\bar{X}\right|e^{i\tau}\\ \Delta\bar{Y}(\tau)&=\frac{\Delta Y(\tau)}{c_r}=\left|\Delta\bar{Y}\right|e^{i\tau}\end{aligned} \tag{2.2.9}$$

$$\begin{aligned}\Delta\dot{\bar{X}}(\tau)&=\frac{d\Delta\bar{X}(\tau)}{d\tau}=i\Delta\bar{X}\\ \Delta\dot{\bar{Y}}(\tau)&=\frac{d\Delta\bar{Y}(\tau)}{d\tau}=i\Delta\bar{Y}\end{aligned} \tag{2.2.10}$$

$$\begin{aligned}\Delta\ddot{\bar{X}}(\tau)&=\frac{d\Delta\dot{\bar{X}}(\tau)}{d\tau}=-\Delta\bar{X}\\ \Delta\ddot{\bar{Y}}(\tau)&=\frac{d\Delta\dot{\bar{Y}}(\tau)}{d\tau}=-\Delta\bar{Y}\end{aligned} \tag{2.2.11}$$

Then, the pressure distribution, the foil deformation and the film thickness can be expressed in Taylor series in terms of the normalized perturbations around an equilibrium position of the journal:

[45] ***J. P. Peng, M. Carpino.*** *Calculation of stiffness and damping coefficients for elastically supported gas foil bearings. Journal of Tribology. 115, pp. 20-27.*

$$\begin{aligned}\overline{p} &= \overline{p}_0 + \overline{p}_{\overline{X}}\Delta\overline{\mathrm{X}} + \overline{p}_{\overline{\mathrm{Y}}}\Delta\overline{\mathrm{Y}} + \overline{p}_{\dot{\overline{X}}}\Delta\dot{\overline{\mathrm{X}}} + \overline{p}_{\dot{\overline{\mathrm{Y}}}}\Delta\dot{\overline{\mathrm{Y}}} \\ \overline{h} &= \overline{h}_0 + \overline{h}_{\overline{X}}\Delta\overline{\mathrm{X}} + \overline{h}_{\overline{\mathrm{Y}}}\Delta\overline{\mathrm{Y}} + \overline{h}_{\dot{\overline{X}}}\Delta\dot{\overline{\mathrm{X}}} + \overline{h}_{\dot{\overline{\mathrm{Y}}}}\Delta\dot{\overline{\mathrm{Y}}} \\ \overline{q} &= \overline{q}_0 + \overline{q}_{\overline{X}}\Delta\overline{\mathrm{X}} + \overline{q}_{\overline{\mathrm{Y}}}\Delta\overline{\mathrm{Y}} + \overline{q}_{\dot{\overline{X}}}\Delta\dot{\overline{\mathrm{X}}} + \overline{q}_{\dot{\overline{\mathrm{Y}}}}\Delta\dot{\overline{\mathrm{Y}}}\end{aligned} \tag{2.2.12}$$

The relationships between the partial derivatives of the film thickness and the foil deformations are given by:

$$\begin{aligned}\overline{h}_{\overline{X}} &= \overline{q}_{\overline{X}} + \sin\theta,\ \overline{h}_{\dot{\overline{X}}} = \overline{q}_{\dot{\overline{X}}} \\ \overline{h}_{\overline{\mathrm{Y}}} &= \overline{q}_{\overline{\mathrm{Y}}} - \cos\theta,\ \overline{h}_{\dot{\overline{\mathrm{Y}}}} = \overline{q}_{\dot{\overline{\mathrm{Y}}}}\end{aligned} \tag{2.2.13}$$

Once the partial derivatives of the pressure distribution are found, the stiffness and damping coefficients are calculated by properly integrating over the bearing's surface. These partial derivatives are now found as follows. Equations (2.2.9) - (2.2.13) are substituted in (2.2.3) - (2.2.8). Terms with the same coefficients $(\Delta\overline{\mathrm{X}}, \Delta\overline{\mathrm{Y}}, \Delta\dot{\overline{\mathrm{X}}}, \Delta\dot{\overline{\mathrm{Y}}})$ are collected yielding to the following equations about the equilibrium position of the journal:

$$-\frac{R}{L_b}\frac{\partial}{\partial\overline{z}}\left(\overline{p}_0\overline{h}_0^{\,3}\frac{\partial\overline{p}_0}{\partial\overline{z}}\right) - \frac{\partial}{\partial\theta}\left(\overline{p}_0\overline{h}_0^{\,3}\frac{\partial\overline{p}_0}{\partial\theta}\right) + \Lambda'\frac{\partial}{\partial\theta}\left(\overline{p}_0\overline{h}_0\right) = 0 \tag{2.2.14}$$

$$(\overline{p}_0 - 1) - \overline{k}_f\left[\overline{h}_0 - 1 - \varepsilon\sin\left(\theta - \theta_0\right)\right] = 0 \tag{2.2.15}$$

, on the domain $\Omega_{2D"}$ in respect to the boundary conditions:

$$\overline{p}_0\left(\theta, \overline{z} = 1/2\right) = 1,\ \overline{p}_0\left(\theta, \overline{z} = -1/2\right) = 1 \tag{2.2.16}$$

$$\overline{p}_0\left(\theta = \chi, \overline{z}\right) = 1,\ \overline{p}_0\left(\theta = \chi + 2\pi, \overline{z} = -1/2\right) = 1 \tag{2.2.17}$$

In equations (2.2.14) , (2.2.15) the unknowns are the dimensionless pressure distribution $\overline{p}_0$, the corresponding dimensionless film thickness $\overline{h}_0$ the eccentricity ε and finally the altitude angle θ_0 . Therefore two more equations are incorporated:

$$-\int_{-1/2}^{1/2}\int_{\chi}^{\chi+2\pi}\overline{p}_0\sin\theta R d\theta d\overline{z} = \overline{W}_{st} \tag{2.2.18}$$

$$\int_{-1/2}^{1/2}\int_{\chi}^{\chi+2\pi}\overline{p}_0\cos\theta R d\theta d\overline{z} = 0 \tag{2.2.19}$$

The dimensionless static load $\overline{W}_{st}$ can easily be evaluated from the static analysis of the rotor-bearing model which will be discussed in section 2.4 . It should be clarified that the term $\left(\overline{p}_0 - 1\right)$ in equation (2.2.15) is artificially introduced and the reason lies between the assumptions of Heshmat et al [46] and R. Dhakad et al[47]. Analytical solution of (2.2.14) can't be

[46] ***H. Heshmat, J. A. Walowit, O. Pinkus.*** *Analysis of gas-lubricated foil journal bearings. Journal of Lubrication Technology. 1983.*

found so a Finite Difference Method (F.D.M.) is again applied to evaluate an approximation of the pressure field $\overline{p}_0$. By applying the discretization formulas thoroughly described in 2.1 the Partial Differential Equation (P.D.E.) (2.2.14) is converted into a system of non-linear algebraic equations $\left(i = 2,..., N_{\overline{x}},\ j = 2,..., N_{\overline{z}}\right)$:

$$\begin{aligned} &A_1 \overline{p}_{0_{i,j}}^2 + A_2 \overline{p}_{0_{i,j}} + A_3 = 0 \\ &A_1 = f_1\left(\overline{p}_{0_{i+1,j}}, \overline{p}_{0_{i-1,j}}, \overline{h}_{0_{i+1,j}}, \overline{h}_{0_{i-1,j}}\right) \\ &A_2 = f_2\left(\overline{p}_{0_{i+1,j}}, \overline{p}_{0_{i-1,j}}, \overline{h}_{0_{i+1,j}}, \overline{h}_{0_{i-1,j}}\right) \\ &A_3 = f_3\left(\overline{p}_{0_{i+1,j}}, \overline{p}_{0_{i-1,j}}, \overline{h}_{0_{i+1,j}}, \overline{h}_{0_{i-1,j}}\right) \end{aligned} \tag{2.2.20}$$

, coupled to $\left(i = 1,..., N_{\overline{x}} + 1,\ j = 1,..., N_{\overline{z}} + 1\right)$:

$$\left(\overline{p}_{0_{i,j}} - 1\right) - \overline{k}_f \left[\overline{h}_{0_{i,j}} - 1 - \varepsilon \sin\left(\theta_i - \theta_0\right)\right] = 0 \tag{2.2.21}$$

$$\sum_i \sum_j s_{1_{i,j}} \overline{p}_{0_{i,j}} = \overline{W}_{st} \tag{2.2.22}$$

$$\sum_i \sum_j s_{2_{i,j}} \overline{p}_{0_{i,j}} = 0 \tag{2.2.23}$$

, with the respective boundary conditions:

$$\overline{p}_{0_{i,j=1}} = 1,\ \overline{p}_{0_{i,j=N_{\overline{z}}+1}} = 1 \tag{2.2.24}$$

$$\overline{p}_{0_{i=1,j}} = 1,\ \overline{p}_{0_{i=N_{\overline{x}}+1,j}} = 1 \tag{2.2.25}$$

, whereas $s_{1_{i,j}}, s_{2_{i,j}}$ are both constants arising from the Simpson's 1/3 law, which is applied to numerically evaluate the integrals in (2.2.18) - (2.2.19). The non-linear system of algebraic equations (2.2.20) - (2.2.23) may now be solved by means of standard iterative solvers under the constraint $\overline{p}_{0_{i,j}} \geq 1$.

It is now more than obvious that the artificial term $\left(\overline{p}_0 - 1\right)$ is introduced in order to ensure that $\overline{q}_{0_{i,j}} \geq 0$ (the equality is applied when sub-ambient pressure is occurred). In addition, it ensures that correct boundary conditions for the top foil deformations are taken into consideration.

After determining pressure distribution and gas film thickness at the equilibrium position of the journal, their partial derivatives can be evaluated solving the following equations (always on the domain $\Omega_{2D"}$):

---

[47] ***R. Dhakad, B. K. Pradhan, J. Kumar, S. Behera.*** *Prediction of Stiffness and Damping of Gas Foil Journal Bearing for High Speed Rotor. TRIBOINDIA. December 2018.*

$$-\left(\frac{R}{L_b}\right)\frac{\partial}{\partial\bar{z}}\left(\bar{p}_0\bar{h}_0^{\,3}\frac{\partial\bar{p}_{\bar{x}}}{\partial\bar{z}}+\bar{p}_{\bar{x}}\bar{h}_0^{\,3}\frac{\partial\bar{p}_0}{\partial\bar{z}}+3\bar{p}_0\bar{h}_0^{\,2}\bar{h}_{\bar{x}}\frac{\partial\bar{p}_0}{\partial\bar{z}}\right)-\frac{\partial}{\partial\vartheta}\left(\bar{p}_0\bar{h}_0^{\,3}\frac{\partial\bar{p}_{\bar{x}}}{\partial\theta}+\bar{p}_{\bar{x}}\bar{h}_0^{\,3}\frac{\partial\bar{p}_0}{\partial\theta}+3\bar{p}_0\bar{h}_0^{\,2}\bar{h}_{\bar{x}}\frac{\partial\bar{p}_0}{\partial\theta}\right)$$
$$+\Lambda'\left(\bar{p}_{\bar{x}}\bar{h}_0+\bar{p}_0\bar{h}_{\bar{x}}\right)-2\Lambda'\gamma\left(\bar{p}_{\bar{x}}\bar{h}_0+\bar{p}_0\bar{h}_{\bar{x}}\right)=0 \tag{2.2.26}$$

$$\bar{p}_{\bar{x}}-\bar{k}_f\bar{h}_{\bar{x}}+\gamma\bar{c}_f{}'\bar{h}_{\bar{x}}+\bar{k}_f\sin\theta=0 \tag{2.2.27}$$

$$-\left(\frac{R}{L_b}\right)\frac{\partial}{\partial\bar{z}}\left(\bar{p}_0\bar{h}_0^{\,3}\frac{\partial\bar{p}_{\bar{x}}}{\partial\bar{z}}+\bar{p}_{\bar{x}}\bar{h}_0^{\,3}\frac{\partial\bar{p}_0}{\partial\bar{z}}+3\bar{p}_0\bar{h}_0^{\,2}\bar{h}_{\bar{x}}\frac{\partial\bar{p}_0}{\partial\bar{z}}\right)-\frac{\partial}{\partial\vartheta}\left(\bar{p}_0\bar{h}_0^{\,3}\frac{\partial\bar{p}_{\bar{x}}}{\partial\theta}+\bar{p}_{\bar{x}}\bar{h}_0^{\,3}\frac{\partial\bar{p}_0}{\partial\theta}+3\bar{p}_0\bar{h}_0^{\,2}\bar{h}_{\bar{x}}\frac{\partial\bar{p}_0}{\partial\theta}\right)$$
$$+\Lambda'\left(\bar{p}_{\bar{x}}\bar{h}_0+\bar{p}_0\bar{h}_{\bar{x}}\right)+2\Lambda'\gamma\left(\bar{p}_{\bar{x}}\bar{h}_0+\bar{p}_0\bar{h}_{\bar{x}}\right)=0 \tag{2.2.28}$$

$$\bar{p}_{\bar{x}}-\bar{k}_f\bar{h}_{\bar{x}}-\gamma\bar{c}_f{}'\bar{h}_{\bar{x}}+\gamma\bar{c}_f{}'\sin\theta=0 \tag{2.2.29}$$

$$-\left(\frac{R}{L_b}\right)\frac{\partial}{\partial\bar{z}}\left(\bar{p}_0\bar{h}_0^{\,3}\frac{\partial\bar{p}_{\bar{y}}}{\partial\bar{z}}+\bar{p}_{\bar{y}}\bar{h}_0^{\,3}\frac{\partial\bar{p}_0}{\partial\bar{z}}+3\bar{p}_0\bar{h}_0^{\,2}\bar{h}_{\bar{y}}\frac{\partial\bar{p}_0}{\partial\bar{z}}\right)-\frac{\partial}{\partial\vartheta}\left(\bar{p}_0\bar{h}_0^{\,3}\frac{\partial\bar{p}_{\bar{y}}}{\partial\theta}+\bar{p}_{\bar{y}}\bar{h}_0^{\,3}\frac{\partial\bar{p}_0}{\partial\theta}+3\bar{p}_0\bar{h}_0^{\,2}\bar{h}_{\bar{y}}\frac{\partial\bar{p}_0}{\partial\theta}\right)$$
$$+\Lambda'\left(\bar{p}_{\bar{y}}\bar{h}_0+\bar{p}_0\bar{h}_{\bar{y}}\right)-2\Lambda'\gamma\left(\bar{p}_{\bar{y}}\bar{h}_0+\bar{p}_0\bar{h}_{\bar{y}}\right)=0 \tag{2.2.30}$$

$$\bar{p}_{\bar{y}}-\bar{k}_f\bar{h}_{\bar{y}}+\gamma\bar{c}_f{}'\bar{h}_{\bar{y}}-\bar{k}_f\cos\vartheta=0 \tag{2.2.31}$$

$$-\left(\frac{R}{L_b}\right)\frac{\partial}{\partial\bar{z}}\left(\bar{p}_0\bar{h}_0^{\,3}\frac{\partial\bar{p}_{\bar{y}}}{\partial\bar{z}}+\bar{p}_{\bar{y}}\bar{h}_0^{\,3}\frac{\partial\bar{p}_0}{\partial\bar{z}}+3\bar{p}_0\bar{h}_0^{\,2}\bar{h}_{\bar{y}}\frac{\partial\bar{p}_0}{\partial\bar{z}}\right)-\frac{\partial}{\partial\vartheta}\left(\bar{p}_0\bar{h}_0^{\,3}\frac{\partial\bar{p}_{\bar{y}}}{\partial\theta}+\bar{p}_{\bar{y}}\bar{h}_0^{\,3}\frac{\partial\bar{p}_0}{\partial\theta}+3\bar{p}_0\bar{h}_0^{\,2}\bar{h}_{\bar{y}}\frac{\partial\bar{p}_0}{\partial\theta}\right)$$
$$+\Lambda'\left(\bar{p}_{\bar{y}}\bar{h}_0+\bar{p}_0\bar{h}_{\bar{y}}\right)+2\Lambda'\gamma\left(\bar{p}_{\bar{y}}\bar{h}_0+\bar{p}_0\bar{h}_{\bar{y}}\right)=0 \tag{2.2.32}$$

$$\bar{p}_{\bar{y}}-\bar{k}_f\bar{h}_{\bar{y}}-\gamma\bar{c}_f{}'\bar{h}_{\bar{y}}-\gamma\bar{c}_f{}'\cos\theta=0 \tag{2.2.33}$$

, with the respective boundary conditions:

$$\bar{p}_{\bar{x}}\left(\theta,\bar{z}=\pm1/2\right)=\bar{p}_{\bar{x}}\left(\theta,\bar{z}=\pm1/2\right)=\bar{p}_{\bar{y}}\left(\theta,\bar{z}=\pm1/2\right)=\bar{p}_{\bar{y}}\left(\theta,\bar{z}=\pm1/2\right)=0 \tag{2.2.34}$$

$$\bar{p}_{\bar{x}}\left(\theta=\chi,\chi+2\pi,\bar{z}\right)=\bar{p}_{\bar{x}}\left(\theta=\chi,\chi+2\pi,\bar{z}\right)=\bar{p}_{\bar{y}}\left(\theta=\chi,\chi+2\pi,\bar{z}\right)=\bar{p}_{\bar{y}}\left(\theta=\chi,\chi+2\pi,\bar{z}\right)=0 \tag{2.2.35}$$

Although equations (2.2.26) - (2.2.33) appear to require sophisticated solutions, it can be observed that they form two sets of coupled equations: Equations (2.2.26) - (2.2.29) for $\bar{p}_{\bar{x}},\bar{p}_{\bar{x}},\bar{h}_{\bar{x}},\bar{h}_{\bar{x}}$ and equations (2.2.30) - (2.2.33) for $\bar{p}_{\bar{y}},\bar{p}_{\bar{y}},\bar{h}_{\bar{y}},\bar{h}_{\bar{y}}$. Furthermore, the highest order of the Partial Differential Equations (P.D.E) is two, enabling relatively simplistic solution by the Finite Difference Method (F.D.M.) thoroughly described before. Thus the following non-linear algebraic system is derived for $\bar{p}_{\bar{x}_{i,j}},\bar{p}_{\bar{x}_{i,j}}$ $\left(i=2,...,N_{\bar{x}},j=2,...,N_{\bar{z}}\right)$:

$$B_1 \overline{p}_{\overline{x}_{i,j}} + B_2 = 0$$
$$B_1 = g_1(\overline{p}_{\overline{x}_{i+1,j}}, \overline{p}_{\overline{x}_{i-1,j}}, \overline{h}_{\overline{x}_{i+1,j}}, \overline{h}_{\overline{x}_{i-1,j}} \overline{p}_{\dot{\overline{x}}_{i+1,j}}, \overline{p}_{\dot{\overline{x}}_{i-1,j}}, \overline{h}_{\dot{\overline{x}}_{i+1,j}}, \overline{h}_{\dot{\overline{x}}_{i-1,j}}) \quad (2.2.36)$$
$$B_2 = g_2(\overline{p}_{\overline{x}_{i+1,j}}, \overline{p}_{\overline{x}_{i-1,j}}, \overline{h}_{\overline{x}_{i+1,j}}, \overline{h}_{\overline{x}_{i-1,j}} \overline{p}_{\dot{\overline{x}}_{i+1,j}}, \overline{p}_{\dot{\overline{x}}_{i-1,j}}, \overline{h}_{\dot{\overline{x}}_{i+1,j}}, \overline{h}_{\dot{\overline{x}}_{i-1,j}})$$

And

$$C_1 \overline{p}_{\dot{\overline{x}}_{i,j}} + C_2 = 0$$
$$C_1 = h_1(\overline{p}_{\overline{x}_{i+1,j}}, \overline{p}_{\overline{x}_{i-1,j}}, \overline{h}_{\overline{x}_{i+1,j}}, \overline{h}_{\overline{x}_{i-1,j}} \overline{p}_{\dot{\overline{x}}_{i+1,j}}, \overline{p}_{\dot{\overline{x}}_{i-1,j}}, \overline{h}_{\dot{\overline{x}}_{i+1,j}}, \overline{h}_{\dot{\overline{x}}_{i-1,j}}) \quad (2.2.37)$$
$$C_2 = h_2(\overline{p}_{\overline{x}_{i+1,j}}, \overline{p}_{\overline{x}_{i-1,j}}, \overline{h}_{\overline{x}_{i+1,j}}, \overline{h}_{\overline{x}_{i-1,j}} \overline{p}_{\dot{\overline{x}}_{i+1,j}}, \overline{p}_{\dot{\overline{x}}_{i-1,j}}, \overline{h}_{\dot{\overline{x}}_{i+1,j}}, \overline{h}_{\dot{\overline{x}}_{i-1,j}})$$

, coupled to $\left(i = 1,..., N_{\overline{x}} + 1,\ j = 1,..., N_{\overline{z}} + 1\right)$:

$$\overline{p}_{\overline{x}_{i,j}} - \overline{k}_f \overline{h}_{\overline{x}_{i,j}} + \gamma \overline{c}_f{}' \overline{h}_{\dot{\overline{x}}_{i,j}} + \overline{k}_f \sin\theta_i = 0 \quad (2.2.38)$$

$$\overline{p}_{\dot{\overline{x}}_{i,j}} - \overline{k}_f \overline{h}_{\dot{\overline{x}}_{i,j}} - \gamma \overline{c}_f{}' \overline{h}_{\overline{x}_{i,j}} + \gamma \overline{c}_f{}' \sin\theta_i = 0 \quad (2.2.39)$$

, with the respective boundary conditions:

$$\overline{p}_{\overline{x}_{i,j=1,N_{\overline{z}}+1}} = \overline{p}_{\dot{\overline{x}}_{i,j=1,N_{\overline{z}}+1}} = 0 \quad (2.2.40)$$

$$\overline{p}_{\overline{x}_{i=1,N_{\overline{x}}+1,j}} = \overline{p}_{\dot{\overline{x}}_{i=1,N_{\overline{x}}+1,j}} = 0 \quad (2.2.41)$$

, under the constraint $\overline{p}_{\overline{x}_{i,j}} \geq 0, \overline{p}_{\dot{\overline{x}}_{i,j}} \geq 0$

An analogous non-linear algebraic system can easily be derived for $\overline{p}_{\overline{y}_{i,j}}, \overline{p}_{\dot{\overline{y}}_{i,j}}$ under the same boundary conditions and constraints. Finally the four stiffness and the four damping coefficients are calculated with respect to the sign convention and the coordinate system of Figure 2.2.1 as:

$$\begin{bmatrix} \overline{K}_{\overline{xx}} & \overline{K}_{\overline{xy}} \\ \overline{K}_{\overline{yx}} & \overline{K}_{\overline{yy}} \end{bmatrix} = \frac{c_r}{p_0 R^2} \begin{bmatrix} K_{xx} & K_{xy} \\ K_{yx} & K_{yy} \end{bmatrix} = -\frac{L_b}{R} \int_{-1/2}^{1/2} \int_{\chi}^{\chi+2\pi} \begin{bmatrix} \overline{p}_{\overline{x}} \sin\theta & \overline{p}_{\overline{y}} \sin\theta \\ -\overline{p}_{\overline{x}} \cos\theta & -\overline{p}_{\overline{y}} \cos\theta \end{bmatrix} d\theta d\overline{z} \quad (2.2.42)$$

$$\begin{bmatrix} \overline{C}_{\overline{xx}} & \overline{C}_{\overline{xy}} \\ \overline{C}_{\overline{yx}} & \overline{C}_{\overline{yy}} \end{bmatrix} = \frac{c_r \Omega}{p_0 R^2} \begin{bmatrix} C_{xx} & C_{xy} \\ C_{yx} & C_{yy} \end{bmatrix} = -\frac{L_b}{R} \int_{-1/2}^{1/2} \int_{\chi}^{\chi+2\pi} \begin{bmatrix} \overline{p}_{\dot{\overline{x}}} \sin\theta & \overline{p}_{\dot{\overline{y}}} \sin\theta \\ -\overline{p}_{\dot{\overline{x}}} \cos\theta & -\overline{p}_{\dot{\overline{y}}} \cos\theta \end{bmatrix} d\theta d\overline{z} \quad (2.2.43)$$

These coefficients will be incorporated in the dimensional discretized rotor model, either as extra stiffness and damping matrices added properly to the stiffness and damping matrices of the full system, or as external excitation sources. In any case, due to the different coordinate systems utilized, the transformation described below is necessary:

$$\begin{bmatrix} K_{xx} & K_{xy} \\ K_{yx} & K_{yy} \end{bmatrix}_{rot} = \begin{bmatrix} 0 & 1 \\ -1 & 0 \end{bmatrix} \begin{bmatrix} K_{xx} & K_{xy} \\ K_{yx} & K_{yy} \end{bmatrix} \begin{bmatrix} 0 & -1 \\ 1 & 0 \end{bmatrix} \quad (2.2.44)$$

$$\begin{bmatrix} C_{xx} & C_{xy} \\ C_{yx} & C_{yy} \end{bmatrix}_{rot} = \begin{bmatrix} 0 & 1 \\ -1 & 0 \end{bmatrix} \left[\begin{bmatrix} C_{xx} & C_{xy} \\ C_{yx} & C_{yy} \end{bmatrix} \right] \begin{bmatrix} 0 & -1 \\ 1 & 0 \end{bmatrix} \tag{2.2.45}$$

2.3 Parametric excitation implementation

As clearly stated in 1.2, parametric excitation is implemented for both the linear and the non-linear approach of the elastoaerodynamic lubrication problem. According to the linear approach, the stiffness and damping coefficients are incorporated to the discretized rotor model either as extra stiffness and damping matrices properly added to the global ones, or as external excitation sources. In any case, these coefficients, under the principles of parametric excitation, are time dependent and change periodically according to:

$$\begin{bmatrix} K_{xx} & K_{xy} \\ K_{yx} & K_{yy} \end{bmatrix}^{p.e.}_{rot} = \begin{bmatrix} K_{xx} & K_{xy} \\ K_{yx} & K_{yy} \end{bmatrix}_{rot} \left(1+\delta \sin\left(\Omega_{ex} t\right)\right) \tag{2.3.1},$$

$$\begin{bmatrix} C_{xx} & C_{xy} \\ C_{yx} & C_{yy} \end{bmatrix}^{p.e.}_{rot} = \begin{bmatrix} C_{xx} & C_{xy} \\ C_{yx} & C_{yy} \end{bmatrix}_{rot} \left(1+\delta \sin\left(\Omega_{ex} t\right)\right) \tag{2.3.2},$$

with the parametric excitation frequency Ω_{ex} and amplitude ratio δ. Note that the stiffness and damping properties of all bearings are varied with the same frequency and without phase-lag, which is referred as synchronous stiffness and damping parametric excitation. In addition, note that all properties are varied with the same amplitude ratio, which is rather unrealistic. Equations (2.3.1) - (2.3.2) should be considered just as a mean to determine excitation frequencies and amplitude ratios which lead to parametric anti-resonances. These desirable parameters is then attempted to be achieved by the time dependent deformation of the initially circular bearing ring (*Figure 2.3.1*)

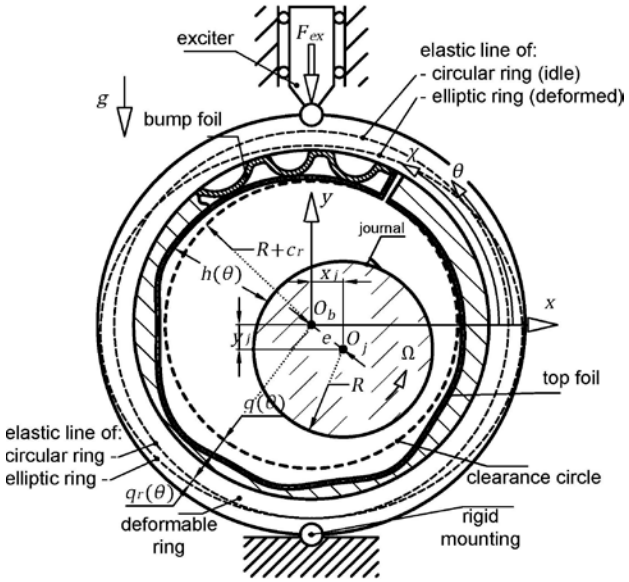

Figure 2.3.1 *The elastic line of the deformable ring under the effect of a vertical periodic load*

The following analysis considers the physical and geometrical properties (inner /outer radius, young modulus of elasticity, Poisson's ratio) of the bearing ring as known and denotes:

$$\kappa_1 = 1 - \frac{\left(R_{o,r}^4 - R_{i,r}^4\right)}{2R_{i,r}^2\left(R_{o,r}^2 - R_{i,r}^2\right)} + \frac{1.33\left(1+2\nu_r\right)R_{o,r}}{\pi\left(R_{o,r}^2 - R_{i,r}^2\right)}$$
$$\kappa_2 = 1 - \frac{\left(R_{o,r}^4 - R_{i,r}^4\right)}{2R_{i,r}^2\left(R_{o,r}^2 - R_{i,r}^2\right)} \tag{2.3.3}$$

Inspired by the analytically computed deformation of a ring under the effect of a periodic vertical load, the author defines the horizontal and vertical deformation of the bearing ring as:

$$q_r\left(\theta = 0, \pi, t\right) = dh = \frac{F_0}{2}\frac{R_{o,r}^3}{4.2\cdot 10^{11} I_r}\left(\frac{2}{\pi}\kappa_2^2 - \kappa_2 + \frac{\kappa_1}{2}\right)\left[1+\sin(\Omega_{ex}t)\right]$$
$$q_r\left(\theta = \pi/2, 3\pi/2, t\right) = dv = \frac{-F_0}{2}\frac{R_{o,r}^3}{4.2\cdot 10^{11} I_r}\left(\frac{\pi}{4}\kappa_1 - \frac{2\kappa_2^2}{\pi}\right)\left[1+\sin(\Omega_{ex}t)\right] \tag{2.3.4}$$

, and their time derivatives:

$$\dot{dh} = \frac{F_0}{2}\frac{R_{o,r}^3}{4.2\cdot 10^{11} I_r}\left(\frac{2}{\pi}\kappa_2^2 - \kappa_2 + \frac{\kappa_1}{2}\right)\left[\Omega_{ex}\cos(\Omega_{ex}t)\right]$$
$$\dot{dv} = \frac{-F_0}{2}\frac{R_{o,r}^3}{4.2\cdot 10^{11} I_r}\left(\frac{\pi}{4}\kappa_1 - \frac{2\kappa_2^2}{\pi}\right)\left[\Omega_{ex}\cos(\Omega_{ex}t)\right] \tag{2.3.5}$$

Therefore:

$$q_r\left(\theta, t\right) = q_r = \sqrt{\left[\left(R_{i,r} + dh\right)\cos\theta\right]^2 + \left[\left(R_{i,r} + dv\right)\sin\theta\right]^2} - R_{i,r}$$
$$\dot{q}_r\left(\theta, t\right) = \dot{q}_r = \frac{\left[\left(R_{i,r} + dh\right)\cos\theta\right]\left[\dot{dh}\cos\theta\right] + \left[\left(R_{i,r} + dv\right)\sin\theta\right]\left[\dot{dv}\sin\theta\right]}{q_r + R_{i,r}} \tag{2.3.6}$$

According to the normalization introduced in 2.2, the normalized deformation of the bearing ring is:

$$\bar{q}_r = \frac{q_r}{c_r}, \dot{\bar{q}}_r = \frac{\dot{q}_r}{c_r \nu} \tag{2.3.7}$$

The aforementioned deformation is considered positive when it is developed towards the outer side of the bearing. Furthermore, it is assumed that the perturbed motion of the journal about an equilibrium position does not affect the ring's deformation. Therefore, equation (2.2.15) is now converted into:

$$\left(\bar{p}_0 - 1\right) - \bar{k}_f\left[\bar{h}_0 - 1 - \varepsilon\sin\left(\theta - \theta_0\right)\right] + \bar{c}_f{}'\gamma\dot{\bar{q}}_r + \bar{k}_f\bar{q}_r = 0 \tag{2.3.8}$$

Since nothing but the structural equation describing the equilibrium position of the journal has been changed, the familiar Finite Difference Method is applied, converting equation (2.2.21) into $\left(i=1,...,N_{\bar{x}}+1,\ j=1,...,N_{\bar{z}}+1\right)$:

$$\left(\bar{p}_{0_{i,j}}-1\right)-\bar{k}_f\left[\bar{h}_{0_{i,j}}-1-\varepsilon\sin\left(\theta_i-\theta_0\right)\right]+\bar{c}_f{}'\gamma\dot{\bar{q}}_{r_i}+\bar{k}_f\bar{q}_{r_i}=0 \qquad (2.3.9)$$

The new non-linear algebraic system of equations can be solved by means of the standard iterative solvers under the constraint $\bar{p}_{0_{i,j}}\geq 1$.

2.4 Rotor modeling

In practice, rotating machines have complex geometry with variable cross sections carrying flexible disks or blades. Such machines can't be modeled by Jeffcott or Laval rotors as it is of great importance to accurately compute the Eigen-frequencies, the vibration modes and the corresponding unbalance responses. To this end, the rotor is discretized with continuous finite beam elements, each element having two nodes and eight degrees of freedom. The equations of motion of the whole rotor system, the multiple degree of freedom system (M.D.O.F.), can be represented in matrix form since the inertia, damping, gyroscopic and stiffness matrices of each finite beam element are derived. In the current work, the rotating finite beam element depicted in *Figure 2.4.1* is introduced. The necessary geometrical and physical properties of such element are presented in *Table 2.4.1*.

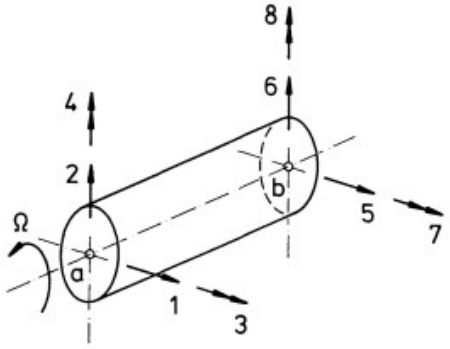

Figure 2.4.1 *Rotating beam element bending in two dimensions*

Table 2.4.1 *Definition of the geometric and physical properties of the rotor finite beam element*

Symbol	***Description***	***Definition***
l_e	*Length of element*	
R_{o,m_e}	*Outer mass radius of element*	
R_{i,m_e}	*Inner mass radius of element*	
R_{o,s_e}	*Outer stiffness radius of element*	
R_{i,s_e}	*Inner stiffness radius of element*	
I_e	*2nd moment of area of the cross section of element*	$\pi\left(R_{o,s_e}^4 - R_{i,s_e}^4\right)/4$
A_e	*Cross section area of element*	$\pi\left(R_{o,m_e}^2 - R_{i,m_e}^2\right)$
ρ_e	*Density of element*	
E_e	*Young's modulus of element*	
G_e	*Shear modulus of element*	
s_{f_e}	*Shear factor of element*	

The elastic line of the element in both vertical and horizontal plane can be approximated by Hermitian polynomials in terms of the nodal translational and rotational degrees of freedom in the form:

$$\begin{Bmatrix} x_e(\zeta,t) \\ y_e(\zeta,t) \end{Bmatrix} = \begin{bmatrix} H_1(\zeta) & 0 & 0 & l_e H_2(\zeta) & H_3(\zeta) & 0 & 0 & l_e H_4(\zeta) \\ 0 & H_1(\zeta) & l_e H_2(\zeta) & 0 & 0 & H_3(\zeta) & l_e H_4(\zeta) & 0 \end{bmatrix} \begin{Bmatrix} x_{1,e}(t) \\ x_{2,e}(t) \\ \varphi_{3,e}(t) \\ \varphi_{4,e}(t) \\ x_{5,e}(t) \\ x_{6,e}(t) \\ \varphi_{7,e}(t) \\ \varphi_{8,e}(t) \end{Bmatrix} = \boldsymbol{\psi}_e(\zeta)\,\mathbf{x}_e(t)$$

(2.4.1)

, where $\zeta = \dfrac{z_e}{l_e}$ denotes the dimensionless axial coordinate and the shape functions:

$$H_1(\zeta) = 1 - 3\zeta^2 + 2\zeta^3, H_2(\zeta) = \zeta - 2\zeta^2 + \zeta^3, H_3(\zeta) = 3\zeta^2 - 2\zeta^3, H_4(\zeta) = -\zeta^2 + \zeta^3$$

(2.4.2)

, represent the Hermitian polynomials of third order**.** Therefore, the lateral bending slope of the element can be approximated in the form:

$$\begin{Bmatrix} \boldsymbol{\varphi}_{x,e}(\zeta,t) \\ \boldsymbol{\varphi}_{y,e}(\zeta,t) \end{Bmatrix} = \begin{bmatrix} 0 & H_1'(\zeta) & l_e H_2'(\zeta) & 0 & 0 & H_3'(\zeta) & l_e H_4'(\zeta) & 0 \\ H_1'(\zeta) & 0 & 0 & l_e H_2'(\zeta) & H_3'(\zeta) & 0 & 0 & l_e H_4'(\zeta) \end{bmatrix} \begin{Bmatrix} x_{1,e}(t) \\ x_{2,e}(t) \\ \varphi_{3,e}(t) \\ \varphi_{4,e}(t) \\ x_{5,e}(t) \\ x_{6,e}(t) \\ \varphi_{7,e}(t) \\ \varphi_{8,e}(t) \end{Bmatrix} = \boldsymbol{\varphi}_e(\zeta)\mathbf{x}_e(t)$$

(2.4.3)

, where:

$$H_1'(\zeta) = -6\zeta + 6\zeta^2, H_2'(\zeta) = 1 - 4\zeta + 3\zeta^2, H_3'(\zeta) = 6\zeta - 6\zeta^2, H_4'(\zeta) = -2\zeta + 3\zeta^2$$

(2.4.4)

The potential energy of the finite beam element is then given by:

$$U_e = \frac{1}{2} E_e I_e \int_0^1 \left(\mathbf{x}_e^T \left(\frac{\partial^2 \boldsymbol{\psi}_e}{\partial \zeta^2}\right)^T \frac{\partial^2 \boldsymbol{\psi}_e}{\partial \zeta^2} \mathbf{x}_e \right) d\zeta \qquad (2.4.5)$$

, or in matrix form:

$$U_e = \frac{1}{2} \mathbf{x}_e^T \mathbf{K}_e \mathbf{x}_e \qquad (2.4.6).$$

Comparison of the equations (2.4.5) - (2.4.6) yields the stiffness matrix of the finite beam element:

$$\mathbf{K}_e = \begin{bmatrix} a_1 & 0 & 0 & -a_2 & -a_1 & 0 & 0 & -a_2 \\ & a_1 & a_2 & 0 & 0 & -a_1 & a_2 & 0 \\ & & a_3 & 0 & 0 & -a_2 & a_4 & 0 \\ & & & a_3 & a_2 & 0 & 0 & a_4 \\ & & & & a_1 & 0 & 0 & a_2 \\ & sym & & & & a_1 & -a_2 & 0 \\ & & & & & & a_3 & 0 \\ & & & & & & & a_3 \end{bmatrix} \qquad (2.4.7)$$

, where:

$$a_1 = \frac{12E_eI_e}{(1+e)l_e^3}, a_2 = \frac{6E_eI_e}{(1+e)l_e^2}, a_3 = \frac{(4+e)E_eI_e}{(1+e)l_e}, a_4 = \frac{(2-e)E_eI_e}{(1+e)l_e}, e = \frac{12E_eI_e}{G_e s_{f,e} A_e l_e^2}$$

(2.4.8)

Similarly, the kinetic energy of the finite beam element is given by the summation of four terms. The first term corresponds to the translational kinetic energy; the second corresponds to the rotational kinetic energy, the third corresponds to the kinetic energy due to tilting phenomena and the last corresponds to the kinetic energy due to gyroscopic phenomena.

$$T_e = \sum_{i=1}^{4} T_{e,i} \tag{2.4.9}$$

, where:

$$\begin{aligned}
T_{e,1} &= \int_0^1 \left(\frac{1}{2} \mu \dot{\mathbf{x}}_e^T \boldsymbol{\psi}^T \boldsymbol{\psi} \dot{\mathbf{x}}_e \right) d\zeta \\
T_{e,2} &= \int_0^1 \left(\frac{1}{2} \Omega^2 \mu_p \right) d\zeta \\
T_{e,3} &= \int_0^1 \left(\frac{1}{2} \mu_d \dot{\mathbf{x}}_e^T \boldsymbol{\varphi}'^T \boldsymbol{\varphi}' \dot{\mathbf{x}}_e \right) d\zeta \\
T_{e,4} &= \int_0^1 \left[\frac{1}{2} \mu_p \Omega \left(\dot{\mathbf{x}}_e^T \boldsymbol{\varphi}_{x,e}^T \boldsymbol{\varphi}_{y,e}' \dot{\mathbf{x}}_e - \dot{\mathbf{x}}_e^T \boldsymbol{\varphi}_{y,e}^T \boldsymbol{\varphi}_{x,e}' \dot{\mathbf{x}}_e \right) \right] d\zeta
\end{aligned} \tag{2.4.10}$$

, or in matrix form:

$$T_e = \frac{1}{2} \dot{\mathbf{x}}_e^T \mathbf{M}_e \mathbf{x}_e + \frac{1}{2} \mu_p l_e \Omega^2 + \frac{1}{2} \Omega \dot{\mathbf{x}}_e^T \mathbf{G}_e \mathbf{x}_e \tag{2.4.11}$$

, where:

$$\mu = \rho_e A_e, \mu_p = 2\rho_e I_e, \mu_d = \rho_e I_e \tag{2.4.12}$$

Comparison of the equations (2.4.10) - (2.4.11) yields the mass and gyroscopic matrices of the finite beam element:

$$\mathbf{M}_e = \begin{bmatrix}
c_1 & 0 & 0 & -c_3 & -c_2 & 0 & 0 & c_4 \\
 & c_1 & c_3 & 0 & 0 & c_2 & -c_4 & 0 \\
 & & c_5 & 0 & 0 & c_4 & -c_6 & 0 \\
 & & & c_5 & -c_4 & 0 & 0 & -c_6 \\
 & & & & c_1 & 0 & 0 & c_3 \\
 & sym & & & & c_1 & -c_3 & 0 \\
 & & & & & & c_5 & 0 \\
 & & & & & & & c_5
\end{bmatrix} \tag{2.4.13}$$

, where:

$$
\begin{aligned}
c_1 &= \frac{1}{(1+e)^2}\left(\frac{13}{35}\mu l_e + \frac{6}{5}\frac{\mu_d}{l_e} + \frac{7}{10}e\mu l_e + \frac{1}{3}e^2\mu l_e\right)\\
c_2 &= \frac{1}{(1+e)^2}\left(\frac{9}{70}\mu l_e - \frac{6}{5}\frac{\mu_d}{l_e} + \frac{3}{10}e\mu l_e + \frac{1}{6}e^2\mu l_e\right)\\
c_3 &= \frac{l_e}{(1+e)^2}\left(\frac{11}{210}\mu l_e + \frac{1}{10}\frac{\mu_d}{l_e} + \frac{11}{120}e\mu l_e + \frac{5}{120}e^2\mu l_e - \frac{1}{2}\frac{e\mu_d}{l_e}\right)\\
c_4 &= \frac{l_e}{(1+e)^2}\left(\frac{13}{420}\mu l_e - \frac{1}{10}\frac{\mu_d}{l_e} + \frac{3}{40}e\mu l_e + \frac{1}{24}e^2\mu l_e - \frac{1}{2}\frac{e\mu_d}{l_e}\right)\\
c_5 &= \frac{l_e^2}{(1+e)^2}\left(\frac{1}{105}\mu l_e + \frac{2}{15}\frac{\mu_d}{l_e} + \frac{1}{60}e\mu l_e + \frac{1}{120}e^2\mu l_e + \frac{1}{6}\frac{e\mu_d}{l_e} + \frac{1}{3}\frac{e^2\mu_d}{l_e}\right)\\
c_6 &= \frac{l_e^2}{(1+e)^2}\left(\frac{1}{140}\mu l_e + \frac{1}{30}\frac{\mu_d}{l_e} + \frac{1}{60}e\mu l_e + \frac{1}{120}e^2\mu l_e + \frac{1}{6}\frac{e\mu_d}{l_e} - \frac{1}{6}\frac{e^2\mu_d}{l_e}\right)
\end{aligned}
\tag{2.4.14}
$$

, and:

$$
\mathbf{G}_e = \begin{bmatrix}
0 & g_1 & g_2 & 0 & 0 & -g_1 & g_2 & 0\\
 & 0 & 0 & g_2 & g_1 & 0 & 0 & g_2\\
 & & 0 & g_4 & g_2 & 0 & 0 & g_3\\
 & & & 0 & 0 & g_2 & g_3 & 0\\
 & & & & 0 & g_1 & -g_2 & 0\\
 & skew-sym & & & & 0 & 0 & -g_2\\
 & & & & & & 0 & g_4\\
 & & & & & & & 0
\end{bmatrix}
\tag{2.4.15}
$$

, where:

$$
g_1 = \frac{6}{5}\frac{\mu_p\Omega}{l_e}, g_2 = \frac{1}{10}\mu_p\Omega, g_3 = \frac{l_e\mu_p\Omega}{30}, g_4 = \frac{2l_e\mu_p\Omega}{15} \tag{2.4.16}
$$

In addition, it is assumed that only nodal forces and moments are affecting the finite beam element, so:

$$
\mathbf{F}_e = \begin{bmatrix} F_1 & F_2 & M_3 & M_4 & F_5 & F_6 & M_7 & M_8 \end{bmatrix} \tag{2.4.17}
$$

Finally it should be noted that the damping matrix is given by the classical Rayleigh damping according to the formula:

$$
\begin{aligned}
&\mathbf{C}_e = \alpha\mathbf{M}_e + \beta\mathbf{K}_e\\
&\alpha, \beta \in \mathbb{R}^+
\end{aligned}
\tag{2.4.18}
$$

After all, it has been observed that small values of α, β make the whole rotor system less numerically stiff without affecting its dynamic behavior. Combination the equations (2.4.7) - (2.4.18) yields the equations of motion of a single finite beam element:

$$
\mathbf{M}_e\ddot{\mathbf{x}}_e + \left(\mathbf{C}_e + \mathbf{G}_e\right)\dot{\mathbf{x}}_e + \mathbf{K}_e\mathbf{x}_e = \mathbf{F}_e \tag{2.4.19}
$$

Finally, the global inertia, damping, gyroscopic and stiffness matrices are assembled by the proper summation of the individual finite beam element matrices and the equations of motion for the whole rotor system are derived:

$$\begin{aligned} &\mathbf{M}\ddot{\mathbf{x}}_r + \left(\mathbf{C}+\mathbf{G}\right)\dot{\mathbf{x}}_r + \mathbf{K}\mathbf{x}_r = \mathbf{F} \\ &\mathbf{x}_r\left(t=0\right) = \mathbf{x}_{r,0}, \dot{\mathbf{x}}_r\left(t=0\right) = \dot{\mathbf{x}}_{r,0} \\ &\mathbf{x}_r \in \mathbb{R}^{Nr} \end{aligned} \tag{2.4.20}$$

Before introducing the criteria which certify the accurate discretization of the rotor, a brief description of the geometrical and physical properties of the segments will be given. At first, inner (if cavities are included) and outer mass diameters D_{i,m_e}, D_{o,m_e} define the geometrical outline of the shaft. The cross section area of each beam element is evaluated based on these diameters, thus stiffness matrices (due to e) and inertia matrices (due to e and μ) are greatly affected by them. In addition, inner and outer stiffness diameters D_{i,s_e}, D_{o,s_e} define the volume of the segment which mainly receives the bending load. The second moment of area and therefore the diametrical and the polar mass moments of inertia of each element are evaluated based on these diameters. It is more than obvious that the effective stiffness of the shaft is influenced by them.

In general, for an accurate representation of the rotor using finite beam elements some very specific rules should be followed. At first, new elements are inserted when the geometrical outline of the shaft changes. Extra elements are utilized if the evaluation of the response is of crucial importance. It is strongly recommended a single element not to have a length to stiffness diameter ratio $l_e \big/ D_{o,s_e}$ less than 0.05 or greater than 0.8. Furthermore, the ratio $\dfrac{l_{e+1}D_{o,s_e}}{l_e D_{o,s_{e+1}}}$ should not be greater than 4.

Additional masses may exist in a rotor segment, such as rotating blades or wiring. It is assumed that these additional masses (which are modeled as hollow disks) affect both the mass and gyroscopic properties of the aforementioned segment. To this end, mass and gyroscopic matrices can be constructed for each disk, since its diameter of gyration D_{gyr_d} and its total mass m_d are known. The aforementioned matrices should finally be added properly to the global mass and gyroscopic matrices of the shaft.

After the accuracy of the discretization is ensured, static bearing loads $\bar{\mathbf{W}}_{st}$ (necessary for the linear approach of the elastoaerodynamic lubrication problem) can easily be evaluated. Equation (2.4.20) leads to:

$$\mathbf{K}\mathbf{x}_r = \mathbf{F} \tag{2.4.21}$$

The force vector $\mathbf{F} \in \mathbb{R}^{Nr}$ consists of the unknown vertical bearing forces $\mathbf{F}^B \in \mathbb{R}^2$ and the known gravity (or zero) forces $\mathbf{F}^G \in \mathbb{R}^{Nr-2}$. Similarly, the state vector $\mathbf{x}_r \in \mathbb{R}^{Nr}$ consists of the known vertical degrees of freedom at each bearing $\mathbf{x}_r^B = \mathbf{0} \in \mathbb{R}^2$ and the unknown displacements $\mathbf{x}_r^G \in \mathbb{R}^{Nr-2}$. If rows and columns of the stiffness matrix corresponding to the known displacements are eliminated, equation (2.4.21) leads to:

$$\mathbf{K}^G \mathbf{x}^G{}_r = \mathbf{F}^G \tag{2.4.22}$$

It is assumed that $\mathbf{K}^G$ is invertible (usually close to singular) so:

$$\mathbf{x}^G{}_r = \left(\mathbf{K}^G\right)^{-1} \mathbf{F}^G \tag{2.4.23}$$

Using the equations previously eliminated, it is now possible to evaluate the vertical bearing forces $\mathbf{F}^B \in \mathbb{R}^2$. Finally, according to the normalization introduced in (2.2.1) – (2.2.2) the non-dimensional bearing load is:

$$\bar{\mathbf{W}}_{st} = \frac{\mathbf{F}^B}{p_0 R^2} \tag{2.4.24}$$

It is of great importance to note that the present finite beam element model is considered as large or in other words, computationally expensive. Therefore, model reduction, whereby the number of degrees of freedom in a model is reduced, is applied in order to compute faster the natural frequencies, mode shapes and responses of the rotor. Possibly the most popular and certainly the simplest reduction method is static (or Guyan) reduction.

According to this method, damping and gyroscopic effects are negligible thus equation (2.4.20) is converted into:

$$\mathbf{M}\ddot{\mathbf{x}}_r + \mathbf{K}\mathbf{x}_r = \mathbf{F} \tag{2.4.25}$$

All vectors and matrices are now split intosub-vectors and sub-matrices respectively, relating to the master degrees of freedom, which are retained and the slave degrees of freedom which will be afterwards eliminated. It is also assumed that no force is applied to the slave degrees of freedom, so equation (2.4.25) becomes:

$$\begin{bmatrix} \mathbf{M}_{mm} & \mathbf{M}_{ms} \\ \mathbf{M}_{sm} & \mathbf{M}_{ss} \end{bmatrix} \begin{Bmatrix} \ddot{\mathbf{x}}_{m,r} \\ \ddot{\mathbf{x}}_{s,r} \end{Bmatrix} + \begin{bmatrix} \mathbf{K}_{mm} & \mathbf{K}_{ms} \\ \mathbf{K}_{sm} & \mathbf{K}_{ss} \end{bmatrix} \begin{Bmatrix} \mathbf{x}_{m,r} \\ \mathbf{x}_{s,r} \end{Bmatrix} = \begin{Bmatrix} \mathbf{F}_m \\ \mathbf{0} \end{Bmatrix} \tag{2.4.26}$$

The sub-scripts m, s relate to the master and slave degrees of freedom respectively. Neglecting the inertia terms of the second set of equations gives:

$$\mathbf{K}_{sm}\mathbf{x}_{m,r} + \mathbf{K}_{ss}\mathbf{x}_{s,r} = \mathbf{0} \tag{2.4.27}$$

, which now may be used to eliminate the slave degrees of freedom according to the formula:

$$\begin{Bmatrix} \mathbf{x}_{m,r} \\ \mathbf{x}_{s,r} \end{Bmatrix} = \begin{bmatrix} \mathbf{I} \\ -\mathbf{K}_{ss}^{-1}\mathbf{K}_{sm} \end{bmatrix} \mathbf{x}_{m,r} = \mathbf{T}_s \mathbf{x}_{m,r} \tag{2.4.28}$$

, where $\mathbf{T}_s$ denotes the static transformation between the full state vector and the master degrees of freedom. The reduced matrices are then given by:

$$\mathbf{M}_r = \mathbf{T}_s^T \mathbf{M} \mathbf{T}_s, \mathbf{K}_r = \mathbf{T}_s^T \mathbf{K} \mathbf{T}_s, \mathbf{C}_r = \mathbf{T}_s^T \mathbf{C} \mathbf{T}_s, \mathbf{G}_r = \mathbf{T}_s^T \mathbf{G} \mathbf{T}_s \tag{2.4.29}$$

It is more than obvious that the reduced matrices construct the following equations of motion for the master nodes of the rotor model:

$$\begin{aligned} &\mathbf{M}_r \ddot{\mathbf{x}}_{m,r} + \left(\mathbf{C}_r + \mathbf{G}_r\right)\dot{\mathbf{x}}_{m,r} + \mathbf{K}_r \mathbf{x}_{m,r} = \mathbf{F}_m \\ &\mathbf{x}_{m,r}\left(t=0\right) = \mathbf{x}_{m,r_0}, \dot{\mathbf{x}}_{m,r}\left(t=0\right) = \dot{\mathbf{x}}_{m,r_0} \\ &\mathbf{x}_{m,r} \in \mathbb{R}^{Nm} \end{aligned} \tag{2.4.30}$$

This page has been intentionally left blank

3. SOLUTION OF THE ROTOR DYNAMIC SYSTEM

3.1 Linear Harmonic Analysis

The well established Linear Harmonic Analysis (L.H.A.) consists of calculating the eigenvalues/eigenvectors of the system and the calculation of synchronous steady state response. First of all, in order to couple the elastoaerodynamic lubrication model with the rotor model the stiffness and damping matrices given by (2.2.44) - (2.2.45) are properly added to the reduced stiffness and damping matrices given by (2.4.29) thus equations (2.4.30) are converted into:

$$\begin{aligned} &\mathbf{M}_r\ddot{\mathbf{x}}_{m,r}+\left(\mathbf{C}'_r+\mathbf{G}_r\right)\dot{\mathbf{x}}_{m,r}+\mathbf{K}'_r\mathbf{x}_{m,r}=\mathbf{F}_m \\ &\mathbf{x}_{m,r}\left(t=0\right)=\mathbf{x}_{m,r_0},\dot{\mathbf{x}}_{m,r}\left(t=0\right)=\dot{\mathbf{x}}_{m,r_0} \\ &\mathbf{x}_{m,r}\in\mathbb{R}^{Nm} \end{aligned} \tag{2.4.31}$$

A new state vector is defined $\mathbf{X}_{m,r}=\begin{Bmatrix}\mathbf{x}_{m,r}\\ \dot{\mathbf{x}}_{m,r}\end{Bmatrix},\mathbf{X}_{m,r}\in\mathbb{R}^{2Nm}$ and equations (3.1.1) are written in the customary state form:

$$\begin{aligned} &\dot{\mathbf{X}}_{m,r}=\mathbf{A}\mathbf{X}_{m,r}+\mathbf{B}\mathbf{F}_m \\ &\mathbf{X}_{m,r}\left(t=0\right)=\mathbf{X}_{m,r_0} \\ &\mathbf{X}_{m,r}\in\mathbb{R}^{2Nm} \end{aligned} \tag{2.4.32}$$

, where:

$$\mathbf{A}=\begin{bmatrix}\mathbf{0} & \mathbf{I}_r\\ -\mathbf{M}_r^{-1}\mathbf{K}'_r & -\mathbf{M}_r^{-1}(\mathbf{C}'_r+\mathbf{G}_r)\end{bmatrix},\mathbf{B}=\begin{bmatrix}\mathbf{0}\\ \mathbf{M}_r^{-1}\end{bmatrix} \tag{2.4.33}$$

The solution can be carried out by means of the modal analysis in the state space. To this end, the free vibration problem is considered $(\mathbf{F}_m=\mathbf{0})$ so the solution has the exponential form:

$$\mathbf{X}_{m,r}\left(t\right)=\boldsymbol{\Phi}e^{\lambda t} \tag{2.4.34}$$

, where λ is a constant scalar and $\boldsymbol{\Phi}$ a constant vector. Inserting equation (3.1.4) into (3.1.2) yields to the algebraic eigenvalue problem which is said to be in standard form:

$$\mathbf{A}\boldsymbol{\Phi}=\lambda\boldsymbol{\Phi} \tag{2.4.35}$$

It should be noted here, that matrix $\mathbf{A}$ is non-symmetric thus the adjoint eigenvalue problem should be considered too:

$$\mathbf{A}^{\mathrm{T}}\boldsymbol{\Psi}=\lambda\boldsymbol{\Psi} \tag{2.4.36}$$

Eigenvalues, right and left eigenvectors can be obtained by solving (3.1.5) - (3.1.6) using Matlab. For the calculation of the synchronous steady state response, it is firstly assumed that the force vector $\mathbf{F}_m$ consists of unbalance forces $\mathbf{F}_m^U$ only. Unbalance forces are considered for selected nodes and for constant rotating speed Ω. Given the total mass of the rotor part

defined between sequential bearing nodes M_k and the unbalance eccentricity e_u (which in this Master Thesis follows the ISO G-grade), the unbalance forces can be formulated as (in horizontal and vertical direction respectively):

$$F_{m,h}^{U} = M_k e_u \Omega^2 \cos\left(\Omega t\right),\ F_{m,v}^{U} = M_k e_u \Omega^2 \sin\left(\Omega t\right) \tag{2.4.37}$$

The steady state synchronous response for synchronous harmonic excitation of the form $\mathbf{F}_m\left(t\right) = \mathbf{F}_{m_c}^{U}\cos\left(\Omega t\right) + \mathbf{F}_{m_s}^{U}\sin\left(\Omega t\right)$ can be written as $\mathbf{X}_{m,r}\left(t\right) = \mathbf{X}_{m,r_c}\cos\left(\Omega t\right) + \mathbf{X}_{m,r_s}\sin\left(\Omega t\right)$. Substituting to the equations of motion, the steady state response can be calculated from the following set of linear algebraic equations:

$$\begin{bmatrix} \mathbf{K}_r' - \Omega^2\mathbf{M}_r & \Omega\left(\mathbf{C}_r' + \mathbf{G}_r\right) \\ -\Omega\left(\mathbf{C}_r' + \mathbf{G}_r\right) & \mathbf{K}_r' - \Omega^2\mathbf{M}_r \end{bmatrix} \begin{Bmatrix} \mathbf{X}_{m,r_c} \\ \mathbf{X}_{m,r_s} \end{Bmatrix} = \begin{Bmatrix} \mathbf{F}_{m_c} \\ \mathbf{F}_{m_s} \end{Bmatrix} \tag{2.4.38}$$

3.2 Time integration

Time integration is mainly implemented in order to evaluate the unbalance response of the non-linear bearing-rotor model. In addition, it contributes to the evaluation of the response of a parametrically excited linear or non-linear bearing- rotor model. Following sections are dedicated to the response of a parametrically excited bearing-rotor model thus the current one emphasizes to the unbalance response of the non-linear bearing-rotor model. To this end, it is of great importance to note that equations (2.4.30) should be transformed in their non-dimensional form, according to (2.1.9) - (2.1.10):

$$\begin{aligned} &\overline{\mathbf{M}}_r \ddot{\overline{\mathbf{x}}}_{m,r} + \left(\overline{\mathbf{C}}_r + \overline{\mathbf{G}}_r\right)\dot{\overline{\mathbf{x}}}_{m,r} + \overline{\mathbf{K}}_r \overline{\mathbf{x}}_{m,r} = \overline{\mathbf{F}}_m \\ &\overline{\mathbf{x}}_{m,r}\left(\tau = 0\right) = \overline{\mathbf{x}}_{m,r_0},\ \dot{\overline{\mathbf{x}}}_{m,r}\left(\tau = 0\right) = \dot{\overline{\mathbf{x}}}_{m,r_0} \\ &\overline{\mathbf{x}}_{m,r} \in \mathbb{R}^{Nm} \end{aligned} \tag{2.4.39}$$

, where:

$$\overline{\mathbf{M}}_r = \mathbf{M}_r \frac{p_0 c_r^5}{36\mu^2 R^5 L_b},\ \overline{\mathbf{C}}_r = \mathbf{C}_r \frac{c_r^3}{6\mu R^3 L_b},\ \overline{\mathbf{G}}_r = \mathbf{G}_r \frac{c_r^3}{6\mu R^3 L_b},\ \overline{\mathbf{K}}_r = \mathbf{K}_r \frac{c_r}{p_0 R L_b} \tag{2.4.40}$$

Furthermore, it should be noted that the dimensionless force vector $\overline{\mathbf{F}}_m$ consists of the dimensionless bearing forces $\overline{\mathbf{F}}_m^B$ given by (2.1.18) - (2.1.19), the dimensionless unbalance forces $\overline{\mathbf{F}}_m^U$ and the dimensionless gravity forces $\overline{\mathbf{F}}_m^G$. Equations (3.2.1) are included in equations (2.1.29) and the non-linear system of first order O.D.E.s is clearly defined.

In an initial value problem such as(2.1.29), the solution is obtained iteratively using the initial condition $\overline{\mathbf{x}}_{s_r,0}$ as well as a period of time over which the solution is to be obtained. At each time step the solver applies a specific algorithm to the results of previous time steps. At the first time step the initial condition provides the necessary information that allows the integration to proceed.

The time step adopted by the solver is sometimes forced down to an unreasonably small level in comparison to the interval of integration. These time steps can be so small that

traversing a small time interval may require thousands of iterations. Usually these integrations are considered as inaccurate or failed and the corresponding system of O.D.E.s is considered as numerically stiff. More specifically, the numerical stiffness of (2.1.29) depends on the shaft properties and the bump foil properties. Thus a stiff solver is more than necessary.

Ode15s is a variable step variable order (V.S.V.O.) solver based on the numerical differentiation formulas of orders 1 to 5. Optionally it can use backward differentiation formulas, which are usually less efficient. In this Master Thesis, this solver is chosen due to its high accuracy.

3.3 Pseudo arc-length continuation with orthogonal collocation

Orthogonal collocation refers to a class of methods for computing periodic solutions of a set of autonomous O.D.E.s by solving the adjoint two-point boundary value problem. To access the stability of this periodic solution, if it actually exists, a special type of fundamental solution matrix must be computed the widely known monodromy matrix. Its eigenvalues are known as Floquet multipliers and for autonomous O.D.E. systems, one of them is by default equal to one. The periodic solution found, is asymptotically stable if all Floquet multipliers except the aforementioned trivial Floquet multiplier have a modulus smaller than one. Given the real and the imaginary part of a Floquet multiplier with modulus greater than one, then the type of instability can be also determined.

Suppose that the autonomous system of O.D.E.s appears explicitly one or more scalar parameters (for example the rotating speed Ω) and the periodic solutions depend on this scalar parameter. A numerical continuation algorithm takes as input the parameterized autonomous system of O.D.E.s and an initial periodic solution evaluated for a specific value of the scalar parameter. The output is a set of periodic solutions for various values of the scalar parameter, continuously connected to the initial periodic solution, which in other words is called solution branch. In present work, the sole scalar parameter (also called bifurcation parameter) is the rotating speed Ω. Therefore only co-dimension 1 bifurcation sets are considered.

Every numerical continuation algorithm incorporates one sub-algorithm which computes a periodic solution for a specific value of the bifurcation parameter and another one which determines the initial guess for the periodic solution given the next value of the bifurcation parameter. Maybe the simplest form of numerical continuation is the so called natural parameter continuation. According to this method, the periodic solution computed for a known value of the bifurcation parameter is the initial guess for the periodic solution which is to be computed for the next value of the bifurcation parameter. One advantage of this method is that it does not require an explicit formula for the stationary problem. On the other hand, the main disadvantage is that it usually fails at turning points, where the sign of the difference between two sequential bifurcation parameters changes.

Another widely applied continuation method (the one used in present work) is pseudo arc-length continuation. This method introduces an independent parameter, the arc-length parameter, and produces an initial guess for the next step in the tangential direction of the current periodic solution step. This enables the method to continue the solution branch at turning points and make larger steps at regions of high curvature. The main drawback of the method is that the bifurcation parameter becomes part of the solution vector and one additional equation is required to proceed.

In the present work, pseudo arc-length continuation is applied to both the linear and the non-linear parametrically excited rotor-bearing model. At first, in order to couple the linear

model of the parametrically excited G.F.B.s to the rotor model, stiffness and damping matrices given by (2.3.1) - (2.3.2) are rewritten as:

$$\begin{aligned}\begin{bmatrix} K_{xx} & K_{xy} \\ K_{yx} & K_{yy} \end{bmatrix}_{rot}^{p.e.} &= \begin{bmatrix} K_{xx} & K_{xy} \\ K_{yx} & K_{yy} \end{bmatrix}_{rot} \left(1+\delta x_{m,s}\right) \\ \begin{bmatrix} C_{xx} & C_{xy} \\ C_{yx} & C_{yy} \end{bmatrix}_{rot}^{p.e.} &= \begin{bmatrix} C_{xx} & C_{xy} \\ C_{yx} & C_{yy} \end{bmatrix}_{rot} \left(1+\delta x_{m,s}\right)\end{aligned} \tag{2.5.1}$$

, where:

$$\begin{aligned}\dot{x}_{m,s} &= x_{m,s} + \Omega_{ex} x_{m,c} - x_{m,s}\left(x_{m,s}^2 + x_{m,c}^2\right) \\ \dot{x}_{m,c} &= x_{m,c} - \Omega_{ex} x_{m,s} - x_{m,c}\left(x_{m,s}^2 + x_{m,c}^2\right)\end{aligned} \tag{2.5.2}$$

The aforementioned matrices are properly added to the reduced stiffness and damping matrices given by (2.4.29) and the equations (2.4.30) are converted to:

$$\begin{aligned}&\mathbf{M}_r \ddot{\mathbf{x}}_{m,r} + \left(\mathbf{C}_r^{p.e.} + \mathbf{G}_r\right)\dot{\mathbf{x}}_{m,r} + \mathbf{K}_r^{p.e.}\mathbf{x}_{m,r} = \mathbf{F}_m \\ &\mathbf{x}_{m,r}\left(t=0\right) = \mathbf{x}_{m,r_0}, \dot{\mathbf{x}}_{m,r}\left(t=0\right) = \dot{\mathbf{x}}_{m,r_0} \\ &\mathbf{x}_{m,r} \in \mathbb{R}^{Nm}\end{aligned} \tag{2.5.3}$$

Now, the force vector $\mathbf{F}_m$ consists of gravity forces $\mathbf{F}_m^G$ only. A new state vector is again defined $\mathbf{Y}_{m,r} = \begin{Bmatrix} \mathbf{x}_{m,r} \\ \dot{\mathbf{x}}_{m,r} \end{Bmatrix}, \mathbf{Y}_{m,r} \in \mathbb{R}^{2Nm}$ and equations (3.3.3) are written in the customary state form:

$$\begin{aligned}&\dot{\mathbf{Y}}_{m,r} = \mathbf{A}'\mathbf{Y}_{m,r} + \mathbf{B}'\mathbf{F}_m \\ &\mathbf{Y}_{m,r}\left(t=0\right) = \mathbf{Y}_{m,r_0} \\ &\mathbf{Y}_{m,r} \in \mathbb{R}^{2Nm}\end{aligned} \tag{2.5.4}$$

, where:

$$\mathbf{A}' = \begin{bmatrix} \mathbf{0} & \mathbf{I}_r \\ -\mathbf{M}_r^{-1}\mathbf{K}_r^{p.e.} & -\mathbf{M}_r^{-1}(\mathbf{C}_r^{p.e.} + \mathbf{G}_r) \end{bmatrix}, \mathbf{B}' = \begin{bmatrix} \mathbf{0} \\ \mathbf{M}_r^{-1} \end{bmatrix} \tag{2.5.5}$$

It is now observed that equations (3.3.1) - (3.3.2) , (3.3.4) clearly define a non-linear autonomous system of first order O.D.E.s. This type of problems can be handled by the orthogonal collocation method.

Furthermore, in order to couple the non-linear model of the parametrically excited G.F.B.s to the rotor model, the top foil deformations given by (2.3.6) are now normalized according to the equations (2.1.9) - (2.1.10):

$$\bar{q}_r^{nl} = \frac{q_r}{c_r}, \dot{\bar{q}}_r^{nl} = \frac{\dot{q}_r}{c_r \Lambda} \tag{2.5.6}$$

The aforementioned deformation is considered positive when it is developed towards the outer side of the bearing. Therefore, equation (2.1.12) is converted to:

$$\bar{p}_m = \bar{c}_f\left(\dot{\bar{q}} - \dot{\bar{q}}_r^{nl}\right) + \bar{k}_f\left(\bar{q} - \bar{q}_r^{nl}\right) \tag{2.5.7}$$

Then, the procedure already described in 3.2 is followed, without considering the unbalance forces $\overline{\mathbf{F}}_m^U$. Therefore, it is considered that both the linear and the non-linear parametrically excited rotor-bearing model can be written as:

$$\begin{aligned} \dot{\mathbf{y}} &= \mathbf{f}\left(\mathbf{y}, \Omega\right) \\ \mathbf{y}\left(\xi_0, 0, \Omega\right) &= \mathbf{y}\left(\xi_0, T, \Omega\right) \end{aligned} \tag{2.5.8}$$

, where Ω stands for the rotating speed of the rotor, the bifurcation parameter, ξ_0 is the initial state vector which belongs to the solution curve $\mathbf{y}$ and T is the unknown period of the solution. According to the orthogonal collocation rules, time t is rescaled to $[0,1]$ and equation (3.3.8) is rewritten as:

$$\begin{aligned} \dot{\mathbf{y}} &= T\mathbf{f}\left(\mathbf{y}, \Omega\right) \\ \mathbf{y}\left(\xi_0, 0, \Omega\right) &= \mathbf{y}\left(\xi_0, 1, \Omega\right) \end{aligned} \tag{2.5.9}$$

Since the period T is unknown, an additional equation, the so called phase condition is required:

$$\phi = \int_0^1 \left\langle \mathbf{y}, \dot{\mathbf{y}}_0 \right\rangle dt = 0 \tag{2.5.10}$$

, where $\left\langle \mathbf{y}, \dot{\mathbf{y}}_0 \right\rangle$ denotes the scalar product of the unknown solution and the time derivative of the previous solution. If the arc-length s is used as a continuation parameter, then as previously stated the rotating speed Ω is unknown too. Thus, an additional equation is required, the so called pseudo arc-length condition:

$$\psi = \int_0^1 \left\langle \mathbf{y} - \mathbf{y}_0, \mathbf{y}_0' \right\rangle dt + \left(T - T_0\right) T_0' + \left(\Omega - \Omega_0\right) \Omega_0' - \Delta s = 0 \tag{2.5.11}$$

, where $\left(\right)'$ denotes the derivative with respect to the arc-length.

The vector containing the unknowns is defined as $\mathbf{u} = \left(\mathbf{y}, T, \Omega\right)^T$ and equations (3.3.9) - (3.3.11) can be written as:

$$\mathbf{H}\left(\mathbf{u}\right) = \begin{Bmatrix} \mathbf{F}(\mathbf{u}) \\ \phi\left(\mathbf{y}\right) \\ \psi\left(\mathbf{u}\right) \end{Bmatrix} = \mathbf{0} \tag{2.5.12}$$

The system of non-linear equations (3.3.12) can be solved by means of a standard iterative method, such as Newton – Raphson method:

$$\mathbf{u}^{i+1} = \mathbf{u}^i - \left[\mathbf{A}(\mathbf{u}^i)\right]^{-1} \mathbf{H}\left(\mathbf{u}^i\right) \tag{2.5.13}$$

, where:

$$\mathbf{A}(\mathbf{u}) = \begin{bmatrix} \dfrac{\partial \mathbf{F}}{\partial \mathbf{y}} & \dfrac{\partial \mathbf{F}}{\partial T} & \dfrac{\partial \mathbf{F}}{\partial \Omega} \\ \dfrac{\partial \phi}{\partial \mathbf{y}} & 0 & 0 \\ \mathbf{y}_0' & T_0' & \Omega_0' \end{bmatrix} \tag{2.5.14}$$

The procedure is iterated until a convergence criterion, inserted by the user, is satisfied. The arc-length derivatives for subsequent continuation steps can be calculated by backward differences. The main goal is to discretize properly in time and thereby calculate $\mathbf{A}$. To this end, the orthogonal collocation at Gauss-Legendre points with piece-wise polynomials is used. A brief overview of the method is given below. The time interval $[0,1]$ is discretized into N time sub-intervals. For the i^{th} sub-interval the collocation equations must be assembled at the following time nodes:

$$t_{i,j} = t_i + h_i \rho_j \tag{2.5.15}$$

, where h_i denotes the length of the time sub-interval and ρ_j is chosen as a zero of the m^{th} order Legendre polynomial. At the above time nodes must be provided an initial solution $\mathbf{y}_{i,j}$, the time derivatives $T\mathbf{f}\left(\mathbf{y}_{i,j}\right)$, the Jacobian matrix $\dfrac{\partial \mathbf{f}\left(\mathbf{y}_{i,j},\Omega\right)}{\partial \mathbf{y}}$ and finally the derivatives with respect to the bifurcation parameter $\dfrac{\partial \mathbf{f}\left(\mathbf{y}_{i,j},\Omega\right)}{\partial \Omega}$.

The initial solution can be extracted at the global time nodes as:

$$\begin{aligned} \mathbf{y}_{i,j} &= \mathbf{y}_i + h_i \sum_{l=1}^{m} a_{j,l} \mathbf{f}_{i,l} \\ \mathbf{y}_{i+1} &= \mathbf{y}_i + h_i \sum_{l=1}^{m} \beta_l \mathbf{f}_{i,l} \end{aligned} \tag{2.5.16}$$

, where $a_{j,l}, \beta_i$ are the quadratic weights. Therefore, the quasi-linearized two-point B.V.P. can be written as shown below:

$$\begin{aligned} &\Delta \dot{\mathbf{y}}_{i,j} = T \frac{\partial \mathbf{f}}{\partial \mathbf{y}}\left(\mathbf{y}_{i,j},\Omega\right)\Delta \mathbf{y}_{i,j} + \mathbf{f}\left(\mathbf{y}_{i,j},\Omega\right)\Delta T + T \frac{\partial \mathbf{f}}{\partial \Omega}\left(\mathbf{y}_{i,j},\Omega\right)\Delta\Omega + \mathbf{r}_{i,j} \\ &\mathbf{y}_{N+1} - \mathbf{y}_1 = 0 \end{aligned} \tag{2.5.17}$$

, where:

$$\mathbf{r}_{i,j} = T\mathbf{f}\left(\mathbf{y}_{i,j},\Omega\right) - \dot{\mathbf{y}}_{i,j} \tag{2.5.18}$$

In order to eliminate the local unknowns at every time interval, parameter condensation is applied. In other words, equations (3.3.16) are substituted in (3.3.17) - (3.3.18):

$$\mathbf{f}_i\left(\Delta\mathbf{y}_{i,j}\right)=\mathbf{f}\left(\Delta\mathbf{y}_i+h_i\sum_{l=1}^{m}a_{j,l}\mathbf{f}_{i,l}\right)=T\frac{\partial\mathbf{f}}{\partial\mathbf{y}}\left(\mathbf{y}_{i,j},\Omega\right)\Delta\mathbf{y}_{i,j}+$$
$$+T\frac{\partial\mathbf{f}}{\partial\mathbf{y}}\left(\mathbf{y}_{i,j},\Omega\right)h_i\sum_{l=1}^{m}a_{j,l}\mathbf{f}_{i,l}+\mathbf{f}\left(\mathbf{y}_{i,j},\Omega\right)\Delta T\frac{\partial\mathbf{f}}{\partial\Omega}\left(\mathbf{y}_{i,j},\Omega\right)\Delta\Omega+\mathbf{r}_{i,j} \tag{2.5.19}$$

Equation (3.3.19) can be written in a matrix form:

$$\mathbf{f}_i=\mathbf{W}_i^{-1}\mathbf{V}_i\Delta\mathbf{y}_i+\mathbf{W}_i^{-1}\mathbf{U}_i\Delta T+\mathbf{W}_i^{-1}\mathbf{S}_i\Delta\Omega+\mathbf{W}_i^{-1}\mathbf{q}_i \tag{2.5.20}$$

, where:

$$\mathbf{W}_i=\mathbf{I}-h_i\begin{bmatrix}a_{11}T\frac{\partial\mathbf{f}}{\partial\mathbf{y}}\left(\mathbf{y}_{i,1},\Omega\right) & \cdots & a_{1m}T\frac{\partial\mathbf{f}}{\partial\mathbf{y}}\left(\mathbf{y}_{i,1},\Omega\right)\\ \vdots & \ddots & \vdots\\ a_{1m}T\frac{\partial\mathbf{f}}{\partial\mathbf{y}}\left(\mathbf{y}_{i,m},\Omega\right) & \cdots & a_{mm}T\frac{\partial\mathbf{f}}{\partial\mathbf{y}}\left(\mathbf{y}_{i,m},\Omega\right)\end{bmatrix} \tag{2.5.21}$$

$$\mathbf{V}_i=\begin{bmatrix}T\frac{\partial\mathbf{f}}{\partial\mathbf{y}}\left(\mathbf{y}_{i,1},\Omega\right)\\ \vdots\\ T\frac{\partial\mathbf{f}}{\partial\mathbf{y}}\left(\mathbf{y}_{i,m},\Omega\right)\end{bmatrix} \tag{2.5.22}$$

$$\mathbf{U}_i=\begin{bmatrix}\mathbf{f}\left(\mathbf{y}_{i,1},\Omega\right)\\ \vdots\\ \mathbf{f}\left(\mathbf{y}_{i,m},\Omega\right)\end{bmatrix} \tag{2.5.23}$$

$$\mathbf{S}_i=\begin{bmatrix}T\frac{\partial\mathbf{f}}{\partial\Omega}\left(\mathbf{y}_{i,1},\Omega\right)\\ \vdots\\ T\frac{\partial\mathbf{f}}{\partial\Omega}\left(\mathbf{y}_{i,m},\Omega\right)\end{bmatrix} \tag{2.5.24}$$

$$\mathbf{q}_i=\begin{bmatrix}T\mathbf{f}\left(\mathbf{y}_{i,1},\Omega\right)-\mathbf{f}_{i,1}\\ \vdots\\ T\mathbf{f}\left(\mathbf{y}_{i,m},\Omega\right)-\mathbf{f}_{i,m}\end{bmatrix} \tag{2.5.25}$$

Substituting equations (3.3.20) - (3.3.25) to (3.3.16) and adding the pseudo arc-length continuation equations, yields the linear algebraic system for the combined collocation – pseudo arc-length continuation method:

$$
\begin{bmatrix}
-\boldsymbol{\Gamma}_1 & \mathbf{I} & \mathbf{0} & \cdots & \cdots & \mathbf{0} & -\boldsymbol{\Lambda}_1 & -\boldsymbol{\Sigma}_1 \\
\mathbf{0} & \boldsymbol{\Gamma} & -\mathbf{I}_2 & \mathbf{0} & & \cdots & \mathbf{0} & \boldsymbol{\Lambda} \\
\vdots & \ddots & \ddots & \ddots & \ddots & \vdots & \vdots & \vdots \\
\mathbf{0} & \boldsymbol{\Gamma} & \cdots & \mathbf{I} & \mathbf{0} & -\mathbf{0}_{N-1} & \boldsymbol{\Lambda} & \boldsymbol{\Sigma} \\
\mathbf{0} & \boldsymbol{\Gamma} & \mathbf{0} & \mathbf{I} & \cdots & \boldsymbol{\Lambda} & \mathbf{0} & \boldsymbol{\Sigma}_N \\
\mathbf{I} & \mathbf{0} & \cdots & \cdots & \mathbf{0} & -\mathbf{I} & \mathbf{0} & \mathbf{0} \\
h_1\mathbf{y}_1 & h_2\mathbf{y}_2 & \cdots & \cdots & h_N\mathbf{y}_N & \mathbf{0} & \mathbf{0} & \mathbf{0} \\
h_1\mathbf{y}_1'^0 & h_2\mathbf{y}_2'^0 & \cdots & \cdots & h_N\mathbf{y}_N'^0 & \mathbf{0} & T'^0 & \Omega'^0
\end{bmatrix}
\begin{Bmatrix}
\Delta\mathbf{y}_1 \\ \Delta\mathbf{y}_2 \\ \vdots \\ \Delta\mathbf{y}_{N-1} \\ \Delta\mathbf{y}_N \\ \Delta\mathbf{y}_{N+1} \\ \Delta T \\ \Delta\Omega
\end{Bmatrix} =
$$

$$
= \begin{Bmatrix}
\mathbf{r}_1 \\ \mathbf{r}_2 \\ \vdots \\ \mathbf{r}_{N-1} \\ \mathbf{r}_N \\ \mathbf{y}_{N+1} - \mathbf{y}_N \\ \sum_{i=1}^{N} h_i \left\langle \mathbf{y}_i, \dot{\mathbf{y}}_i^0 \right\rangle \\ \sum_{i=1}^{N} h_i \left\langle \mathbf{y}_i - \mathbf{y}_i^0, \mathbf{y}_i'^0 \right\rangle + \left(T - T_0\right) T'^0 + \left(\Omega - \Omega_0\right) \Omega'^0 - \Delta s
\end{Bmatrix} \tag{2.5.26}
$$

, where:

$$
\boldsymbol{\Gamma}_i = \mathbf{I} + h_i \begin{bmatrix} \beta_1 \mathbf{I} & \cdots & \beta_m \mathbf{I} \end{bmatrix} \mathbf{W}_i^{-1} \mathbf{V}_i \tag{2.5.27}
$$

$$
\boldsymbol{\Lambda}_i = h_i \begin{bmatrix} \beta_1 \mathbf{I} & \cdots & \beta_m \mathbf{I} \end{bmatrix} \mathbf{W}_i^{-1} \mathbf{U}_i \tag{2.5.28}
$$

$$
\boldsymbol{\Sigma}_i = h_i \begin{bmatrix} \beta_1 \mathbf{I} & \cdots & \beta_m \mathbf{I} \end{bmatrix} \mathbf{W}_i^{-1} \mathbf{S}_i \tag{2.5.29}
$$

$$
\mathbf{r}_i = h_i \begin{bmatrix} \beta_1 \mathbf{I} & \cdots & \beta_m \mathbf{I} \end{bmatrix} \mathbf{W}_i^{-1} \mathbf{q}_i \tag{2.5.30}
$$

The solution can be achieved by various methods. Iterative methods are applied in this work. Floquet multipliers are evaluated as the eigenvalues of the matrix $\Gamma_1 \cdot \Gamma_2 \cdots \Gamma_N$ when the solution of the linear algebraic system is determined. Calculating the Floquet multipliers in this way severely reduces the evaluation time compared to other methods, such as shooting method.

4. RESULTS AND DISCUSSION

In this chapter, several results concerning the validity of the novel method for the prediction of the stiffness and damping coefficients for a G.F.B. are presented. Ever since the validity of the method is ensured, the stiffness and damping coefficients for a parametrically excited G.F.B. can extensively be studied. More specifically, results concerning the influence of the amplitude and the frequency of the predefined displacements of the deformable ring on the equivalent stiffness and damping coefficients of the G.F.B. are presented and properly commented. Given the fact that the stiffness and damping coefficients of a periodically excited G.F.B. are similar to those given be the equations (2.3.1) - (2.3.2) the stability maps for the linear and the non – linear approach of parametrically excited rotor – bearing models can be compared. Special emphasis has been given on the bearing and rotor properties which enhance parametric anti – resonances.

4.1 Validation of the stiffness and damping coefficients for G.F.B.s

In this section the validity of the method for the calculation of the stiffness and damping coefficients for a G.F.B. is proved. In other words, the procedure thoroughly described in section 2.2 was followed and the results are compared to the respective results carried out by J. P. Peng and M. Carpino[48] and H. Heshmat et.al.[49]. The bearing properties as well as the number of mesh points in both the circumferential and axial direction are presented in *Table 4.1.1*. It should be noted that the aforementioned discretization was selected according to a sensitivity analysis based on the integration of the pressure distribution over the bearing surface.

Table 4.1.1 *Constant parameters for the validation process*

Parameters	***Values***
Ambient pressure, $p_0\left[N/m^2\right]$	10^5
Viscosity, $\mu\left[mNs/m^2\right]$	0.018
Radius of the bearing, $R\left[m\right]$	0.015
Length of the bearing, $L_b\left[m\right]$	0.03
Clearance, $c_r\left[m\right]$	$3.106\cdot10^{-5}$
Starting/ending angle, $\chi\left[rad\right]$	$\pi/2$
Mesh intervals in circ. Direction, $N_{\bar{x}}$	43
Mesh intervals in axial Direction, $N_{\bar{z}}$	23

In *Figure 4.1.1*, the predictions of the four stiffness coefficients are depicted for three different cases of the dimensionless compliance $\bar{a}_f$ and for three different values of the bearing number Λ. It should be noted that according to J. P. Peng and M. Carpino zero compliance is not identical to rigid foil as in the case of former the top foil is not loosing contact to the foundation when sub – ambient pressure occurs. It can easily be observed that

[48] ***J. P. Peng, M. Carpino.*** *calculation of stiffness and damping coefficients for elastically supported gas foil bearings. Journal of Tribology. 115, pp. 20-27.*

[49] ***H. Heshmat, J. A. Walowit, O. Pinkus.*** *Analysis of gas-lubricated foil journal bearings. Journal of Lubrication Technology. 1983.*

the predictions show very good agreement if the foil is not assumed rigid. Actually in case of zero compliance (or according to J. P. Peng and M. Carpino in case of rigid foil) slight discrepancies are observed and a possible explanation can be found in the numerous differences between the current method and that proposed by them (F.E. method and two less equations for the prediction of the equilibrium position).

In general, the four stiffness coefficients of the G.F.B are decreased as the compliance is increased, due to the increased deflection of the top foil. Furthermore, in case of $\bar{a}_f = 1, \bar{a}_f = 5$ and at low rotating speeds which means small bearing numbers something quite interesting occurs. The compliance of the overall bearing depends on the lubricant film which is rather softer than the so-assumed elastic foundation. This is demonstrated by the four stiffness coefficients which tend to approach the same value, independent to the foil's compliance. In contrast, at high rotating speeds or large bearing numbers the compliance of the overall bearing depends on the elastic foundation. This is demonstrated by the four stiffness coefficients which tend to be constant at high speeds independent to the foil's compliance. Finally as it was expected in case of $\bar{a}_f = 0$ the four stiffness coefficients are solely a function of the lubricant film. These observations will be proved of significant importance, when the stability margins of the whole rotor – bearing model will be examined.

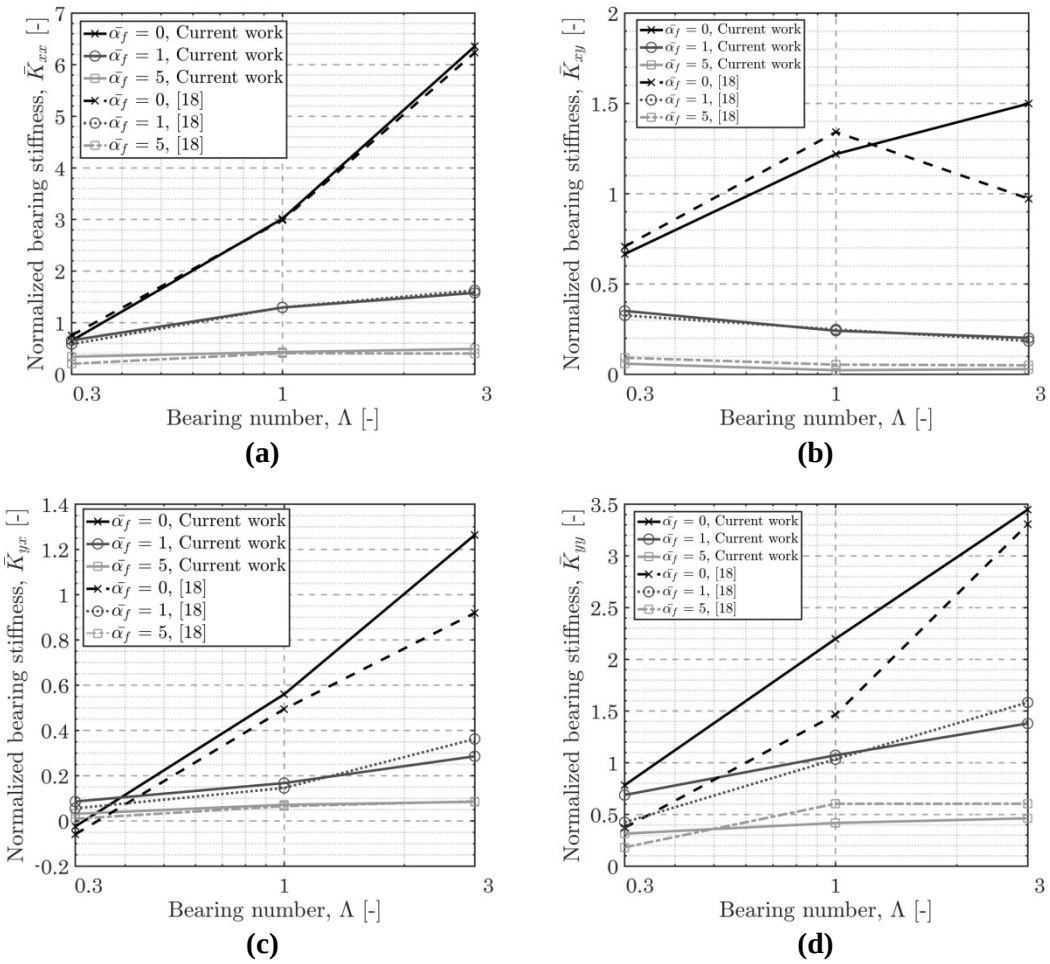

Figure 4.1.1 *Comparison of normalized bearing stiffness coefficient* ***(a)*** $\bar{K}_{xx}$ ***(b)*** $\bar{K}_{xy}$ ***(c)*** $\bar{K}_{yx}$ ***(d)*** $\bar{K}_{yy}$

In *Figure 4.1.2* the predictions of the four damping coefficients are depicted for the same three cases of the dimensionless compliance $\bar{a}_f$ and the same three values of the bearing

number Λ . It is again easily observed that the damping coefficients decrease as the compliance is increased due to the increased deflection of the foil. Furthermore, as stiffness coefficients clearly depict, at low rotating speeds the complinace of the overall bearing depends on the lubricant film. This is the reason why all four damping coefficients approach the same value for small bearing numbers independent of the compliance of the foundation. Finally, as one may observe damping coefficients decrease at higher rotating speeds due to the increased stiffness of the gas film which prevents energy dissipation.

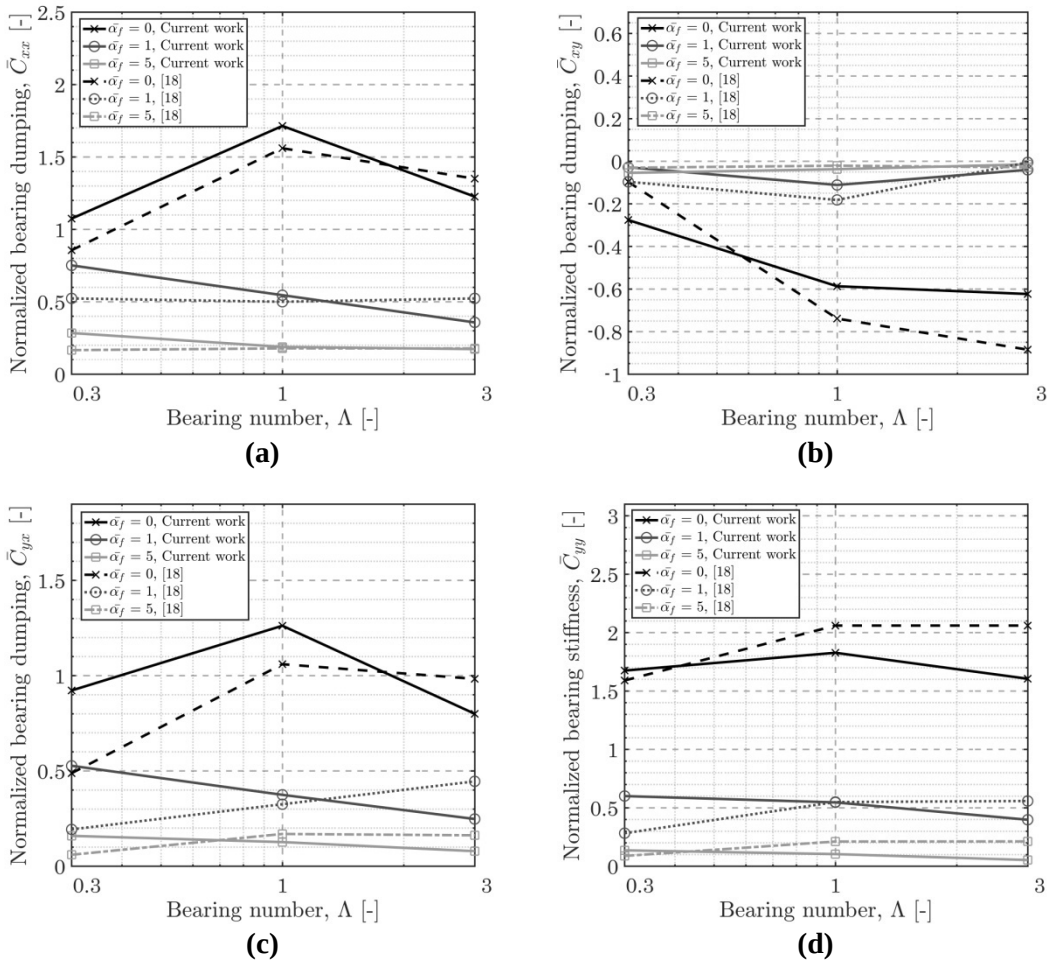

Figure 4.1.2 *Comparison of normalized bearing damping coefficient* ***(a)*** $\bar{C}_{xx}$ ***(b)*** $\bar{C}_{xy}$ ***(c)*** $\bar{C}_{yx}$ ***(d)*** $\bar{C}_{yy}$

H. Heshmat et. al. have computed the stiffness coefficients for three different values of Sommerfeld number S and for two different cases of the dimensionless compliance $\bar{a}_f$ (*Figure 4.1.3*). In each operating condition finite numerical perturbations are applied in a static model. It should be mentioned that the Cartesian coordinate system used by H. Heshmat is different from the one used in current work. Therefore, in order to make clear comparisons those values reported by H. Heshmat are converted to the coordinate system used now. As one may observe there are significant discrepancies in the predictions of stiffness coefficients even though the steady state properties of all three approaches show sufficiently good agreement. These discrepancies increase in the calculation of cross couple terms and in the cases of low eccentricity ratios. An explanation can be found in the difference between the three approaches. First of all, H. Heshmat et. al. neglect any damping effect in the bearing since a static model has been utilized. In addition, if sub – ambient pressure occurs for a

specificate value of the circumferential coordinate ϑ_p the film thickness is equalized to the thickness evaluated at ϑ_{p-1}.

J. P. Peng and M. Carpino on the other hand, if sub – ambient pressure occurs, permit negative top – foil's displacements. Additionally in the case of formers, the equilibrium position of the journal has been evaluated neglecting (2.2.18) - (2.2.19) and using a F.E. method. In any case, the results of current work lie between the results by J. P. Peng, M. Carpino and H. Heshmat et. al.

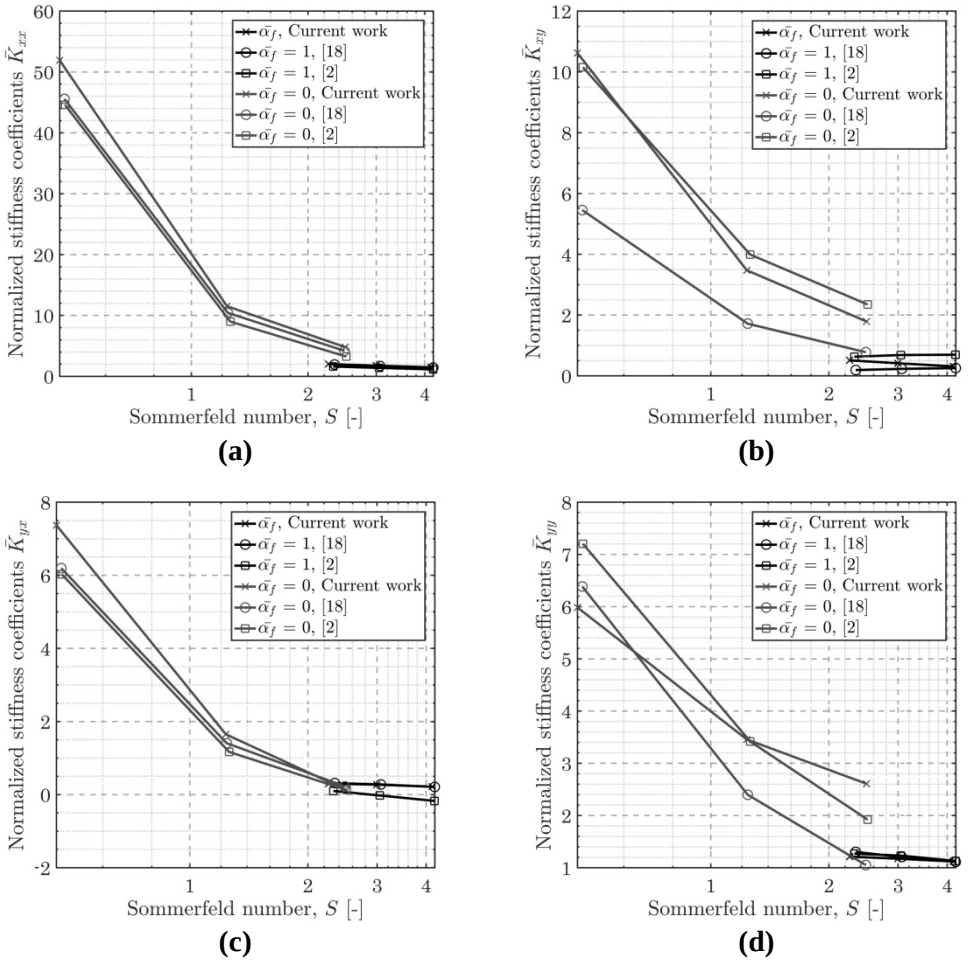

Figure 4.1.3 *Comparison of normalized bearing stiffness coefficient* ***(a)*** $\bar{K}_{xx}$ ***(b)*** $\bar{K}_{xy}$ ***(c)*** $\bar{K}_{yx}$ ***(d)*** $\bar{K}_{yy}$

The last and most important validation test is the comparison of the dynamic characteristics of three different analytical models. The first analytical model is the reduced non – linear one, thoroughly described in 2.1, which includes the Guyan reduction method and the Reynolds equation reduction method. The second model is the reduced linear one, thoroughly described in 2.2, according to which the bearing forces are evaluated via the four stiffness and four damping coefficients and the behavior of the rotor can be approximated by the static reduction method. Finally, the third analytical model is the full linear one, which just includes the linearized stiffness and damping coefficients of the bearings. In other words, the last validation test ensures the validity of the Guyan reduction method, the Reynolds equation reduction method and the linearized stiffness and damping coefficients.

The reference key properties of the rotor's analytical model are presented in *Table 4.1.2*.

Table 4.1.2 *Reference key properties of the rotor*

Property	***Value***
Slenderness ratio, $SR[-]$	20
Bearing span, $L_s\,[m]$	0.37
Young's modulus, $E\,[GPa]$	70
Rotor's mass, $m_r\,[Kg]$	2.51
Shaft's mass, $m_s\,[Kg]$	1.11
Natural frequency of the equivalent, rigidly supported Jeffcott rotor, $\omega_n\,[rad/s]$	1000

In the beginning of the section, some constant parameters regarding the physical properties of the bearings and the number of mesh points in both the axial and the circumferential direction are given. To an extension, some extra properties regarding the static load and the bump foil's compliance and loss factor are presented in *Table 4.1.3*.

Table 4.1.3 *Bearings' extra properties for the validation process*

Property	***Value***
Non – dimensional static load at bearings, $\overline{W}_{st}\,[-]$	0.5
Non – dimensional structural compliance, $\overline{a}_f\,[-]$	1
Loss factor, $\eta[-]$	0.1

In *Figure 4.1.4* **(a), (b)** the unbalance response of both the horizontal and vertical degree of freedom at first gas – foil bearing's node is depicted respectively. For all the three cases single unbalance of grade G1 is considered. It is more than obvious that the unbalance grade is low in order not to trigger strongly non – linear bearing forces, or in other words in order to keep the journal's orbit sufficiently close to its equilibrium position. In the case of linear analytical models, the responses are evaluated via the Linear Harmonic Analysis (described in Linear Harmonic Analysis3.1) and in the case of the non – linear model the response is calculated via Time Integration (described in 3.2) considering low rotating acceleration. Sufficiently good agreement between the three models is observed until the threshold rotating speed of instability. Resonance frequencies are identical among the three models while resonance amplitudes appear very similar. The negligible discrepancies arise from the imperfect estimation of the damping ratio of the non – linear analytical model.

Linear Harmonic Analysis (described in Linear Harmonic Analysis3.1) provides an estimation of the eigenvalues and the corresponding eigenvectors of the linear system. Each eigenvalue has its own damped natural frequency and its own stability factor which is directly related to its logarithmic decrement δ . In turn, logarithmic decrement is directly related to the damping ratio of the corresponding eigenvalue. In the case of the non – linear analytical model, all the aforementioned information is accessed via a linearization around an equilibrium position. The comparison of the results is depicted in *Figure 4.1.4* **(c)**. As one may easily observe the damped natural frequencies of all the three cases and of all modes are

almost identical but the corresponding damping ratios are not. As explained before, these slight discrepancies arise from the imperfect calculation of the linearized stiffness and damping coefficients.

It is of significant importance to note that in case of such structural compliance as in *Table 4.1.3* low damping ratios is expected to be predicted. Therefore, either the structural compliance should be lower or the perturbation method thoroughly described in 2.2 should consider the top – foil deformation too.

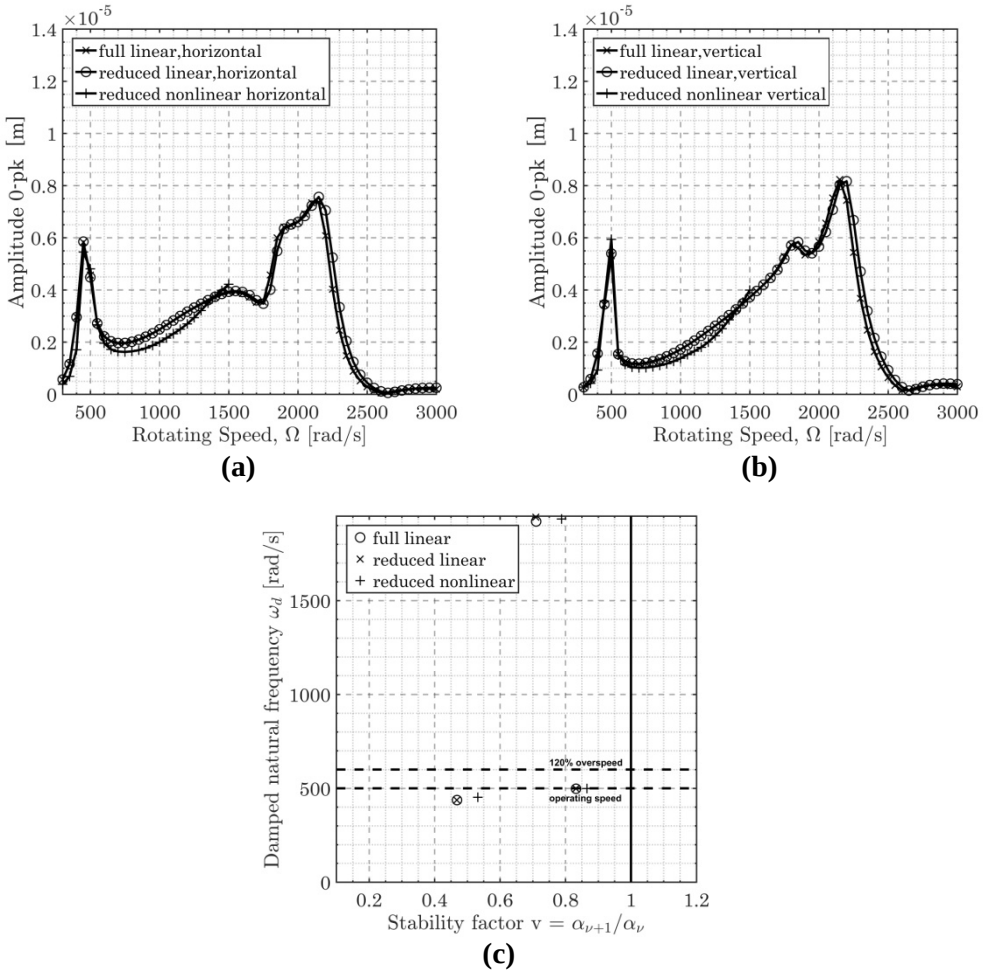

Figure 4.1.4 (a), (b) *GFB #1 journal unbalance response with single unbalance G1* ***(c)*** *Stability factor v of the modes of the system when operating at 500 rad/s*

4.2 Stiffness and damping coefficients for parametrically excited G.F.B.s

It is supposed that the validity of the derivation of the method for the linearized stiffness and damping coefficients is ensured. In this section results regarding the implementation of parametric excitation (described in 2.3) are presented. More specifically, the capability of achieving the desirable amplitude ratios and excitation frequencies (for the stiffness and damping coefficients) under the effect of the predefined periodic deformation of the ring is investigated. Therefore, the main purpose of the section is to determine the appropriate dh, dv given by (2.3.4) which will be then tested again by the non – linear approach of the elastoaerodynamic approach. If parametric antiresonance occurs for both linear and the non – linear approach then the main goal of this Master thesis is achieved.

In Figure 4.2.1 the variation of the stiffness coefficients for three different values of the bearing number and for three different cases of the excitation frequency is depicted. The bearing's properties are already presented in *Table 4.1.1*, *Table 4.1.3* while the horizontal maximum displacement of the outer ring is $dh = 0.005 \cdot c_r$. The normalization of the excitation frequency has been done using the rated rotating speed of the rotor $\Omega_r = 1000[rad/s]$.

It is expected that the mean value of these coefficients (calculated for low excitation frequency) for a fixed bearing number to be equal to the corresponding coefficient of the previous section, due to the low amplitude of the deformation of the ring. As one may easily observe this is not verified, due to the formulation of the vertical periodic load which is depicted in *Figure 2.3.1*. It is of significant importance to note once more that the aforementioned load is given by:

$$F = F_0\left[1+\varepsilon \sin\left(\Omega_{ex} t\right)\right] \tag{3.2.1}$$

Thus, the mean value of the ring's deformation is not equal to zero and the mean equilibrium position as well as the mean value of the stiffness and damping coefficients is affected. In addition, it is observed that all four stiffness coefficients reach their maximum value at $\Omega_{ex} t = \pi, [rad]$, when the ring's deformation reaches its mean value with maximum negative radial velocity. This effect can be interpreted. First of all, in equation (2.3.8) the most important term which disturbs the predefined equilibrium position is the term containing the radial velocity of the ring, due to the high value of the excitation frequency? Thus, when this term becomes negative, the equilibrium position is removed from the bearing's centre and the corresponding stiffness coefficients are higher. Due to the same reason, the amplitude of all the stiffness coefficients gets higher as the excitation frequency gets higher. Finally it can be concluded that the direct couple terms are much more affected by the ring's deformation than the cross couple ones.

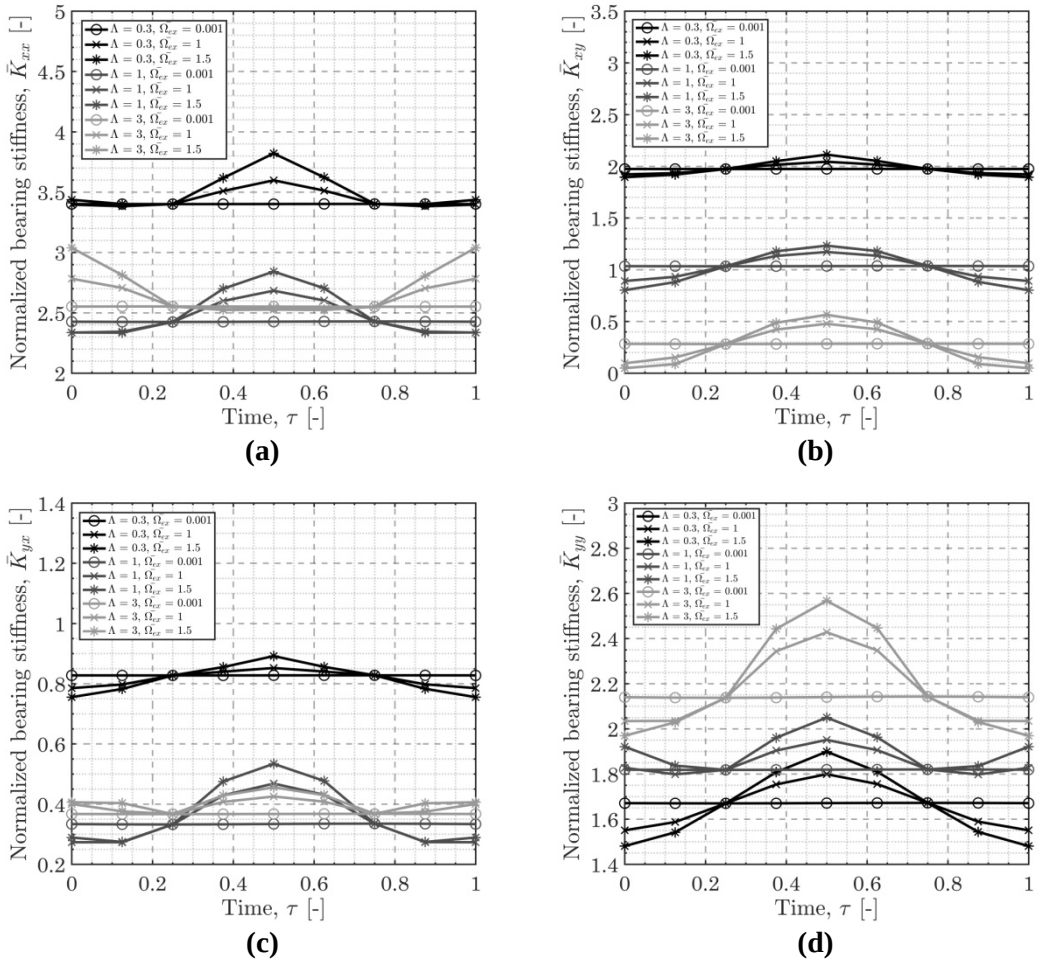

Figure 4.2.1*Variation of stiffness coefficient under the effect of ring's periodic deformation with horizontal amplitude* $dh = 0.005 \cdot c_r$ ***(a)*** $\bar{K}_{xx}$ ***(b)*** $\bar{K}_{xy}$ ***(c)*** $\bar{K}_{yx}$ ***(d)*** $\bar{K}_{yy}$

In Figure 4.2.2 the corresponding damping coefficients for the same three values of the bearing number and for the same three cases of the excitation frequency are presented. The bearing's configuration as well as the ring's deformation remains the same. As thoroughly explained in the previous paragraph, the mean value of these coefficients (calculated for low excitation frequency) for a fixed bearing number is not equal to the corresponding coefficient of the previous section. In addition, at low bearing numbers the complinace of the bearing depends on the lubricant film thus the main source of energy dissipation is the hydrodynamic gas film itself. In contradiction, at higher bearing numbers the compliance of the bearing depends on the structural compliance thus the most significant source of energy dissipation is the bump foil. The two different sources of energy dissipation is the reason why the damping coefficients do not systematically reach their minimum value at $\Omega_{ex} t = \pi, [rad]$.Of course, as the higher the excitation frequency is, the higher the variance of all damping coefficients is.

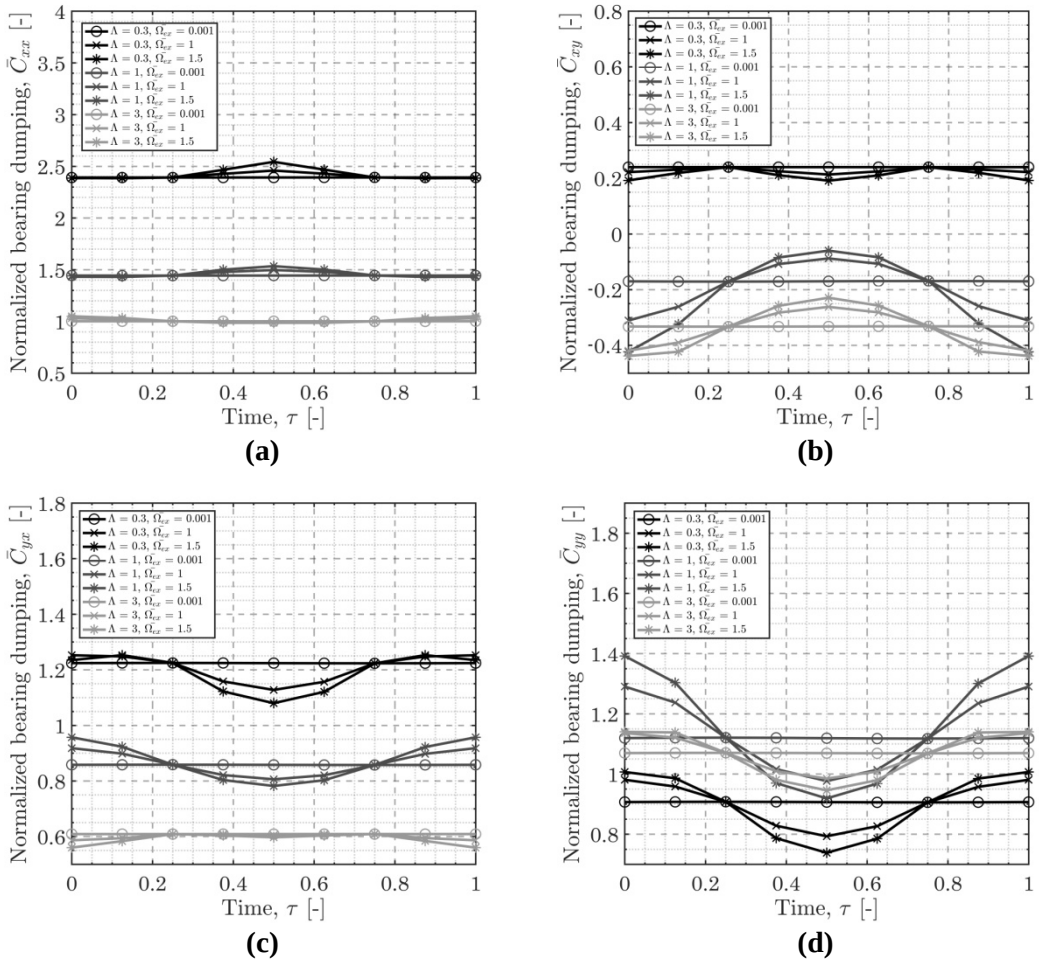

Figure 4.2.2*Variation of damping coefficients under the effect of ring's periodic deformation with horizontal amplitude* $dh = 0.005 \cdot c_r$ ***(a)*** $\bar{C}_{xx}$ ***(b)*** $\bar{C}_{xy}$ ***(c)*** $\bar{C}_{yx}$ ***(d)*** $\bar{C}_{yy}$

In Figure 4.2.3 and in Figure 4.2.4 all stiffness and damping coefficients are presented respectively for the same bearing's configuration but with one major discrepancy. The maximum horizontal displacement of the outer ring is $dh = 0.01 \cdot c_r$ which practically means that the mean value of the vertical periodic load is doubled. As one may suppose, the higher the former mean value is, the greater the affect of the equilibrium position is, the higher the variance of both stiffness and damping coefficients is. It is also observed that the mean values of both stiffness and damping coefficients are not notably affected by the increased maximum horizontal displacement of the ring (the term of deformable ring's radial velocity is still dominant). It is of significant importance to note that if the mean value of the vertical periodic load exceeds a predefined maximum value all the aforementioned observations are not valid, since the most important term in equation (2.3.8) is the term containing the ring's deformation.

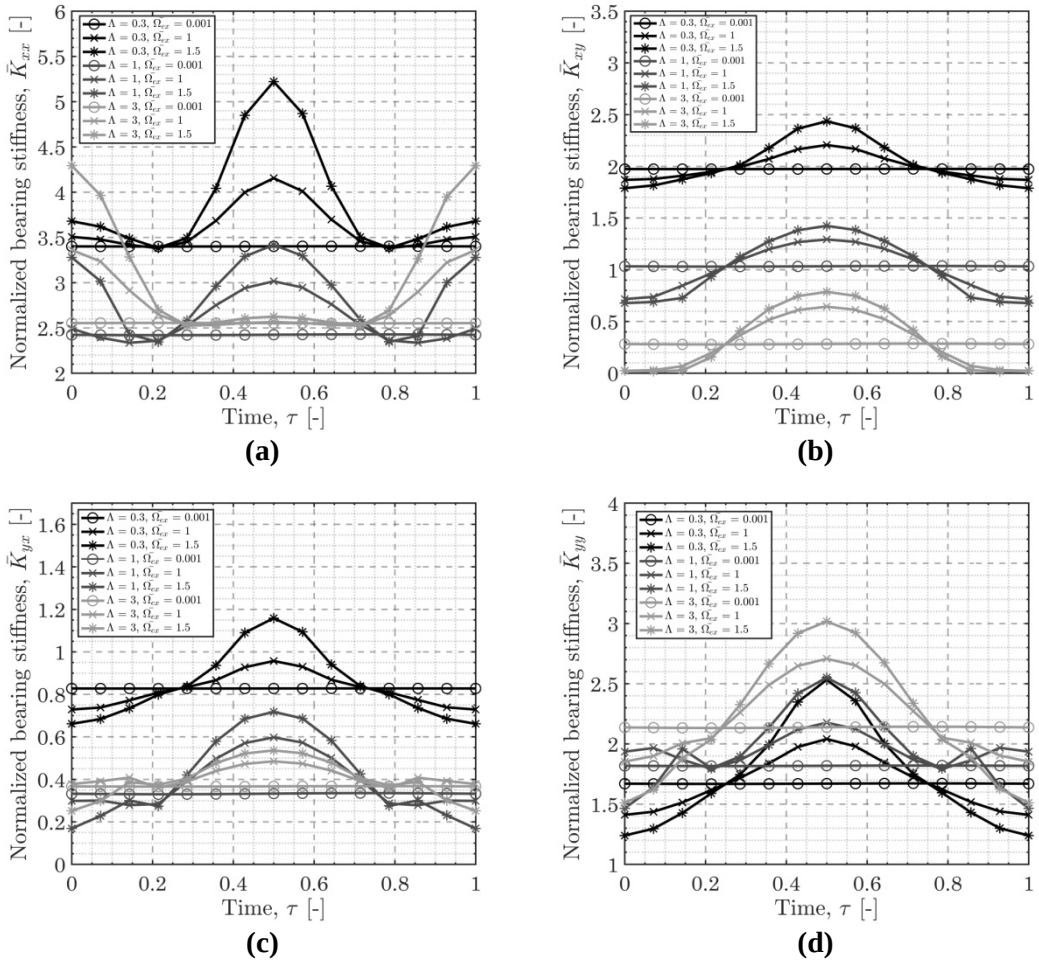

Figure 4.2.3*Variation of stiffness coefficients under the effect of ring's periodic deformation with horizontal amplitude* $dh = 0.01 \cdot c_r$ ***(a)*** $\bar{K}_{xx}$ ***(b)*** $\bar{K}_{xy}$ ***(c)*** $\bar{K}_{yx}$ ***(d)*** $\bar{K}_{yy}$

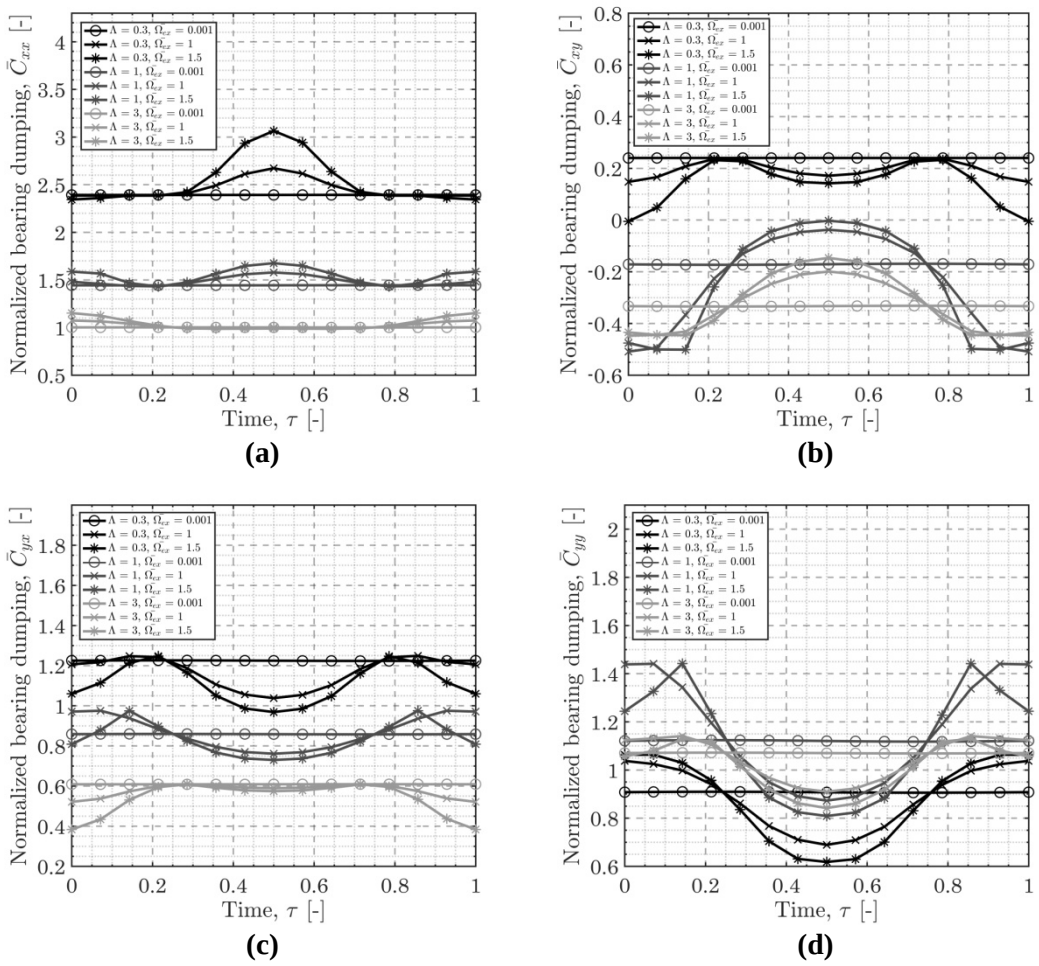

Figure 4.2.4 *Variation of damping coefficients under the effect of ring's periodic deformation with horizontal amplitude* $dh = 0.01 \cdot c_r$ ***(a)*** $\bar{C}_{xx}$ ***(b*** $\bar{C}_{xy}$ ***(c)*** $\bar{C}_{yx}$ ***(d)*** $\bar{C}_{yy}$

4.3 Stability maps for the linear and the non - linear approach of the parametrically excited rotor – bearing model

According to the previous section stiffness and damping coefficients can change periodically under the effect of a vertical periodic load. It is concluded that the frequency of such variation is the same as the frequency of the periodic load and the amplitude ratio strongly depends on the mean value of the vertical load and the excitation frequency itself. Furthermore, it is concluded that it is rather unrealistic to suppose that both stiffness and damping coefficients have the same amplitude ratio. Although it is observed that for the excitation frequencies of interest, a variation of $\delta \in [0.3 \;\; 0.4]$ is quite feasible. Finally it is concluded that synchronous stiffness and damping parametric excitation is not feasible as by default in present case, there are two different types of energy dissipation source.

In current section, the stability maps for the linear and the non – linear approach of the parametrically excited rotor – bearing model are presented. In the case of the linear approach, the bearing forces are calculated via the periodically changed stiffness and damping coefficients assuming no phase lug between them and assuming the same amplitude ratio for all of them (see (2.3.1) - (2.3.2)). Even if these assumptions are rather an oversimplification, they provide us a first impression about the excitation frequency and the amplitude ratios which finally lead to parametric antiresonance. Finally according to the aforementioned desirable excitation frequencies and amplitude ratios the non – linear stability threshold is calculated, proving that parametric antiresonance is feasible in G.F.B.s.

In *Figure 4.3.1* the maximum and minimum value of the periodic limit cycles of the response of the horizontal degree of freedom at the first G.F.B. is depicted for three ascending values of the amplitude ratio. The physical properties of the rotor and of the two identical bearings are already presented in *Table 4.1.1* - *Table 4.1.3*. The range of both the excitation frequency and the rotating speed is selected in order to physically interpret the phenomenon of parametric antiresonance. Black dots obviously denote stable periodic limit cycles and white dots denote unstable periodic limit cycles. All the periodic solutions have been evaluated via pseudo arc – length continuation method thoroughly described in 3.3 assuming a perfectly balanced rotor model (i.e. the only source of excitation is the periodically changing bearing's properties). This continuation scheme is implemented accounting the rotating speed as bifurcation parameter. The continuation among the excitation frequencies has been simplistically achieved via parameter continuation scheme. As aforementioned in 3.3 pseudo arc – length continuation method incorporates orthogonal collocation. The former, based on Floquet's theorem determines the stability of the periodic solution as well as the type of the bifurcation possibly occurs.

First of all, one may observe that stable periodic limit cycles are found in both low and high rotating speeds independent on the excitation frequency. The corresponding stability analysis clearly states that the transition from stable to unstable limit cycles in all excitation frequencies and rotating speeds is accompanied by Neimark – Sacker bifurcation. In other words, the eigenvalues of the monodromy matrix which have magnitude greater than one present both real and imaginary non – zero part. It is of great interest to see that as the amplitude ratio is increased, these Neimark – Sacker bifurcations come closer to each other and the stable periodic limit cycles become more. Finally, double Neimark – Sacker bifurcation occurs and the stability of the periodic solutions is restored. Figure 4.3.1 also proves that parametric excitation has beneficial effects to the quality of motion of the bearing – rotor system. Around a fundamental excitation frequency (e.g. the excitation frequency

around which parametric antiresonance occurs), as the amplitude ratio is increased, the extent of the corresponding periodic limit cycles is decreased. Finally it is of significant importance to note that the fundamental excitation frequency can be approximately evaluated by the formula:

$$\Omega_f \simeq \Omega_{cr2} - \Omega_{cr1} \tag{3.3.1}$$

, where Ω_{cr} denotes the critical speed of the system, approximately depicted in *Figure 4.1.4* (due to the damping ratio of the modes). This notation shows full agreement with[50].

[50] ***F. Dohnal, H. Ecker, H. Springer.*** *Enhanced damping of a cantilever beam by axial parametric excitation. Archive of Applied Mathematics. December 2008.*

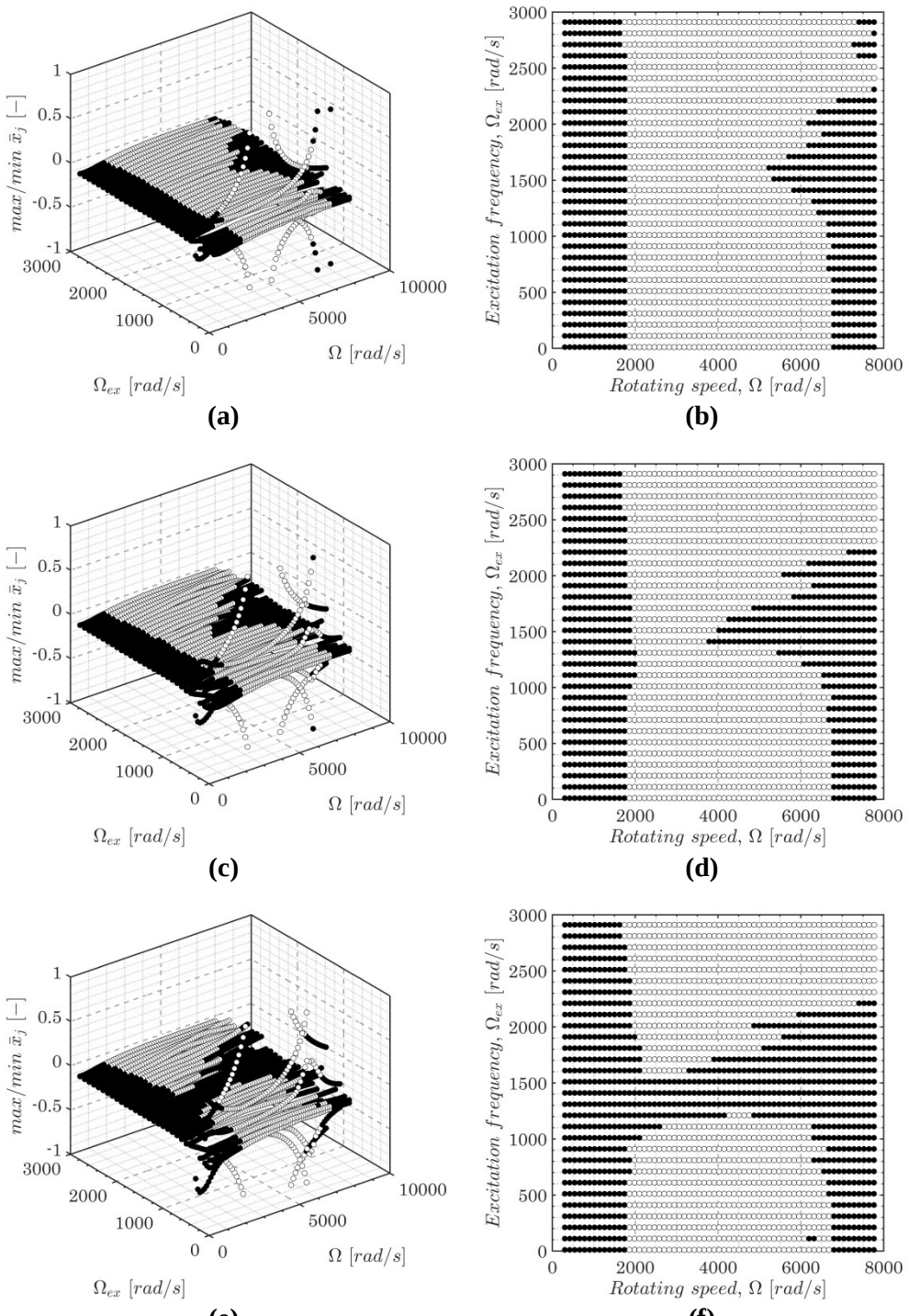

Figure 4.3.1 *Stability maps according to the linear approach of the elastoaerodynamic lubrication problem for the reference rotor – bearing model* ***(a), (b)*** $\delta = 0.2$ ***(c), (d)*** $\delta = 0.3$ ***(e), (f)*** $\delta = 0.4$

In *Figure 4.3.2* the maximum and minimum of the periodic limit cycles of the response of the horizontal degree of freedom at the first G.F.B. is depicted again, for two ascending values of the amplitude ratio. The one and only discrepancy is the value of the non – dimensional structural compliance, which now is $\overline{a}_f = 0.01$. As mentioned in the previous section, the reason of the phase lag between the periodically changing damping coefficients is the two different types of energy dissipation. If the bump foil becomes stiffer, the amplitude of the top – foil deformation is lower thus the amount of dissipated energy (due to the structural damping) is lower. It is then expected that all four damping coefficients mainly depend on the gas film, thus no phase lug between them exists (still the excitation is not synchronous since stiffness and damping coefficients do not reach their maximum value simultaneously). All the aforementioned observations regarding the quality of the periodic limit cycles are validated. The stability of the overall rotor – bearing system is restored by double Neimark – Sacker bifurcation around an excitation frequency approximately given by (4.3.1). Of course one may consider the new critical speeds of the dynamic system. Once again the extent of the periodic limit cycles evaluated around this fundamental excitation frequency is decreased. The current configuration of the G.F.B. is now utilized to evaluate the same periodic solutions (if possible) with the non – linear approach of the elastoaerodynamic lubrication problem.

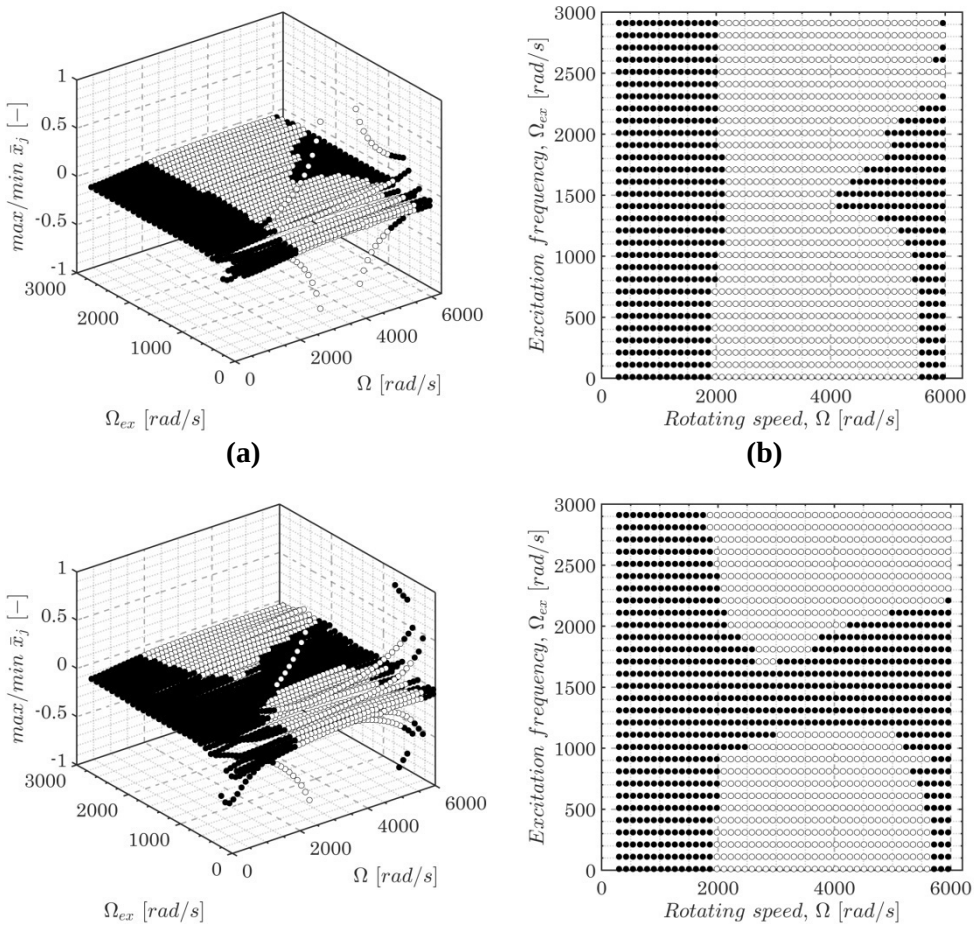

Figure 4.3.2*Stability maps according to the linear approach of the elastoaerodynamic lubrication problem for the modified rotor – bearing model* ***(a), (b)*** $\delta = 0.2$ ***(c), (d)*** $\delta = 0.4$

In *Figure 4.3.3* the linear stability threshold is compared to the non – linear one. It is encouraging that parametric antiresonance still occurs according to the non – linear approach. The strength (i.e. the zone of excitation frequencies) of parametric antiresonance strongly depends on the amplitude of the variation of the stiffness and damping coefficients. Therefore the significant discrepancies between the linear and the non – linear stability threshold can be interpreted. Additionally, it should be noted that the method of evaluating the stiffness and damping coefficients, thoroughly described in 2.2 for G.F.B.s is not as accurate as possible, even for such high values of the non – dimensional structural compliance.

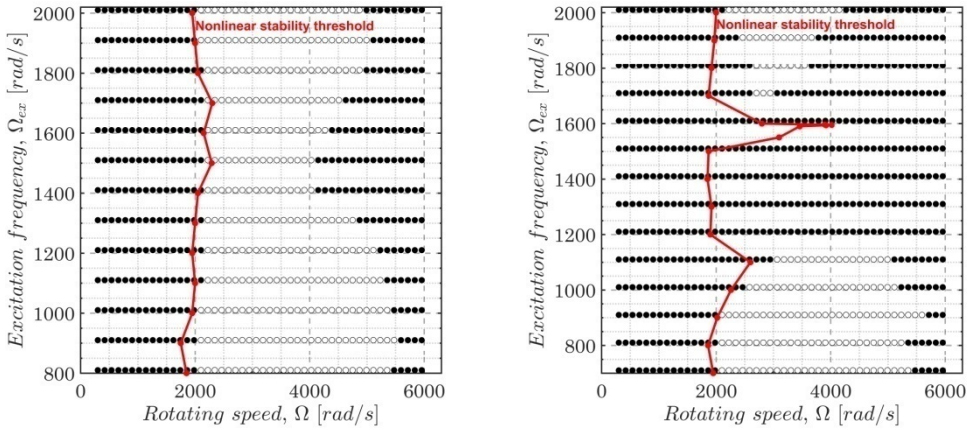

Figure 4.3.3 *Comparison between the linear and the non - linear stability threshold of the modified rotor – bearing system* ***(a)*** $\delta = 0.2$ ***(b)*** $\delta = 0.4$

5. CONCLUSIONS AND RECOMMENDATIONS FOR FUTURE WORK

The current work mainly proves that parametric antiresonance is feasible in realistic turbo-pump rotor – active gas foil bearing systems. Parametric excitation has been implemented by a vertical periodic load, acting on the deformable ring of the gas foil bearings, whose elastoaerodynamic behavior is described by a novel linear and a non – linear method. The stability and the extent of periodic limit cycles are evaluated via pseudo arc – length continuation method combined with an orthogonal collocation method. Based on the following conclusions this thesis aims to raise further concerns on parametrically excited rotating systems.

It is desirable to periodically change stiffness and damping properties of the gas foil bearing with the same amplitude ratio and without phase lag between them. According to a rather simplistic implementation of parametric excitation it is difficult to keep the same amplitude ratio for all the stiffness and damping coefficients. In contradiction, phase lug (between damping coefficients only) can be eliminated mainly by decreasing the compliance of the bump foil structure. In general, the strength (i.e. the zone of the excitation frequencies) of parametric antiresonance strongly depends on the amplitude ratios of the periodically changing stiffness and damping coefficients.

The accuracy of the applied continuation scheme is significant. As aforementioned, orthogonal collocation method applies a quasi linearization method in order to solve the two point boundary value problem, thus analytically computed Jacobian matrices is recommended to be used. In current work, due to the mathematical formulation of the dynamic model only numerically computed Jacobian matrices are used. Therefore either a different mathematical formulation is necessary or another method for evaluating periodic limit cycles and their stability could be implemented.

Additionally, the investigation of the full bifurcation set at lower rotating speeds and higher excitation frequencies is recommended. Up to now it is observed that a few period - doubling bifurcations occur at low rotating speeds independent on the excitation frequency. Due to difficulties regarding the accuracy of pseudo arc – length continuation method this investigation is not curried out in current work.

Finally, parametric antiresonance can simplistically be interpreted as modal interaction. Consequently, it is quite interesting to evaluate the energy flow between the interacting modes (e.g. the 1^{st} and 2^{nd} bending mode) when actually parametric antiresonance occurs. This can be achieved by evaluating the unbalance response of a parametrically excited unbalanced rotor. It should be noted though, that in this case classical methods such as Linear Harmonic Analysis or classical continuation methods such as pseudo arc – length continuation method can no longer be implemented.

"If you want to find the secrets of the universe, think in terms of energy, frequency and vibration."

Nikola Tesla *(July 9/10, 1856 – January 7, 1943)*

BIBLIOGRAPHY

1. ***T.Leister, C.Baum, W.Seemann.*** *On the Importance of Frictional Energy Dissipation in the Prevention of Undesirable Self-Excited Vibrations in Gas Foil Bearing Rotor Systems. TECHNISCHE MECHANIK. 2017.*

2. ***H. Heshmat, J. A. Walowit, O. Pinkus.*** *Analysis of gas-lubricated foil journal bearings. Journal of Lubrication Technology. 1983.*

3. ***S. A. Howard, R. J. Bruckner, C. DellaCorte, K. C. Radil.*** *Gas foil bearing technology advancements for closed Brayton cycle turbines. United States of America : National Aeronautics and Space Administration, 2007.*

4. ***Howard, S. A.*** *Rotordynamics and design methods of an oil-free turbocharger. United States of America : National Aeronautics and Space Administration, 1999.*

5. ***S. A. Howard, R. J. Bruckner, K. C. Radil.*** *Advancements toward oil-free rotorcraft propulsion. United States of America : National Aeronautics and Space Administration, 2010.*

6. ***C. DellaCorte, A. Zaldana, K. C. Radil.*** *A Systems Approach to the Solid Lubrication of Foil Air Bearings for Oil-Free Turbomachinery. STLE/ASME . Joint International Tribology Conference, 2004.*

7. ***Gross, W. A.*** *Gas Film Lubrication. s.l. : John Wiley and Sons, Inc, 1962.*

8. ***M. J. Baum, F. K. Choy, M. Dzodzo, J. Hsu.*** *Two-Dimensional Dynamic Simulation of a Continuous Foil Bearing. Tribology International. 1996, pp. 61-68.*

9. ***C. A. Heshmat, H. Heshmat.*** *An Analysis of Gas Lubricated Multileaf Foil Journal Bearings with Backing Springs. J. Tribol. 1995, 117, pp. 437-443.*

10. ***H. Heshmat, W. Sharpino, S. Gray.*** *Development of Foil Journal Bearings for High Load Capacity and High Speed Whirl Stability. J. Lubr. Technol. 1982, pp. 149-156.*

11. ***C. DellaCorte, J. C. Wood.*** *High Temperature Solid Lubricant Materials for Heavy Duty and Advanced Heat Engines. NASA TM-106570. 1994.*

12. ***C. DellaCorte, K. C. Radil, R. J. Bruckner, S. A. Howard.*** *Design, Fabrication and Performance of Open Source Generation I and II Compliant Hydrodynamic Gas Foil Bearings. NASA TM-214691. 2007.*

13. ***Bolotin, V.*** *The Dynamic Stability of Elastic Systems. Holden-Day. 1964.*

14. ***A. P. Seyramian, A. A. Mailybaev.*** *Multiparameter Stability Theory with Mechanical Applications. World Scientific Pub. Co. 13, 2003.*

15. ***Schmidt, G.*** *Parametererregte Schwingungen (In German, Translated Title 'Parametrically Excited Oscillations'). Deutcher Verlag der Wissenschaften. 1975.*

16. ***Tondl, A.*** *On the interaction between self excited and parametric vibrations. Monographs and Memoranda, National Research Institute for Machine Design. 25, 1978.*

17. —. To the problem of quenching self-excited vibrations. ACTA Technology. 1998, pp. 109-116.

18. ***J. P. Peng, M. Carpino.*** *calculation of stiffness and damping coefficients for elastically supported gas foil bearings. Journal of Tribology. 115, pp. 20-27.*

19. —. Finite element approach to the prediction of foil bearing rotor dynamic coefficients. Journal of Tribology. 119, pp. 85-90.

20. ***L. San Andres, T. H. Kim.*** *Improvements to the analysis of gas foil bearings: Integration of top foil 1D and 2D structural models. ASME turbo expo 2007, Power for land, sea and air. 2007, pp. 779-789.*

21. ***T. H. Kim, L. San Andres.*** *Heavily loaded gas foil bearings: a model anchored to test data. Journal Engineering for Gas Turbines and Power 012504-012508. 130, 2007.*

22. ***Kim, L. San Andres T. H.*** *Forced non-linear response of gas foil bearing supported rotors. Tribology International. 41, pp. 704-715.*

23. ***C. Baum, H. Hetzler, S. Schroders, T. Leister, W. Seemann.*** *A Computationally Efficient Nonlinear Foil Air Bearing Model for Fully Coupled Transient Rotor Dynamic Investigations. Tribology International. 2020.*

24. ***F. Dohnal, H. Ecker, H. Springer.*** *Enhanced damping of a cantilever beam by axial parametric excitation. Archive of Applied Mathematics. December 2008.*

25. ***T. Breunung, F. Dohnal, B. Pfau.*** *An approach to account for interfering parametric resonances and anti-resonances applied to examples from rotor dynamics. Springer Nature B.V. 2019.*

26. ***H. Ecker, A. Tondl.*** *Stabilization of a rigid rotor by a time-varying stiffness of the bearing mounts. Vibration of Rotating Machinery. 2004.*

27. ***F. Dohnal, A. Chasalevris.*** *Improving stability and operation of turbine rotors using adjustable journal bearings. Tribology International. 2016.*

28. ***Mallon, N. J.*** *Collocation: A method for computing periodic solutions of ordinary differential equations. Eindhoven : s.n., 2002.*

29. ***K. Georg, E. L. Allgower.*** *Introduction to Numerical Continuation Methods. Society for Industrial and Applied Mathematics. 2003.*

30. ***H. Meijer, F. Dercole, B. Olderman.*** *Numerical bifurcation analysis. Encyclopedia of Complexity and Systems Science. 2003, pp. 6329-6352.*

31. ***Kuznetsov, Y. A.*** *Elements of applied bifurcation theory. New York : Applied Mathematical Sciences, Springer, 1998. 2.*

32. ***A. H. Nayfeh, B. Balachandran.*** *Applied Nonlinear Dynamics. s.l. : Wiley Series in nonlinear science, J.Wiley & Sons, 1995. 1.*

33. ***Doedel, E. J.*** *Lecture Notes on Numerical Analysis of Nonlinear Equations. Montreal, Canada : Department of Computer Science.*

34. ***Boyaci, A.*** *Analytical bifurcation Analysis of a rotor supported by floating bearings. Nonlinear Dunamics. 57, 497-507.*

35. ***A. Boyaci, D. Lu, B. Schweizer.*** *Stability and bifurcation phenomena of Laval/Jeffcott rotors in semi-floating ring bearings. Nonlinear Dynamics. 2015, pp. 1535-1561.*

36. ***Breemen, F. C. Van.*** *Stability analysis of a laval rotor on hydrodynamic bearings by numerical continuation: Investigating the influence of rotor flexibility, rotor damping and external rotor oil pressure on the rotordynamic behavior. M.Sc Thesis, Delft University of Technology. 2016.*

37. ***Rubel, J.*** *Vibrations in nonlinear rotordynamics, Ph.D. Thesis. Heidelberg : Ruprecht-Karls-Universitat, 2009.*

38. ***A. Amanou, M. Couchane.*** *Bifurcation of limit cycles in fluid film bearings. International Journal of Non-Linear Mechanics. 2011, pp. 1258-1264.*

39. ***R. Sghir, M. Couchane.*** *Prediction of the nonlinear hysterisis loop for fluid-film bearings by numerical continuation. Proc. IMechE Part C: Mechanical Engineering Science . 2015, pp. 651-662.*

40. —. Non-linear stability analysis of a flexible rotor-bearing system by numerical continuation. Journal of Vibration and Control. 2016, pp. 3079-3089.

41. ***Becker, K.*** *Dynamisches Verhalten hydrodynamisch gelagerter Rotoren unter berucksichtigung veranderlicher Lagergeometrien, Ph.D Thesis. Karlsruhe : Karlsruhe Institute of Technology, 2019.*

42. ***Leister, T.*** *Dynamics of Rotors on Refrigerant Lubricated Gas Foil Bearings, Ph.D Thesis. Karlsruhe : Karlsruhe Institute of Technology, 2021.*

43. ***R. Dhakad, B. K. Pradhan, J. Kumar, S. Behera.*** *Prediction of Stiffness and Damping of Gas Foil Journal Bearing for High Speed Rotor. TRIBOINDIA. December 2018.*

44. ***Ioannis Gavalas, Athanasios Chasalevris.*** *NONLINEAR DYNAMICS OF TURBINE GENERATOR SHAFT TRAINS: EVALUATION OF BIFURCATION SETS APPLYING NUMERICAL CONTINUATION. Proceedings of ASME Turbo Expo . June 2022.*